IMPACTS OF IRRIGATION ON LAND-ATMOSPHERE INTERACTIONS IN HIGH-RESOLUTION MODEL SIMULATIONS

by

Patricia M. Lawston

A dissertation submitted to the Faculty of the University of Delaware in partial fulfillment of the requirements for the degree of Doctor of Philosophy in Climatology

Winter 2017

IMPACTS OF IRRIGATION ON LAND-ATMOSPHERE INTERACTIONS IN HIGH-RESOLUTION MODEL SIMULATIONS

by

Patricia M. Lawston

Approved: ______________________________
Delphis F. Levia, Ph.D.
Chair of the Department of Geography

Approved: ______________________________
Mohsen Badiey, Ph.D.
Acting Dean of the College of Earth, Ocean, and Environment

Approved: ______________________________
Ann L. Ardis, Ph.D.
Senior Vice Provost for Graduate and Professional Education

I certify that I have read this dissertation and that in my opinion it meets the academic and professional standard required by the University as a dissertation for the degree of Doctor of Philosophy.

Signed: ______________________________

Brian Hanson, Ph.D.
Professor in charge of dissertation

I certify that I have read this dissertation and that in my opinion it meets the academic and professional standard required by the University as a dissertation for the degree of Doctor of Philosophy.

Signed: ______________________________

Daniel Leathers, Ph.D.
Member of dissertation committee

I certify that I have read this dissertation and that in my opinion it meets the academic and professional standard required by the University as a dissertation for the degree of Doctor of Philosophy.

Signed: ______________________________

Cristina Archer, Ph.D.
Member of dissertation committee

I certify that I have read this dissertation and that in my opinion it meets the academic and professional standard required by the University as a dissertation for the degree of Doctor of Philosophy.

Signed: ______________________________

Sara Rauscher, Ph.D.
Member of dissertation committee

I certify that I have read this dissertation and that in my opinion it meets the academic and professional standard required by the University as a dissertation for the degree of Doctor of Philosophy.

Signed: ______________________________

Joseph A. Santanello, Jr., Ph.D.
Member of dissertation committee

ACKNOWLEDGMENTS

Thank you to the Department of Geography for the funding and resources needed to complete this work, as well as for providing ample teaching opportunities throughout my graduate career. The NASA Earth and Space Science Fellowship provided additional funding for the final year and a half of this dissertation. Thank you to my committee for lending their expertise; in particular to my primary advisor Brian Hanson, who trusted me to work independently but was also always available when I needed guidance and reassurance. Thank you also to my mentor Joe Santanello for providing computational resources, summer jobs, and numerous opportunities that I never even dreamed would be available to me and for helping me to grow into a real scientist. Thank you also to Cristina Archer, whose expertise was imperative in the third study. I also appreciate the friendship and support of my fellow graduate students, especially Carly Buxton and Chrissy Finan, who have made spending a significant portion of my 20's in grad school more enjoyable. Most importantly, it is only by the Grace of God and the love and support of my parents, siblings, and boyfriend Michael Parker that I was able to complete this dissertation and program.

TABLE OF CONTENTS

LIST OF FIGURES viii
ABSTRACT xii

Chapter

1 INTRODUCTION 1

2 IMPACT OF IRRIGATION METHODS ON LAND SURFACE MODEL SPINUP AND INITIALIZATION OF WRF FORECASTS 3

2.1 Introduction 3
2.2 Background 5

2.2.1 Irrigation Methods 5
2.2.2 Coupled Impacts of Irrigation 6

2.3 Methods 9

2.3.1 Model and Experimental Design 9
2.3.2 Irrigation Parameterizations 11
2.3.3 Evaluation 13

2.4 Results 15

2.4.1 Offline Spinups 15

2.4.1.1 Regional and Multi-Year Impacts 15
2.4.1.2 Spinup Results in a Dry and Wet Regime 16

2.4.2 Coupled Results 17
2.4.3 LoCo Diagnostics 19

2.4.3.1 Mixing Diagrams and EF-PBLH 19
2.4.3.2 LCL Deficit 21

2.4.4 Evaluation against observations 23

2.5 Discussion and Conclusions 26

3 ASSESSMENT OF IRRIGATION PHYSICS IN A LAND SURFACE MODELING FRAMEWORK AND EVALUATION WITH NON-TRADITIONAL AND HUMAN-PRACTICE DATASETS 44

3.1 Introduction 44
3.2 Background 46

3.2.1 Irrigation Physics 46
3.2.2 Evaluation of Irrigation in LSMs 47
3.2.3 Cosmic Ray Neutron Probe (CRNP) 49

3.3 Methods 51

3.3.1 Models and experiment design 51
3.3.2 Irrigation scheme 54

3.4 Results 55

3.4.1 Model results at the interannual scale 55
3.4.2 Model results at the seasonal scale 57
3.4.3 Model results at the local scale 57
3.4.4 Model performance 58

3.4.4.1 Evaluation of irrigation amounts and CRNP soil moisture evaluation 58
3.4.4.2 Evaluation with CRNP gridded product 60

3.5 Discussion 62
3.6 Conclusions 64
3.7 Data availability 66

4 ASSESSMENT OF IRRIGATION AND WIND TURBINE WAKE EFFECTS ON LAND-ATMOSPHERE INTERACTIONS IN A DESERT REGIME 76

4.1 Introduction 76
4.2 Background 78

4.2.1 Irrigation 78
4.2.2 Wind Turbines 79
4.2.3 Turbines and Irrigation 81

4.3 Methods 82

4.3.1 Model Configuration and Study Area 82
4.3.2 Experimental Design 85

4.4 Results 86

4.4.1 Irrigation Impacts 86
4.4.2 Turbine Impacts 88
4.4.3 Combined Impacts 89

4.5 Discussion 90
4.6 Conclusions 91

5 CONCLUSIONS 103

REFERENCES 106

Appendix

PERMISSIONS 116

LIST OF FIGURES

Figure 2.1. LSM and coupled simulations were run in a single domain in the central Great Plains of the United States, denoted by the yellow box in the inset. Simulation domain has green dots to denote grid cells classified as ‘irrigated’ according to the USGS land cover data. Stars mark the sites used for analysis, including irrigated and rainfed sites in Mead Nebraska (blue); ARM-SGP site E4 in Plevna, Kansas (orange); and point A (purple). 30

Figure 2.2. Domain-averaged monthly change from Control during the 5-year LIS-Noah spinup for top-layer (upper 0-10 cm) SM (top), Qle (middle), Qh (bottom). 31

Figure 2.3. Seasonally averaged (May-September) change in top layer SM content during the dry regime of 2006 using (a) Flood25, (b), Flood75, (c) Drip, and (d) Sprinkler irrigation methods. 32

Figure 2.4. As in Figure 2.3, but for wet regime of 2008. 33

Figure 2.5. As in Figure 2.3, but for Qle. 34

Figure 2.6. As in Figure 2.4, but for Qle. 35

Figure 2.7. Difference from Control in LIS-WRF simulated T2 using (a) Flood25, (b) Flood75, (c) Drip, and (d) Sprinkler methods at 1400 LT 31 Jul 2006 (dry regime). All methods decrease T2 over irrigated grid cells, ranging from a slight reduction (Drip) to almost 5 K (Sprinkler). 36

Figure 2.8. As in Figure 2.7, but for Q2. 37

Figure 2.9. As in Figure 2.7, but for total accumulated precipitation over the 2-day LIS-WRF simulation on 25-26 May 2008 (wet regime). 38

Figure 2.10. MDs for the LIS-WRF simulations during the (top-left) dry regime and (top right) wet regime at point A. The line representing the Control simulations is boldface. The solid lines are T2 and Q2 plotted in energy space from 0700 to 1700 LT. The tail of the surface vector has its tail at the final time point above. The entrainment ratio of heat Ah gives the proportion of sensible heat input to the PBL by entrainment Hent compared to that of the surface Hsfc and similarly for latent heat input Ale. (bottom left) Daytime mean evaporative fraction versus daily max PBLH at point A on 31 July (dry regime) and (bottom right) 25 May (wet regime). Each simulation is represented by a marker of a particular color and style. Note there is overlap in the markers in both the dry and wet regimes. 39

Figure 2.11. Hourly LCL deficit at point A on 31 July (dry regime). 40

Figure 2.12. Change from Control in LCL deficit using the Sprinkler method at (top) 1000 and (bottom) 1800 LT 31 July (dry regime). 41

Figure 2.13. (top) The LCL deficit and (bottom) vertically integrated cloud water mixing ratio for the LIS-WRF Control simulation at 0800 LT 25 May (wet regime). 42

Figure 2.14. Hourly RMSE for (top) T2 and (bottom) Q2 for each of the LIS-WRF and the NoSpin simulations generated by the MET toolkit for the dry regime. 43

Figure 3.1 (Top) Comparison of the GRIPC irrigation intensity given by Salmon et al. (2015, left) used in the Standard and SPoRT simulations and the observationally tuned irrigation intensity (right) used in the Tuned simulation. (Bottom) Average July 2012 greenness vegetation fraction given by NCEP climatology (left) used in the Standard and Tuned simulations and (right) SPoRT real-time dataset used in the SPoRT run. 67

Figure 3.2 Domain and monthly averaged GVF from the NCEP climatological GVF dataset, used in the Standard run, the SPoRT GVF dataset used in the SPoRT run, and the difference between the two (SPoRT – Climatology). 68

Figure 3.3 Domain and monthly averaged irrigation amount for each irrigation simulation. 69

Figure 3.4 Change from control (IRR - CTRL) in soil moisture for each experiment (line style) and each layer (line color). Layer designations are the Noah LSM default layers Layer 1 (top layer) is 0 to 10 cm depth, layer 2 is 10 to 40 cm (delta Z = 30cm), layer 3 is 40 cm to 1 m (delta Z = 60 cm) and layer 4 is 1 m to 2 m (100 cm depth). 70

Figure 3.5 May to September 2012 (top) and 2014 (bottom) domain average daily change from control (IRR-CTRL) in latent (blue) and sensible (red) heat fluxes for each irrigation simulation (left axis) and domain average daily accumulated precipitation from the NLDAS2 forcing data (right axis). 71

Figure 3.6 Domain average change in latent heat flux for three diurnal cycles in July 2012 (top). Change in latent heat flux (IRR-CTRL) at noon on July 6, 2012 for each irrigation simulation (bottom). 72

Figure 3.7 Volumetric soil water content at the rainfed (top) and irrigated maize (bottom) sites (left axis). The black solid line shows observations from the CRNP probe, the gray and green lines show the LIS control and irrigation simulations, respectively. Dark gray bars show accumulated daily precipitation from the Automated Daily Weather Network in York, Nebraska and pink bars show the accumulated irrigation amount at the irrigated maize and soybean sites (right axis). 73

Figure 3.8 Spatial CDF for 25 July 2014 (top) and 30 Jul 2014 (bottom), two dates when irrigation was applied at the irrigated maize and soybean sites in practice and in the model simulations. 74

Figure 3.9 Temporal CDF of normalized domain averaged (top) and irrigated/non-irrigated spatial average (bottom) SWC values from May 5 to Sept 16 from the COSMOS observational product (black) and the model simulations (colors). 75

Figure 4.1 The nested domain configuration for the LIS-WRF simulation. Each domain contains 249 x 315 grid points. The spatial resolution of each nest is 9 km, 3 km, and 1 km, for the outermost, middle, and innermost domains, respectively. 92

Figure 4.2 Locations of individual turbines (red) overlaid on the irrigation intensity map (shades of blue) in the innermost (1 km resolution) domain. The locations of surface based temperature (orange) and wind profiling (purple) instruments are also noted and will be used in future studies to validate the model results. 93

Figure 4.3 Change from control (IRR – CTRL) in top layer soil moisture at the time of initialization for each of the coupled LIS-WRF cases. 94

Figure 4.4 Change from control (IRR – CTRL) in surface latent (blue) and sensible (red) fluxes averaged over all gridcells with irrigation intensity greater than zero. Light colors show the six diurnal cycles for the three cases. The darker shades of blue and red are the case averages of latent and sensible heat fluxes, respectively. 95

Figure 4.5 As in Figure 4.4, but for (a) near surface humidity (b) and near surface temperature. 96

Figure 4.6 Change from control (IRR – CTRL) in near surface temperature at 2 am (top) and 10am (bottom) on the first day of case study 3. 97

Figure 4.7 Hourly surface latent (blue) and sensible heat (red) fluxes in CTRL averaged over all gridcells containing at least one turbine (top). As in (top) but for change from control (WIND – CTRL). 98

Figure 4.8 As in Figure 4.7 but for near surface temperature (top) and humidity (bottom). 99

Figure 4.9 Change from control in T2 resulting from the simulation that includes both turbines and irrigation (WIND_IRR – CTRL) averaged over gridcells that are irrigated added to the average over turbine gridcells (top) Difference between WIND_IRR impacts (WIND_IRR – CTRL) and the sum of the linear impacts of irrigation and turbines individually (bottom; IRR – CTRL and WIND – CTRL, respectively). 100

Figure 4.10 As in Figure 4.9, but for near surface humidity. 101

Figure 4.11 Scatterplot of the hourly difference in sensible heat flux in the simulation that contains both irrigation and turbines as compared to only using turbines and the corresponding difference in power produced. All differences are (WIND_IRR – WIND) and color of the dots indicates the hour of the day of each data point. 102

ABSTRACT

In the United States, irrigation represents the largest consumptive use of freshwater and accounts for approximately one-third of total water usage. Irrigation impacts soil moisture and can ultimately influence clouds and precipitation through land–planetary boundary layer (PBL) coupling processes. This dissertation is a collection of three studies that analyze the impact of irrigation on the atmosphere using NASA modeling tools the Land Information System (LIS) and the NASA Unified Weather Research and Forecasting Model (NU-WRF) framework.

The first study investigates the effects of drip, flood, and sprinkler irrigation methods on land–atmosphere interactions, including land–PBL coupling and feedbacks at the local scale. The offline and coupled simulation results show that regional irrigation impacts are sensitive to time, space, and method and that irrigation cools and moistens the surface over and downwind of irrigated areas, ultimately resulting in both positive and negative feedbacks on the PBL depending on the time of day and background climate conditions.

The second study assesses the sprinkler irrigation scheme physics and model sensitivity to choice of irrigation intensity and greenness fraction over a small, high resolution domain in Nebraska and evaluates the model performance with Cosmic Ray Neutron Probe (CRNP) observations. Results show that differences between experiments are small at the interannual scale, but become more apparent at seasonal and daily time scales. In addition, field-scale heterogeneity resulting from the individual actions of farmers is not captured by the model and the amount of irrigation

applied by the model exceeds that applied at the two irrigated fields. However, the seasonal timing of irrigation and soil moisture contrasts between irrigated and non-irrigated areas are simulated well by the model.

The third study assesses the individual and combined impacts of irrigation and wind turbines on surface fluxes, near surface temperature, and humidity. Results show that irrigation repartitions surface sensible and latent heat fluxes, reduces daytime temperatures and increases temperatures at night. Turbines weaken surface sensible heat fluxes minimally during the day but enough at nighttime to slightly reduce near surface temperature. The simulations that include both turbines and irrigation show that wind power production is slightly reduced when irrigation is included and irrigation contributes to a greater reduction in daytime surface sensible heat fluxes than would be realized with only turbines. Taken together, these three studies showcase the dramatic alterations that irrigation induces to the water and energy cycles and demonstrates the potential for human impacts on weather and climate.

Chapter 1

INTRODUCTION

Irrigation has been shown to modify local hydrology and regional climate through a repartitioning of water among the surface, soil, and atmosphere with potential to drastically change the terrestrial energy budget in agricultural areas during the growing season (Qian et al. 2013). Vegetation cover and soil moisture primarily control water and energy fluxes from the surface into the planetary boundary layer (PBL), so accurate representation of the land surface characteristics is key to determining and predicting atmospheric conditions. Chapter 2 investigates the impacts of irrigation methods on offline land surface model spinups and coupled land-atmosphere interactions. The model sensitivity to method, time, and space is assessed and recommendations are made for future modeling studies.

Irrigation parameterizations are becoming more common in land surface models and are growing in sophistication, but there is difficulty in assessing the realism of these schemes, due to limited observations (e.g., soil moisture, evapotranspiration) and unknown timing of real world application that may impact these observations. As a result, most irrigation parameterizations are implemented in models without a robust evaluation of the irrigation physics or full understanding of the scheme behavior, making definitive conclusions about downstream impacts on regional weather, precipitation, and long term climate difficult. Chapter 3 assesses the offline land surface model irrigation scheme physics and evaluates the performance of the model with human practice and soil moisture observations available within a small area of eastern Nebraska.

In the United States, the most commonly irrigated regions are often also areas that boast great wind power resource potential (NREL, 2016). Wind turbines, however, also have the potential to impact local land-atmosphere (L-A) interactions within and downwind of the farm. The extraction of kinetic energy by the turbine to produce electricity creates a wake in which wind speed is reduced and turbulent kinetic energy (TKE) is increased (Baidya Roy et al. 2004). As few observations exist within operational wind farms, previous studies have used large eddy simulations (LES; Calaf et al. 2011; Lu and Porté-Agel 2011), mesoscale models (Fitch et al. 2013; Cervarich et al. 2013) and global models (Wang and Prinn 2009)to explore the persistence of wind turbine wakes and their impact on near surface vertical mixing, surface fluxes, and temperature. Despite the fact that turbines are often located in agriculturally productive, potentially irrigated farms, the combined influence of turbines and irrigation has not been investigated. Chapter 4 assesses the potential impacts of irrigation and wind turbines on land-atmosphere interactions. Chapter 5 synthesizes and discusses the conclusions of all three studies more generally.

Chapter 2

IMPACT OF IRRIGATION METHODS ON LAND SURFACE MODEL SPINUP AND INITIALIZATION OF WRF FORECASTS

2.1 Introduction

Almost 55 million acres of farmland is irrigated in the United States, accounting for more than 29 trillion gallons of water usage per year (NASS 2009). Most of this irrigation water is applied to the soil surface, creating an anthropogenic change to the land that impacts soil moisture but can ultimately influence clouds and precipitation through land–planetary boundary layer (PBL) coupling processes. The process chain by which soil moisture can impact clouds and precipitation [as defined by Santanello et al. (2011a)] involves various pathways of positive and negative feedbacks dependent on the relative sensitivities of 1) surface fluxes to soil moisture, 2) PBL evolution to surface fluxes, 3) entrainment fluxes at the top of the PBL to PBL evolution, and 4) the collective feedback of the atmosphere on the surface fluxes.

The local, direct impacts of irrigation on the surface flux–soil moisture component of this process chain are well understood. Modeling and observational studies agree that irrigation application reduces temperature and increases humidity via the repartitioning of latent heat flux and sensible heat flux (Moore and Rojstaczer 2002; Adegoke et al. 2003, 2007; Douglas et al. 2006; Bonfils and Lobell 2007; DeAngelis et al. 2010; Kueppers and Snyder 2012; Jiang et al. 2014). The ability of a numerical model to reproduce irrigation's modifications to the surface energy balance is therefore essential for studies of land-use change impacts on climate (Zaitchik et al.

2005) and could potentially improve forecast skill in numerical weather prediction models (Ozdogan et al. 2010).

Irrigation-induced cloud and precipitation changes originate at the local scale and are regulated by feedbacks within the PBL. However, regional impacts of irrigation are more uncertain and vary by geographical area and climatological conditions. Past modeling studies have found irrigation can affect regional circulations (Chase et al. 1999; Lo and Famiglietti 2013; Huber et al. 2014) or induce remote precipitation responses (Im et al. 2014; Harding and Snyder 2012a,b), but others suggest that irrigation's effects on surface climate are localized and do not extend very far into non-irrigated areas (Sorooshian et al. 2011). Further contributing to this regional-scale uncertainty is the fact that the atmospheric response produced by a regional simulation can be affected by differences in the details of irrigation representation, such as the timing and frequency of water application (Sorooshian et al. 2012). Irrigation's regional impact could be dependent on the degree to which the land and atmosphere communicate changes to one another, as land–atmosphere (LA) coupling has been shown to influence precipitation patterns in studies of soil moisture feedbacks (Koster et al. 2002; Lawrence and Slingo 2005). Thus, a prerequisite to piecing together these regional impacts is an understanding of each irrigation method's effect on land–PBL coupling and feedbacks at the local scale (i.e., the foundation of the process chain described above).

This paper seeks to address this research need by presenting a comprehensive assessment of irrigation's impact on LA interactions using a high-resolution model test bed, multiple irrigation methods, and evaluation with a variety of surface observations. The purpose of this study is to 1) evaluate the sensitivity of a land surface model

(LSM) multiyear spinup to several different irrigation methods and thresholds, 2) assess the impacts of irrigated spinups on regional coupled forecasts, 3) determine the effects of irrigation on land–PBL coupling, and 4) suggest recommendations for future irrigation implementation in LSMs. Previous studies and relevant background information are discussed in section 2, followed by a description of the model and data in section 3. Results from offline and coupled simulations, diagnosis of land–PBL coupling and evaluation with observations are discussed in section 4, with conclusions presented in section 5.

2.2 Background

2.2.1 Irrigation Methods

The irrigation method chosen by a farmer is the product of numerous factors, including the associated monetary investment and labor intensity, the availability of water resources, and the topography of the landscape (S. Howser 2013, personal communication). In the central Great Plains states of Nebraska, Kansas, Iowa, and Missouri, center pivot sprinkler irrigation systems are by far the most widely utilized by farmers. As the method of choice on 68% of farms, sprinklers irrigate 80% of the total farmland acreage in this region (NASS 2009). Gravity systems, similar to flood irrigation, are inefficient from a water resources perspective, but are inexpensive, leading to their use on approximately 31% of farms. The most water-efficient method, drip irrigation systems, are costly and labor intensive and, as a result, are used on only 1% of farms in this area.

Recently, there has been a push for irrigation parameterizations that realistically reflect the variety and complexity of these irrigation practices. A popular representation of irrigation for regional applications forces soil moisture to saturation at a defined time interval in a manner similar to that of flood irrigation (Adegoke et al. 2003; Kueppers et al. 2007; Kueppers and Snyder 2012; Zaitchik et al. 2005; Jiang et al. 2014). Other parameterizations represent irrigation from an evapotranspiration (ET) or vapor flux perspective (Douglas et al. 2006; Segal et al. 1998; Evans and Zaitchik 2008), which best represents the water efficiencies of the drip irrigation method, or require soil moisture thresholds be exceeded before irrigation application occurs (Lobell et al. 2009; Qian et al. 2013; Tuinenburg et al. 2014). Ozdogan et al. (2010) simulated sprinkler irrigation by applying water as precipitation when the root-zone soil moisture fell below a triggering threshold. In some of the more sophisticated treatments of irrigation to date, Leng et al. (2014) used an offline land surface model to simulate the effects of irrigation on both surface fluxes and groundwater withdrawals while other studies have used an ‘‘irrigation demand factor’’ to prevent over irrigating the model soil surface (Pokhrel et al. 2012; Vahmani and Hogue 2014). The increasing complexity of these model parameterizations introduces the need to systematically assess their impacts on the LA interface.

The work presented in this paper is the first to comprehensively compare and evaluate drip, sprinkler, and flood irrigation parameterizations. As these methods are representative of the most common irrigation parameterizations in use today, this work should provide value to a range of future irrigation studies.

2.2.2 Coupled Impacts of Irrigation

Modeling studies utilizing irrigation parameterizations have shown that irrigation can significantly impact the surface energy balance and near-surface temperature from local to global scales. Boucher et al. (2004) estimated that irrigation produces a radiative forcing in the range of 0.03–0.1 W m^{-2} at the global scale because of the additional atmospheric water vapor, and it induces surface cooling of up to 0.8 K over irrigated land areas. Using the Community Atmosphere Model, version 3.3 (CAM3.3), Lobell et al. (2009) concluded that irrigation significantly reduced the model's warm bias over several heavily irrigated areas in the United States, such as California and Nebraska. In a study using the Noah LSM (Chen et al. 1996) over the continental United States, Ozdogan et al. (2010) found increases in surface latent heat flux of up to 100 W m^{-2} in California, as well as other regions across the United States, when simulating sprinkler irrigation. Similarly, in a study using the Regional Atmospheric Modeling System (RAMS), Adegoke et al. (2007) found irrigation increased latent heat flux by 36% in Nebraska, decreasing temperatures by 1.28° C and increasing dewpoints by 2.38° C. These cross-scale modeling results are corroborated by observational studies that have found decreases in surface temperature correlated with increasing spatial extent of irrigated agriculture in California (Bonfils and Lobell 2007) and the high plains aquifer of the southern Great Plains (Mahmood et al. 2013).

The potential ability of irrigation to mitigate or reinforce wet and dry periods through its impact on precipitation has important implications, as these climatological extremes can influence farmers' yields. Observational datasets have shown an enhancement of precipitation downwind of heavily irrigated areas in the Great Plains and Texas high plains (DeAngelis et al. 2010; Moore and Rojstaczer 2002), but irrigation-enhanced precipitation can actually lead to a net water loss as recycled precipitation often falls away from the source and is outweighed by ET increases (Harding and Snyder 2012a,b; Wei et al. 2013). Simulating the effects of irrigation on precipitation amounts and patterns often yields results that are dependent on the model used (Tuinenburg et al. 2014), the antecedent soil moisture conditions (Harding and Snyder 2012b), or the region of interest (Kueppers et al. 2008). Irrigation has even shown the potential to weaken the Great Plains low-level jet, thus increasing July precipitation by almost 50% downwind of irrigated areas (Huber et al. 2014).

Despite the importance of LA coupling and PBL evolution in the soil moisture–precipitation process chain, it can be seen from the aforementioned studies that much of the irrigation research to date either restricts analysis to surface flux–soil moisture interactions or is motivated to discern precipitation impacts with little regard for the PBL feedbacks that connect soil moisture to precipitation. An exception is a recent study by Qian et al. (2013), which explored the impacts of irrigation on the diurnal cycle of near-surface fluxes, temperature, clouds, and precipitation in the southern Great Plains using the Weather Research and Forecasting (WRF) Model (Skamarock et al. 2005). Their study showed irrigation repartitions surface fluxes and also increases the probability of shallow clouds by decreasing the lifting condensation level (LCL) more than the PBL height (PBLH).

The work presented in this paper takes an even more comprehensive approach by using an irrigated LSM spinup to capture soil moisture anomalies and by evaluating the model sensitivity to irrigation algorithms that differ in frequency, timing, and application. Furthermore, this work diagnoses the LA coupling and feedbacks using a high-resolution modeling environment forced by best available surface and satellite observations and utilizes the observational datasets necessary to evaluate irrigation schemes and coupled impacts.

2.3 Methods

2.3.1 Model and Experimental Design

This study utilizes NASA's Land Information System (LIS; Kumar et al. 2006), version 6.1, to complete offline spinups and generate initial conditions for coupled forecasts with the Advanced Research version of the WRF (ARW). LIS is a flexible land surface modeling and data assimilation framework that allows users to choose from a variety of LSMs that are forced and constrained by best available surface and remote sensing observations. The ARW is a community mesoscale research model with an Eulerian mass solver, a terrain following vertical coordinate system, and multiple physics options (Skamarock et al. 2005). LIS has been fully coupled to WRF under the NASA Unified WRF (NU-WRF; Peters-Lidard et al. 2015) framework. This model configuration allows for long-term offline land surface model spinups using observed atmospheric forcing and creates a better representation of LA interactions through the ability to characterize the land surface at the same spatial scales as cloud and precipitation processes (Kumar et al. 2006). In this way, the LIS–WRF configuration has shown skill in studies in which soil moisture anomalies and LA interactions play a prominent role (Santanello et al. 2009, 2011a, 2013b).

The study area is a 500 km by 600 km region of the central Great Plains including portions of Nebraska, Kansas, Iowa, and Missouri, shown in Fig. 2.1. This area provides a steep irrigation gradient, as the western region is heavily irrigated, but minimal irrigation occurs in the eastern section. Present in the domain are three flux observation sites from which data will be used to evaluate model results, discussed more in section 3c. The Noah LSM, version 3.2, was run offline (uncoupled) within the LIS framework at 1-km resolution for 5 years (2005–10) using four different irrigation schemes, discussed further in section 3b, and a control run (no irrigation; hereafter Control). In addition to offline sensitivity experiments, each LIS–Noah spinup was used to initialize a 2-day WRF forecast to study the relative impacts of each irrigation method on the PBL evolution and regional weather forecast. Two simulation periods were chosen, one in a wetter-than-normal year and one in a drier-than-normal year, to evaluate the sensitivity of the model to the background climate conditions. The wet and dry years were determined from the domain-averaged Phase 2 of the North American Land Data Assimilation System (NLDAS-2) soil moisture data, which showed 2006 to have the lowest and 2008 to have the highest soil moisture over the 5-yr spinup period. The LIS–WRF configuration was run for 48 h at 1-km resolution on 30–31 July 2006 (dry) and 25–26 May 2008 (wet). These 2-day periods exhibited the driest and wettest soil moisture in the NLDAS-2 forcing data in the dry and wet year, respectively, during the irrigation season.

The LIS–WRF simulations were completed using a single domain with 43 vertical levels and a time step of 5 s. The Monin–Obukhov surface-layer scheme as well as Goddard microphysics and short- and longwave radiation were utilized. To allow the model to explicitly resolve convection at 1-km resolution, a cumulus parameterization was not used. Initial and boundary conditions were provided by the North American Regional Reanalysis (NARR; Mesinger et al. 2006) at 3-hourly intervals. The Mellor–Yamada–Janjic (MYJ; Janjic 1994) PBL scheme was used for this study, which exhibits oscillatory PBLH estimations in the daytime hours based on TKE. Thus, in analysis of the model output, PBLH is estimated using a bulk Richardson approach, in which the pressure corresponding to the first model level where the bulk Richardson number exceeds 0.25 is assumed to be the top of the PBL

(Sivaraman et al. 2013). An additional NU-WRF run without a spinup (hereafter referred to as NoSpin) was completed for each case to demonstrate the impact of initializing from an LIS spinup versus that of the coarse atmospheric analysis (i.e., NARR) data.

To ensure the land surface states were fully equilibrated by the desired initialization time in 2006, a second spinup from 2003 to 2010 was completed and compared to the original. The 2005 spinup reached equilibrium in less than a year for soil moisture for the top three layers and for all layers with regards to soil temperature. Fourth-layer (bottom) soil moisture equilibrated by mid- 2007. However, differences in fourth-layer soil moisture in July 2006 are small (less than 0.02 $m^3\,m^{-3}$) and negligible for the purposes of this study. Therefore, we determined the model to be appropriately spun up by the July 2006 WRF initialization time.

2.3.2 Irrigation Parameterizations

This study uses three irrigation schemes—flood, sprinkler, and drip—each differing in the frequency, type, and timing of water application. These methods are implemented in the Noah LSM within the LIS framework.

The sprinkler method (hereafter referred to as Sprinkler) is derived from Ozdogan et al. (2010) but has been modified to employ a user-specified irrigation rate as opposed to one based on crop water demand. In this way, the Sprinkler scheme used here closely represents the farmer's perspective of water application and application rates. Water is applied uniformly as precipitation at a rate of 5 mm h^{-1} when the root-zone moisture availability (RZMA) falls to 10% above the stress point. The irrigation water shuts off when the RZMA reaches 80% of the maximum soil moisture.

The flood (hereafter Flood) method builds on Evans and Zaitchik (2008) by adding a threshold used to evaluate the soil moisture state before triggering irrigation. This method applies water to the root zone at 0900 local time (LT) if the root-zone soil moisture falls below a threshold with respect to the wilting point (Yilmaz et al. 2014). Water is then applied until the top layer is saturated and saturation is sustained for 30min. To evaluate the model sensitivity to this threshold, two Flood irrigation spinups were completed: one using a threshold of 25% above the wilting point and the other at 75% (hereafter Flood25 and Flood75, respectively).

The drip (hereafter Drip) method originates from Evans and Zaitchik (2008) and is designed to provide an optimal amount of water—enough to allow for transpiration without stress but without any excess water application. Soil moisture impacts ET in the Noah land surface model through the canopy resistance. The Drip parameterization calculates the canopy resistance and resultant ET twice—once using the current soil moisture and the second time assuming no soil moisture stress. The unstressed transpiration value is used in the simulation and the difference between the two values is the irrigation requirement to avoid stress. This approach results in soil moisture being largely unchanged during the simulation, as the water required is immediately transpired rather than added to the soil column.

The irrigation algorithms are applied homogeneously to each 1-km grid cell exhibiting an irrigable land-use classification. In this study, the 24-class category U.S. Geological Survey (USGS) land-use classification data were used within LIS. This dataset contains two irrigable categories: irrigated cropland and pasture (fully irrigated) and mixed dryland–irrigated cropland and pasture (partially rain fed). The Drip and Sprinkler methods do not distinguish between these categories, but the Flood algorithm uses half (all) of the maximum soil moisture content in calculating the irrigation water requirement for partially rainfed (fully irrigated) grid cells. However, of the two irrigable land-use categories, only fully irrigated grid cells appear in our domain. An additional important criterion needed to activate the methods ensures that it is irrigation season by requiring that the gridcell greenness vegetation fraction (GVF) exceed 40% of the climatological annual range of GVF, after Ozdogan et al. (2010). In LIS–Noah, GVF is derived from satellite-based monthly climatology data also at 1-km resolution.

2.3.3 Evaluation

Several techniques and observational datasets were employed to evaluate the offline and coupled model output. The Land Verification Toolkit (LVT; Kumar et al. 2012) is a software tool designed to enable robust evaluation of LIS output against observations from a variety of sources. This study employs the LVT for analysis of LIS–Noah output against observations of fluxes, soil moisture, and soil temperature from the U.S. Department of Energy (DOE) Atmospheric Radiation Measurement Program in the southern Great Plains (ARM-SGP). In addition, the Model Evaluation Tools (MET) software is used to compare the coupled LIS– WRF output to point observations within the study area (Developmental Testbed Center 2013). MET was developed at the National Center for Atmospheric Research (NCAR) through grants from the U.S. Air Force Weather Agency (AFWA) and the National Oceanic and Atmospheric Administration (MET user's guide). Additional point data were provided by the AmeriFlux group of the DOE's Oak Ridge National Laboratory and were analyzed to create average daily cycles of fluxes to verify those simulated by LIS–Noah.

LA coupling is examined through the use of local-scale land–atmosphere coupling diagnostics (LoCo; Santanello et al. 2011b), including mixing diagrams (MDs; Santanello et al. 2009, 2011a, 2013b), PBL–evaporative fraction (EF) analyses (Santanello et al. 2009), and the concept of the LCL deficit (Santanello et al. 2011a, 2013b). These tools have proven useful in determining the impact of soil moisture perturbations on surface forcing and the subsequent PBL response as well as the sensitivity of WRF to various LSM and PBL combinations. This makes LoCo diagnostics ideal for intercomparison of the impacts of various irrigation schemes as well.

Mixing diagrams represent the diurnal evolution of near-surface humidity and potential temperature using vectors in energy space, allowing for the quantification of heat and moisture budgets in the PBL and several related metrics (e.g., Bowen and entrainment ratios). These diagrams are constructed using the 2-m temperature and humidity at a particular point converted to heat and moisture energy space via multiplication by the specific heat of water and the latent heat of vaporization, respectively. The resultant values for each daytime hour are plotted, creating the solid line shown in the mixing diagrams. The dashed lines are vectors, which represent the fluxes of heat and moisture from the surface and atmosphere. In this analysis, we treat the residual vector of the mixing diagrams as the atmospheric response vector (Santanello et al. 2013a), which is typically dominated by entrainment fluxes but also includes horizontal advection. The slope of the surface (atmospheric response) vector is exactly equal to the surface (entrainment) Bowen ratio, and the magnitude of the vector components are proportional to the surface (entrainment) fluxes of heat, given by the y component, and moisture, given by the x component. For a more comprehensive discussion ofmixing diagram theory and LoCo diagnostics, interested readers are referred to Santanello et al. (2009) and Betts (1992).

2.4 Results

2.4.1 Offline Spinups

2.4.1.1 Regional and Multi-Year Impacts

Figure 2.2 shows monthly, domain-averaged differences from Control in top-layer soil moisture SM, latent heat flux Qle, and sensible heat flux Qh for each of the irrigation methods during the 5-yr spinup. The seasonal cycle of irrigation application is evident, with peaks in mid-year and decreases toward the end of each year. Of particular note is the memory of the soil to the previous growing season's irrigation practices, shown in SM increases that linger through the winter season. However, this residual SM anomaly has only a negligible impact on winter fluxes. The 25% threshold imposed on the Flood irrigation method is more restrictive than the 75% case, requiring the soil dry to a greater degree before irrigation will be triggered. Thus, Flood75 results in greater increases in soil moisture than Flood25, while Sprinkler irrigation shows the largest changes of all methods. As anticipated, Drip exhibits zero changes to soil moisture content because of the nature of the algorithm, as additional water is immediately used for transpiration.

The increased soil moisture repartitions the surface fluxes in the Sprinkler and Flood runs, consistent with previous modeling studies' findings of the impact of SM on fluxes (Adegoke et al. 2007; Qian et al. 2013). Flood75 and Sprinkler increase latent heat flux by up to 7.0 and 8.0 W m^{-2}, respectively. Although no soil moisture changes are noted in the Drip method, the ET modification causes latent heat flux to rise by as much as 3.5 W m^{-2}. Sensible heat flux decreases by a complimentary amount for each of the methods. The greatest changes to the energy balance during the 5-yr spinup occur in 2006, noted as a dry regime for the study area, while the wetter regimes of 2007 and 2008 exhibit the smallest changes. Such results are expected as dry periods are characterized by a lack of precipitation, low soil moisture values, greater plant stress, and decreased evapotranspiration—conditions that will trigger the irrigation algorithms to turn on more frequently than in a wet or normal regime.

Irrigated grid cells are most commonly found in the western third of the domain and account for only 4% of the total study area. Thus, impacts are minimized in the previous analyses because of the heavy weight of non-irrigated grid cells and the averaging of the model output twice—once temporally and a second time spatially with a majority of non-irrigated areas. The following section presents analyses for a dry (2006) and wet (2008) year spatially to determine the variation of impacts within the domain during contrasting antecedent soil moisture conditions.

2.4.1.2 Spinup Results in a Dry and Wet Regime

Irrigation impacts vary across the study area and are sensitive to time and method. Seasonally averaged changes in SM for the dry and wet regimes are presented in Figs. 2.3 and 2.4, respectively. In this case, ‘‘seasonal’’ refers to the irrigation season, defined as from 1 May to 30 September, as this is the primary growing season in Nebraska (Adegoke et al. 2003). Sprinkler irrigation impacts SM and fluxes the most, increasing SM by 0.16– 0.2m3m23 and latent heat flux by at least 100 W m^{-2} over most irrigated grid cells. Increases in latent heat flux (Figs. 2.5, 2.6) as a result of the Drip algorithm slightly exceed those due to SM effects in Flood25 with increases of up to 85 and 50 W m^{-2} for the two methods, respectively. Complementary decreases in sensible heat flux are apparent in these irrigated areas. The effects of irrigation are muted when the background precipitation is greater, as the impacts of each method are consistent with those during the dry regime, but are smaller in magnitude. This is especially noticeable near the Nebraska–Kansas border (western part of the domain near 40°N), where irrigation generally reduces sensible heat flux by 40–50 W m^{-2} more in the dry regime as compared to the wet. The energy balance is consistently impacted the most in the southwestern part of the domain, regardless of method or regime. This feature could potentially indicate that the soil in this region dries out more quickly than over the other irrigated areas, or that this area consistently experiences less precipitation in relation to the rest of the domain during these two regimes.

LIS–Noah spinups provide initial conditions for the WRF runs in the form of soil moisture and soil temperature. It is important to note that although soil moisture is not impacted directly by Drip irrigation, the method does have an effect on soil temperature. Latent heat flux increases caused by the Drip algorithm impact the land surface energy balance calculated by the Noah LSM, which simultaneously solves for fluxes and surface temperature. Thus, initial conditions for soil temperature are impacted by the Drip method via changes to the latent heat flux and surface temperature and are of similar magnitude to impacts seen via Flood25.

2.4.2 Coupled Results

Figures 2.7 and 2.8 present the change from Control in the midday 2-m temperature T2 and humidity Q2, respectively, for each of the irrigation methods in the coupled LIS–WRF simulations. Quiescent synoptic conditions in the dry regime forecast period amplify the impact of the irrigation-induced soil moisture perturbations in the coupled run forecast. Evidence of this is apparent in the comparison of Drip, which exhibits no direct soil moisture changes and therefore only small forecast changes, to Sprinkler, Flood75, and Flood25, which exhibit both direct and indirect impacts. Increased soil moisture and latent heat flux at the surface cause sensible heat flux and temperature to drop while increasing humidity over irrigated areas in the coupled run. Midday T2 decreases by as much as 4 K in the Sprinkler and Flood75 runs over irrigated grid cells while water vapor mixing ratio increases by up to 4 g kg^{-1}.

Although the greatest changes to soil moisture and fluxes occurred in the southwestern part of the domain in the spinup results, the greatest impacts in the coupled run appear just north of the Nebraska–Kansas border (near 40°N). Southerly winds advect the irrigation-cooled and moistened air northward, reducing the temperature downwind by 1–2 K and increasing water vapor by 1.5 g kg^{-1}. Thus, the maximum impact in southern Nebraska is likely due to a combination of the direct impacts, resulting from the densely irrigated area, with the indirect effects stemming from its location downwind of other irrigated grid cells.

The wet regime simulation period featured precipitation events associated with a cold frontal passage, leading to a greater impact of the initial conditions on cloud and precipitation patterns than on surface states. Temperature is still reduced by 1–2 K and humidity increases by up to 2 g kg^{-1} near the Nebraska–Kansas border, but overall, the direct surface impacts are muted as compared to the dry regime. Irrigation causes precipitation to vary in timing and location from Control, but changes to the magnitude of total accumulated precipitation over the simulation period are small (Fig.

2.9). Sprinkler increases rainfall by only 2.6%, while Drip creates a 1.8% reduction in precipitation.

2.4.3 LoCo Diagnostics

2.4.3.1 Mixing Diagrams and EF-PBLH

Figure 2.10 presents mixing diagrams illustrating the diurnal change in temperature and humidity for each of the experiments at an irrigated grid cell (Fig. 2.1, point A). Point A was chosen as an analysis site as it has an irrigated land-cover classification and interannual soil moisture characteristics that are representative of the dry and wet regimes. At this site, the NoSpin run is the driest as compared to the spinup simulations, which were run with observed forcing, consistent with the idea of a dry bias in the warm regimes in the Noah LSM (Chen et al. 2007). The ‘‘shepherd’s hook’’ appearance of the mixing diagram evolution is indicative of a moistening of the PBL through strong surface evaporation in the morning (staff– handle portion) followed by drying due to PBL growth and entrainment in the afternoon (bowed top). This evolution is consistent with previous results of LoCo analysis during dry regimes (Santanello et al. 2009).

The Control and Drip irrigation simulations exhibit almost the same diurnal evolution of temperature and humidity, suggesting that changes to the SM initialization are required to significantly impact T2, Q2, and fluxes. In these runs, the surface sensible heat flux is greatest, leading to the most PBL growth and dry air entrainment and a PBL that is mostly balanced between surface and atmospheric/entrainment inputs. In contrast, the surface provides energy to the atmosphere predominately in the form of latent heat for the Flood75, Sprinkler, and

Flood25 runs. In fact, negative Bowen ratios in the Flood75 and Sprinkler runs are a result of negative sensible heat flux, indicating heat loss from the atmosphere to the surface—a common microclimate situation over irrigated fields, referred to as the ‘‘oasis effect’’ (Oke 1978) or ‘‘sensible heat advection’’ (Brakke et al. 1978). With the exception of Drip, the surface sensible heat input is reduced to such an extent in the irrigated runs that the entrainment flux of sensible heat, even though reduced because of slower PBL growth, becomes the dominant source of heat input to the PBL.

The impact of irrigation on the PBL budget is muted in the wet year. Qualitatively, these mixing diagrams indicate strong surface moisture input and a much smaller range in temperature and humidity as compared to the dry year. This is consistent with the results of Santanello et al. (2013a), where the impacts of different LSM choices were maximized during dry regimes and much less during wet. Flood75 and Sprinkler methods result in more evaporation, but these impacts are not translated downstream as the changes to T2, Q2, fluxes, and entrainment are negligible.

Daily maximum PBLH and daytime mean EF [defined as the ratio of Qle to (Qle + Qh)] are integrative metrics of the land surface and PBL and thus allow evaluation of the PBL response to changes in surface forcing. Plots of PBLH versus EF are shown in Fig. 2.10 for the dry and wet year. In the dry year, EF is proportional to the amount of water applied by the irrigation methods (e.g., EF > 1 for Flood75 and Sprinkler but nearly unchanged for Drip), while the PBLH decreases in response to this surface forcing. The relatively dry surfaces of the Control and Drip runs (low EF) force the PBL to grow rapidly, ultimately reaching more than 2 km. Flood25 increases EF by about 0.5, reducing PBLH by a few hundred meters. However, the greatest changes occur with Flood75 and Sprinkler, as these methods reduce PBLH by almost 1 km at this location. This analysis makes apparent the sensitivity of the PBL response to irrigation method and the range of impacts of each scheme in the dry year.

Wet regime impacts to PBLH and EF indicate that irrigation only minimally impacts the PBL at this site. The effect of irrigation on EF is dependent on method, with small increases for the most water intensive methods (Flood75 and Sprinkler), but the differences in EF are quite small compared to the dry regime. As a result, PBLH is not affected, as maximum height remains around 1.4km for all runs.

2.4.3.2 LCL Deficit

Essential to the development of convective clouds is the requirement of the PBLH to exceed the LCL. A comparison of the PBLH and LCL evolution on diurnal time scales, referred to as LCL deficit (Santanello et al. 2011a), is analyzed at point A as well as spatially over the domain. A negative LCL deficit reveals that the PBLH (millibars) has exceeded the LCL, therefore indicating the potential for cloud development. Figure 2.11 shows a time series of the LCL deficit at point A for the second day of the dry regime coupled runs. In this case, the LCL deficit never becomes negative, but Sprinkler and Flood75 steadily decrease the LCL deficit throughout the morning hours (during the moistening and PBL growth phase seen in the mixing diagrams), allowing both to approach zero around 1000 LT.As the day progresses, the LCL rises faster than the PBL, resulting in an increasingly positive LCL deficit for all simulations.

Although the LCL deficit stays positive at this site, there are other regions of the domain where irrigation creates a negative LCL deficit in the morning. At 1000 LT, Sprinkler irrigation reduces the LCL deficit by about 60 mb over irrigated areas in the western portion of the domain (Fig. 2.12, top). This decrease is large enough to make the LCL deficit negative over those grid cells. Both PBLH and LCL are reduced (higher pressure), but the LCL reduction outweighs that of PBLH, thus driving the LCL deficit decrease. Another notable feature is the advection of moistened and cooled air northward that lowers the LCL in regions downstream of irrigated grid cells (as a function of the advection of the impacts on T2 and Q2). However, toward early evening (1700 and 1800 LT), the LCL deficit increases over the heavily irrigated areas as the PBL breaks down sooner than in the Control run (Fig. 2.12, bottom).

Although irrigation in Flood75 and Sprinkler create a negative LCL deficit in the morning, these changes are not reflected in the cloud field, as cloud development is not simulated until 1400 LT. Thus, irrigation moves the PBL toward a more saturated state in the morning, increasing the proclivity for clouds, but the dry conditions are extreme enough to prevent cloud formation.

At point A in the wet year, the LCL deficit is strongly negative for all methods, and although it increases steadily after 0900 LT, it remains negative throughout the day. As compared to Control, the irrigation methods only slightly reduce the LCL deficit between 1000 and 1300 LT. Spatially, the wet year exhibits large areas of sustained negative LCL deficit values that agree with the location of clouds indicated by the cloud water mixing ratio, shown in Fig. 2.13. Once again, the LCL deficit is reduced over the irrigated areas, but synoptic rather than surface forcing is the catalyst for clouds and precipitation on this day.

Synthesizing the results from the dry and wet year indicates that cloud development requires a strongly negative LCL deficit over many hours. Furthermore, in the absence of larger-scale forcing, as in the dry year, irrigation results in both positive and negative feedbacks on the PBL depending on the time of day. In the morning when the PBL and LCL are shallow, the irrigation perturbation decreases the LCL more than PBLH, consistent with the results of Qian et al. (2013), thereby increasing the chance for convective cloud development (positive feedback). However, the integrative nature of the PBL is such that the memory of reduced heating over the course of the day in irrigated areas causes the PBL to collapse sooner, reducing the chance of convective cloud development in the late afternoon (negative feedback). Advection of moistened and cooled air northward lowers the LCL downwind of the irrigated areas while minimally impacting PBLH, thereby creating a positive feedback downwind that is present throughout the day. Analyses that do not consider the diurnal cycle or changes to background conditions from day to day are likely to average across these feedback mechanisms.

2.4.4 Evaluation against observations

Because of the inherent human and plot-scale influences on irrigation practices, evaluation of irrigation physics in models is not as straightforward as traditional model validation of thermodynamic states or fluxes. Here, we survey at first order an array of potential validation approaches ranging from point to satellite-retrieved scales.

Observations from the ARM-SGP site E4 in Plevna, Kansas, were used to assess the offline and coupled simulations using the Land Verification Toolkit and LoCo diagnostics, respectively. The land-use category for the grid cell representing the E4 location in the model is not irrigable, thereby limiting the comparisons to only the Control and NoSpin simulations. LIS–Noah underestimates the July 2006 average daily cycle of Qle by more than 50 W m^{-2} in the afternoon followed by a smaller overestimation during the nighttime hours. As a result, Qh is overestimated in the afternoon and underestimated during the early morning hours, causing soil temperature to fluctuate more over the daily cycle than what is observed.

Average daily cycles generated from AmeriFlux towers at a rainfed and an irrigated site in Mead, Nebraska, reveal that LIS–Noah overestimates Qh and underestimates Qle at each location, in a way similar to that at the E4 site. The model grid cell associated with the irrigated Mead site is not of an irrigable land use, again preventing an intercomparison of the irrigation methods, but the observations expose some insight into the microclimate at these sites. Of particular note is the negative sensible heat flux in the observations associated with the oasis effect— the same effect noted at Point A with Flood75 and Sprinkler methods. Thus, it is possible that the simulation of the fluxes at this site would have been improved if the land use were irrigable, allowing the irrigation methods, especially Flood75 or Sprinkler, to activate here.

For a more robust evaluation against observations, the MET toolkit was used to match point observations within the domain to the complementary model grid cell (together called a pair) and to generate statistics assessing the skill of the coupled LIS–WRF runs. In the study area, the number of available observations, and therefore pairs, varies between 60 and 80 depending on the hour. It should be noted that only one of these pairs is located at a grid cell of irrigable land-cover classification. Thus, any differences in statistics revealed between the Control and irrigation methods are mostly a result of the indirect impacts of irrigation.

The most noteworthy feature apparent in the statistical analysis is the fact that the coupled runs initialized from any of the LIS spinups consistently show reduced daytime RMSE (Fig. 2.14) and MAE for temperature and humidity in the dry year. In addition, Sprinkler irrigation reduces the daytime warm temperature bias the most and improves the dry bias in Q2. In the wet year, model bias is initially reduced in the first 6 h by the spinups, but the precipitation events thereafter confound the statistics. The impact of simply including any type of spinup is generally dominant over any individual irrigation scheme effects because of the non-irrigated land-cover classification associated with most of the pairs. Overall, the Plevna, Mead, and MET analyses highlight the importance of using an LSM spinup, as well as the difficulties inherent in the evaluation of irrigation methods with point observations.

Observation-based analysis of fluxes within irrigated areas was challenging because of the problem of evaluating short model simulations against limited observations when the exact timing of real world irrigation applications is unknown. Nevertheless, we were able to confirm the realism of the USGS irrigated areas map by comparison with county-level freshwater withdrawal data from a USGS report on U.S. water use (Hutson et al. 2004). The report confirms the most heavily irrigated areas are located in the western part of the domain, as is the case in the land-use classification data. We also compared the USGS product to the MODIS-derived, contiguous U.S. irrigation map of Ozdogan and Gutman (2008) and found reasonable agreement across the simulation domain (not shown), but that the spatial extent of irrigated area in the USGS land cover is less than the MODIS-derived dataset. The USGS data give an irrigated area of 12,341 km^2 for the entire study area, but it is estimated by the Census of Agricultural Farm and Ranch Irrigation Survey that 15 505 km^2 are irrigated in Nebraska alone (NASS 2009).

Evapotranspiration as a proxy for irrigation is a promising avenue for validation as irrigated regions exhibit a markedly different ET signature than surrounding areas during dry years. The general pattern of ET produced by LIS–Noah is comparable to that of the MODIS–surface radiation budget (SRB; Tang et al. 2009) ET product from the University of Washington. However, a single MODIS overpass per day is not capable of reproducing the dynamics influencing the model output, and the dates of irrigation in the model do not necessarily match the exact dates of irrigation in the real world, thereby ruling out a rigorous validation of absolute ET magnitudes. The planned spatial expansion of the University of Nebraska– Lincoln's products using the Mapping Evapotranspiration at High Resolution and Internalized Calibration (METRIC; Irmak et al. 2011) technique will likely make it a valuable high-resolution spatial dataset for validation of ET and irrigation in future studies. Although these spatial and satellite-derived products are currently limited, by and large, they show more potential for future validation of irrigation schemes at the regional scale.

2.5 Discussion and Conclusions

This study has used a high-resolution model test bed and several irrigation parameterizations and thresholds to assess the impact of irrigation on LA interactions during a dry and a wet regime. Irrigation's ability to mitigate the soil moisture stress imposed by dry regimes directly impacts the surface energy budget, PBL growth, and ambient weather. The extent to which these irrigation impacts propagate downstream is dependent on the LA coupling processes as well as the irrigation method employed.

This study has demonstrated that there are several key components necessary to effectively represent irrigation in coupled prediction models, including accurate land-cover classification, GVF, and an appropriate irrigation method and physics.

Similar impacts, in terms of soil moisture and fluxes (both offline and coupled) and feedbacks within the PBL, are expected should these generic irrigation approaches be applied to other LSMs. The extent to which an irrigated LSM spinup will impact the atmosphere in a coupled simulation is likely dependent on the details of LA coupling and model configuration used (physics options, resolution, etc.), but first-order impacts of introducing water to the land surface should be similar regardless of the LSM or coupled model used.

As the focus of this study is on the intercomparison of irrigation methods during the offline period and their cumulative impacts over the 5-yr spinup on the WRF initial condition, irrigation was not turned on in the coupled run. This allowed us to analyze the impact of the irrigated spinup alone on the physical processes while avoiding case study or time-dependent conclusions. The applicability of the coupled Drip results may be somewhat limited since the soil moisture remains largely unchanged, but this approach provided important results related to when and where, in terms of soil moisture and fluxes, the impacts of the Drip algorithm are manifested. Future work, especially that including longer-term and seasonal simulations, will use coupled irrigation.

Irrigation's greatest impact on temperature and humidity occurs in regions that are both densely irrigated and downwind of other irrigated areas, because of the combination of direct and advected irrigation effects. In addition, the necessary conditions for cloud formation are most likely met if the LCL is low and the PBLH is high. Irrigation lowers both the PBLH and the LCL, resulting in competing effects on cloud formation. This study has found that in the absence of more dominant synoptic-scale forcing, irrigation results in both positive and negative feedbacks on the PBL depending on the time of day and the proximity to irrigation. Directly over irrigated areas, temperature drops, humidity rises, and the likelihood of surface-forced cloud development is increased in the morning, but the earlier PBL collapse breaks down the LoCo analyses late in the day. However, the advection of cooled and moistened air from irrigated areas reduces the LCL downwind but less directly impacts PBL growth, leading to greater chances of convective cloud development downwind of irrigation regardless of the time of day. These results may help explain the observational findings of Adegoke et al. (2007), who, using GOES infrared and visible images, detected peak convective cloud development that occurred 2 h earlier over cropland than over forested areas in Michigan on days featuring high pressure and light winds (< 5 m s^{-1}).

Even with a high-resolution simulation, evaluation of the irrigation methods with point observations proved to be difficult because of a number of factors, including the underrepresentation of irrigated areas in the USGS landuse classification data. Biophysical characteristics that determine transpiration amounts differ between crops, but the vegetation parameters in LIS–Noah do not account for different crop types. Thus, these land-use category differences not only complicated the point observations for the LSM evaluation by turning off irrigation and thus any differences between the methods at the Mead sites, but they also likely contributed to the underestimation of latent heat (through less ET) simulated by the model. Furthermore, this study used a climatological GVF, but in reality, phenology, and therefore ET, will vary based on the background climate conditions.

As the demand for food and fuel increases with a growing world population, the need to efficiently produce high crop yields will likely lead to further expansion of irrigated fields. The inclusion of irrigation physics then has the potential to improve forecasts, which will offer farmers a better tool to adapt to increasing crop demands. This study has shown that regional irrigation impacts are sensitive to time, space, and method and that irrigation cools and moistens the surface over and downwind of irrigated areas, ultimately resulting in both positive and negative feedbacks on the PBL. Future work will address these issues by using real-time GVF and a satellite-derived map of irrigated area (e.g., Ozdogan and Gutman 2008) and by addressing the interaction of irrigation with the assimilation of soil moisture in an LSM.

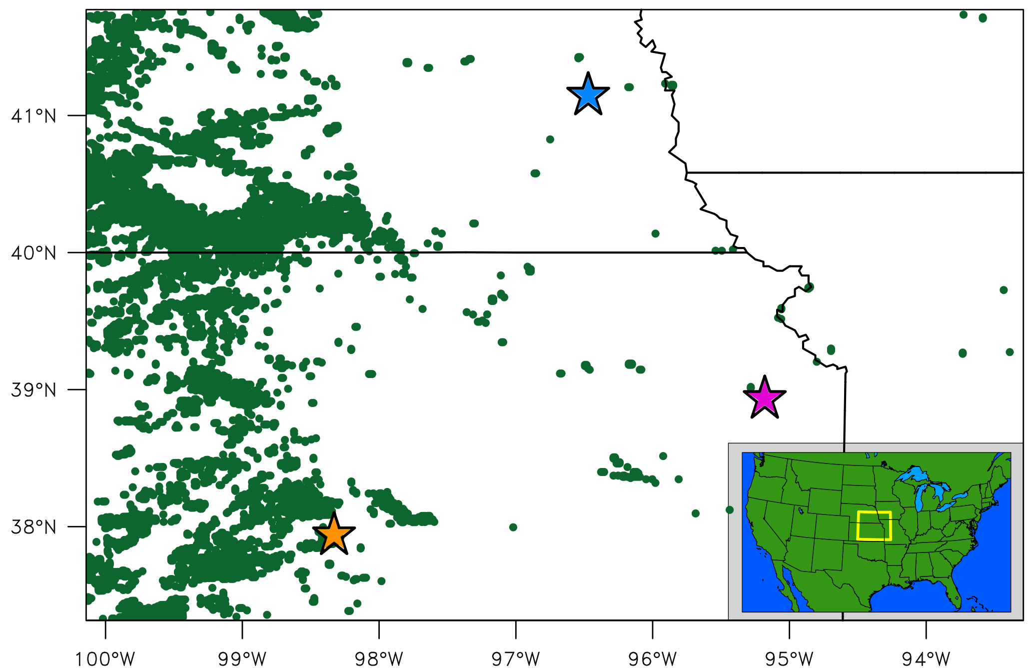

Figure 2.1. LSM and coupled simulations were run in a single domain in the central Great Plains of the United States, denoted by the yellow box in the inset. Simulation domain has green dots to denote grid cells classified as ‘irrigated’ according to the USGS land cover data. Stars mark the sites used for analysis, including irrigated and rainfed sites in Mead Nebraska (blue); ARM-SGP site E4 in Plevna, Kansas (orange); and point A (purple).

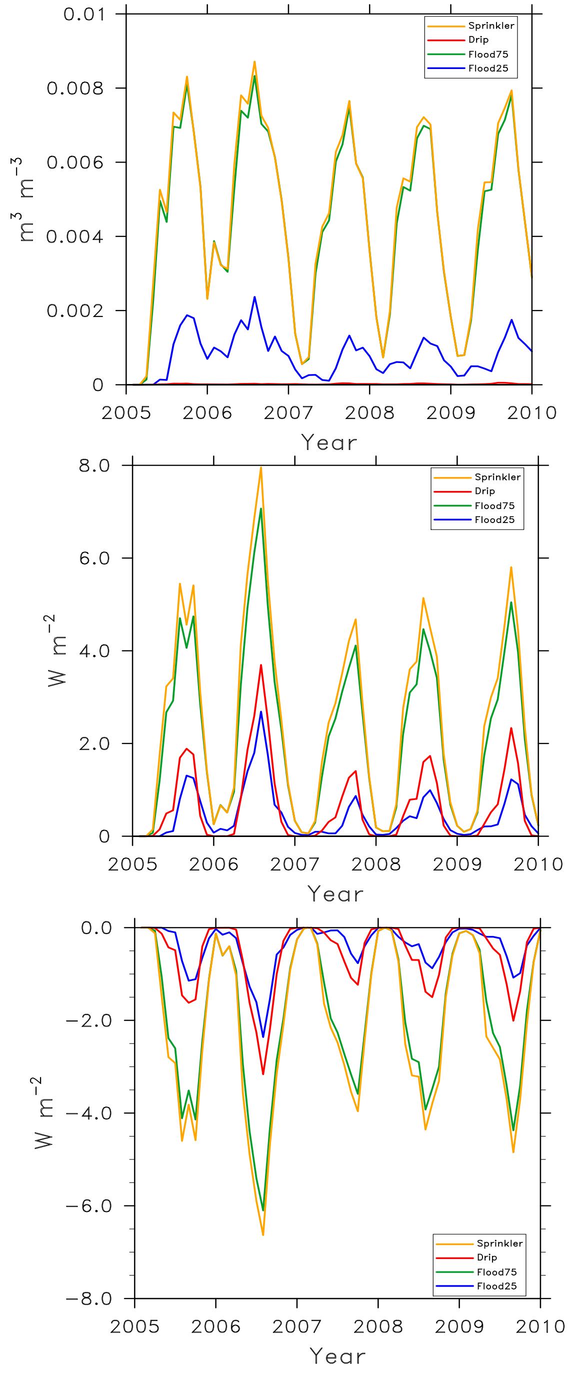

Figure 2.2. Domain-averaged monthly change from Control during the 5-year LIS-Noah spinup for top-layer (upper 0-10 cm) SM (top), Qle (middle), Qh (bottom).

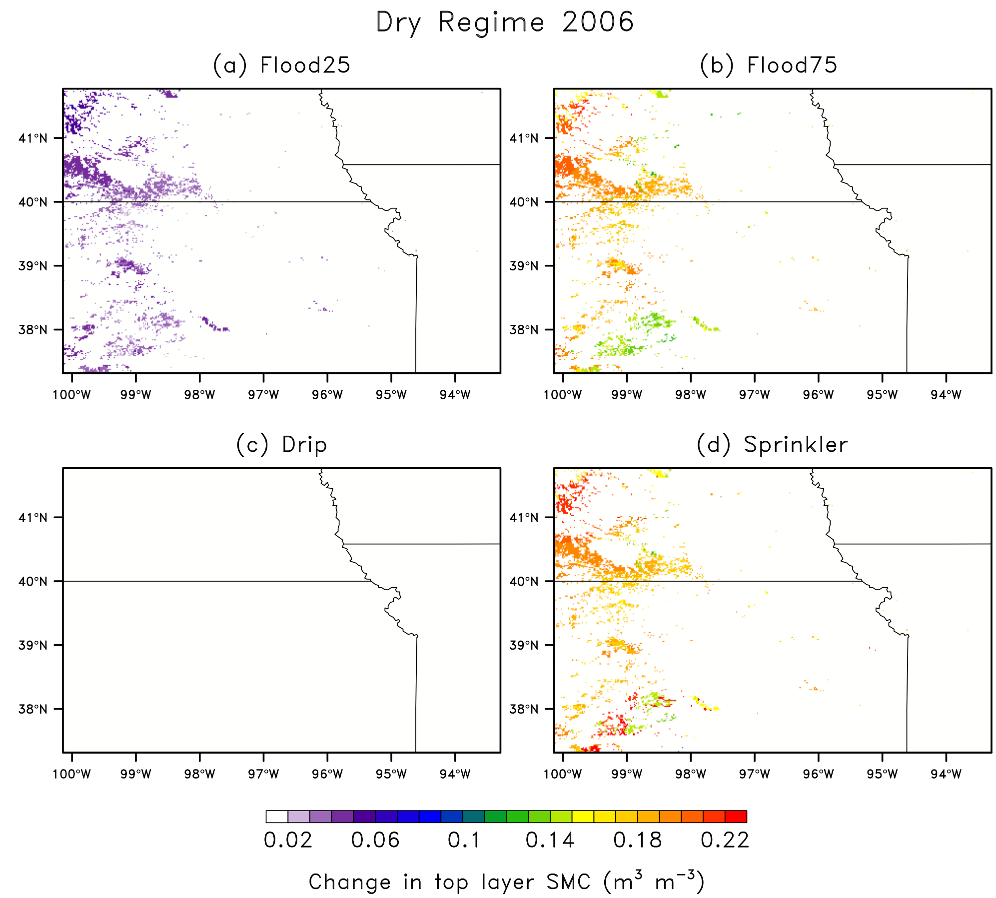

Figure 2.3. Seasonally averaged (May-September) change in top layer SM content during the dry regime of 2006 using (a) Flood25, (b), Flood75, (c) Drip, and (d) Sprinkler irrigation methods.

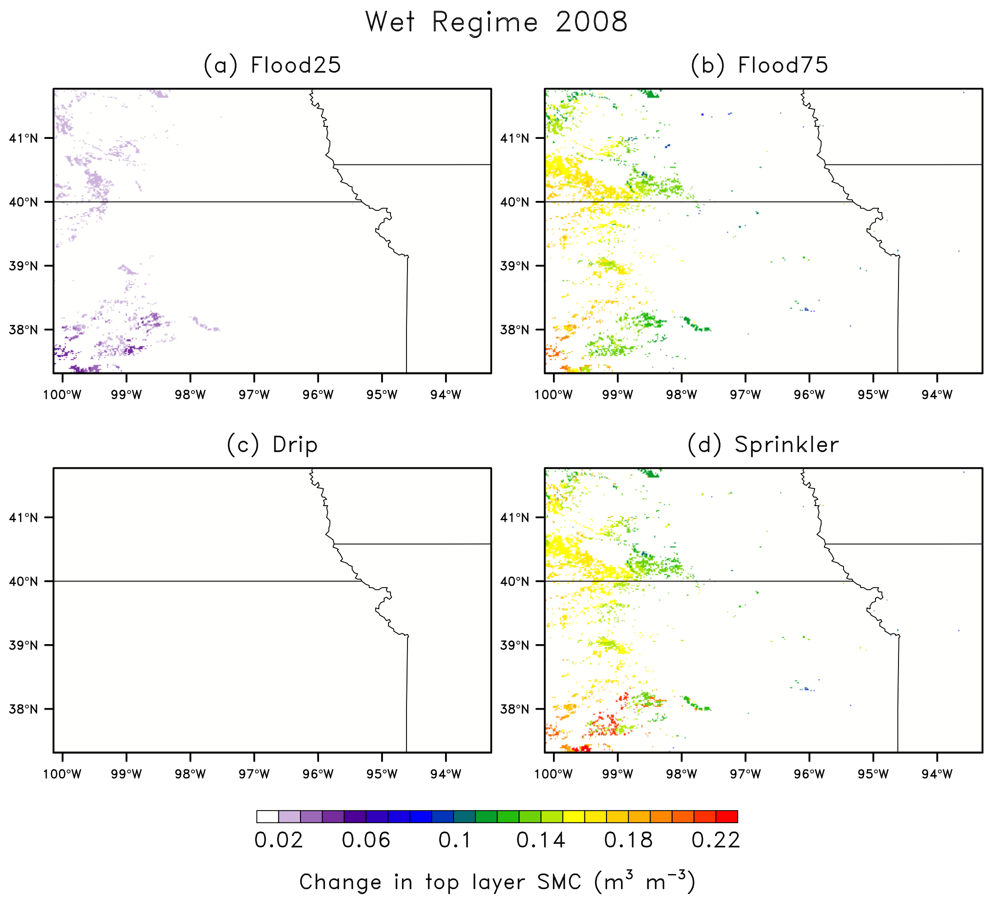

Figure 2.4. As in Figure 2.3, but for wet regime of 2008.

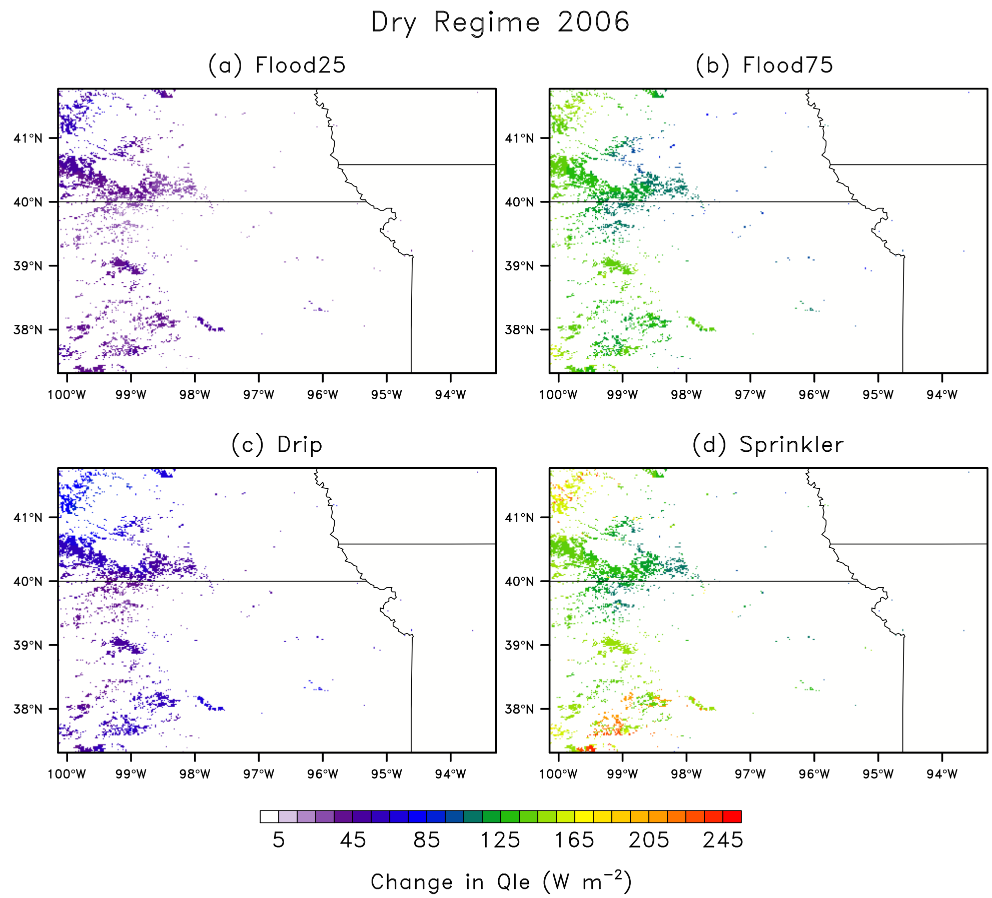

Figure 2.5. As in Figure 2.3, but for Qle.

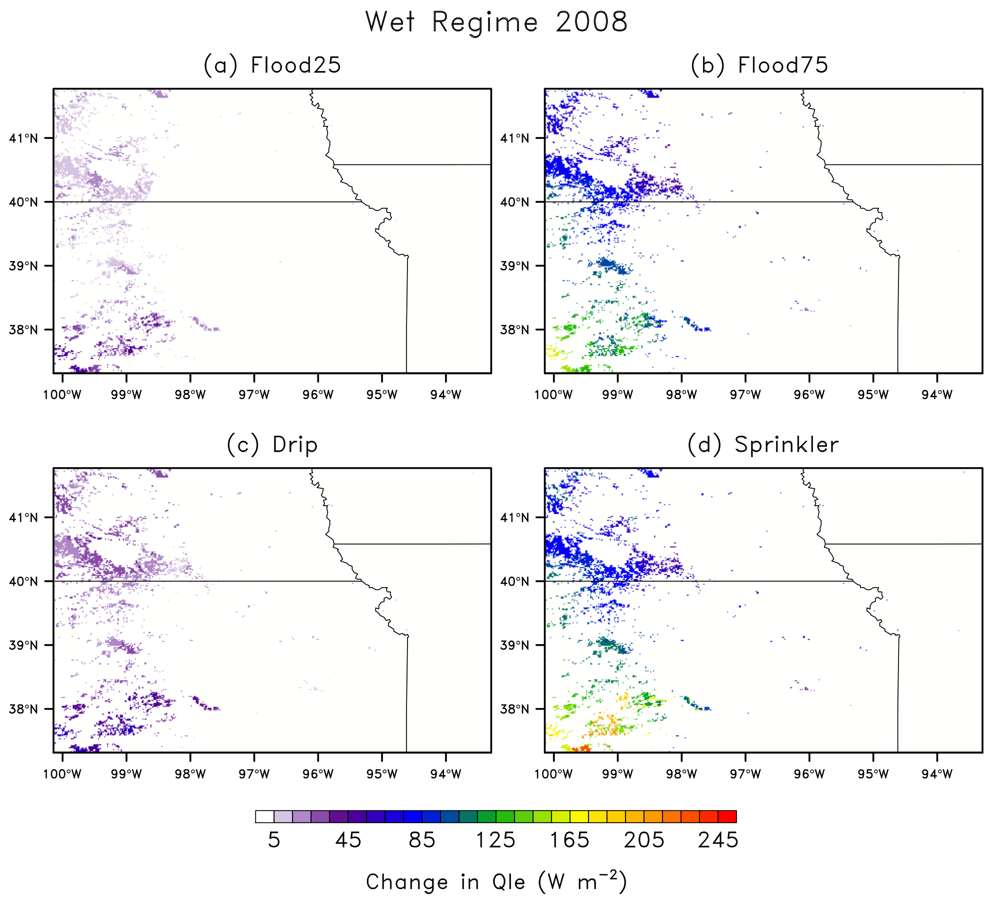

Figure 2.6. As in Figure 2.4, but for Qle.

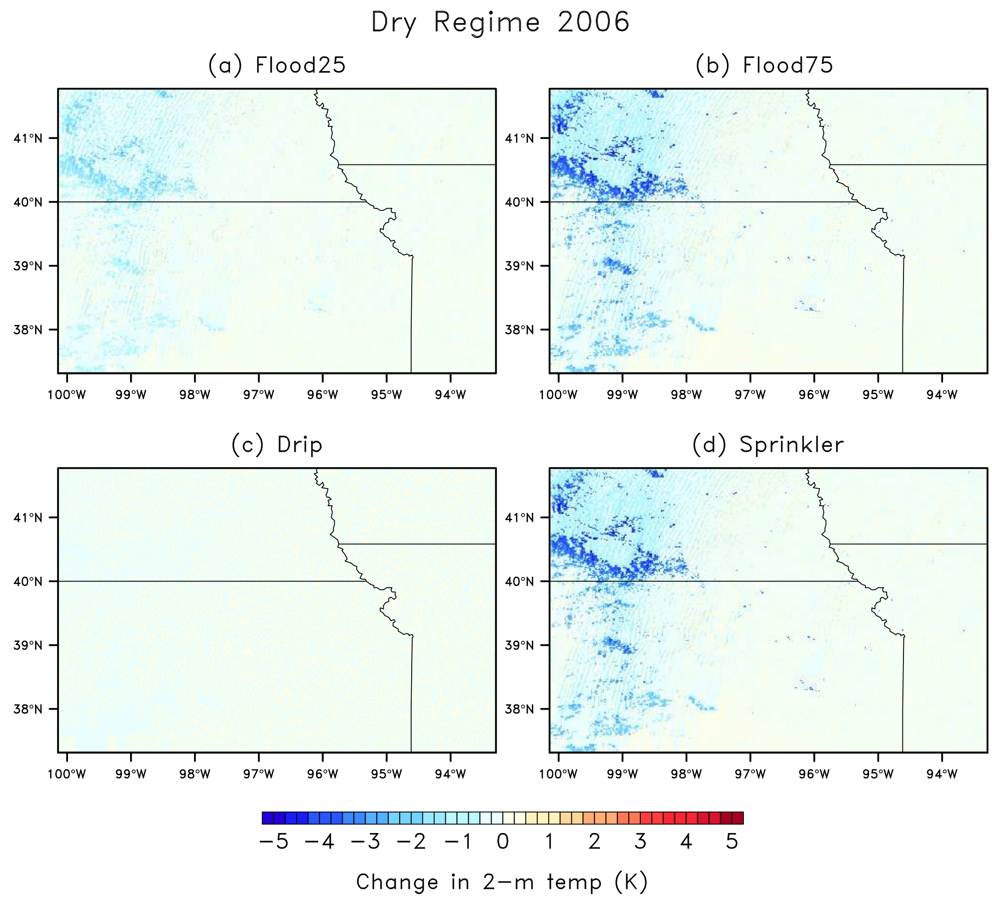

Figure 2.7. Difference from Control in LIS-WRF simulated T2 using (a) Flood25, (b) Flood75, (c) Drip, and (d) Sprinkler methods at 1400 LT 31 Jul 2006 (dry regime). All methods decrease T2 over irrigated grid cells, ranging from a slight reduction (Drip) to almost 5 K (Sprinkler).

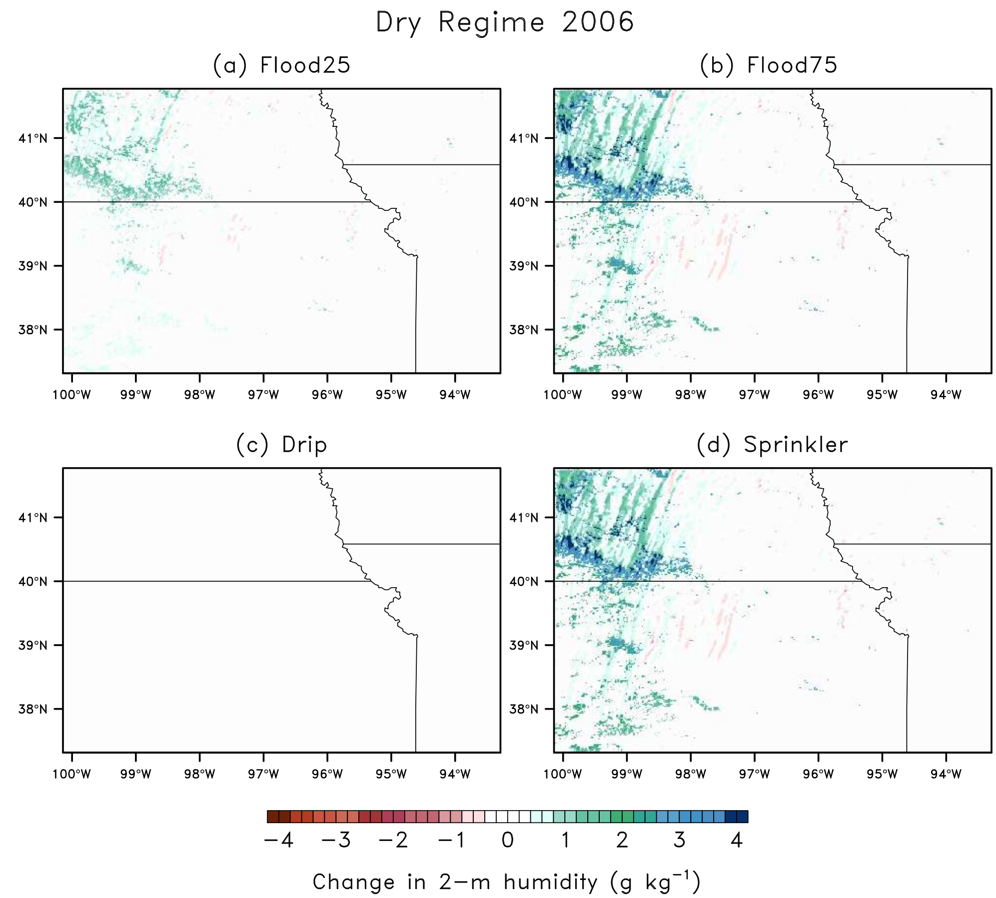

Figure 2.8. As in Figure 2.7, but for Q2.

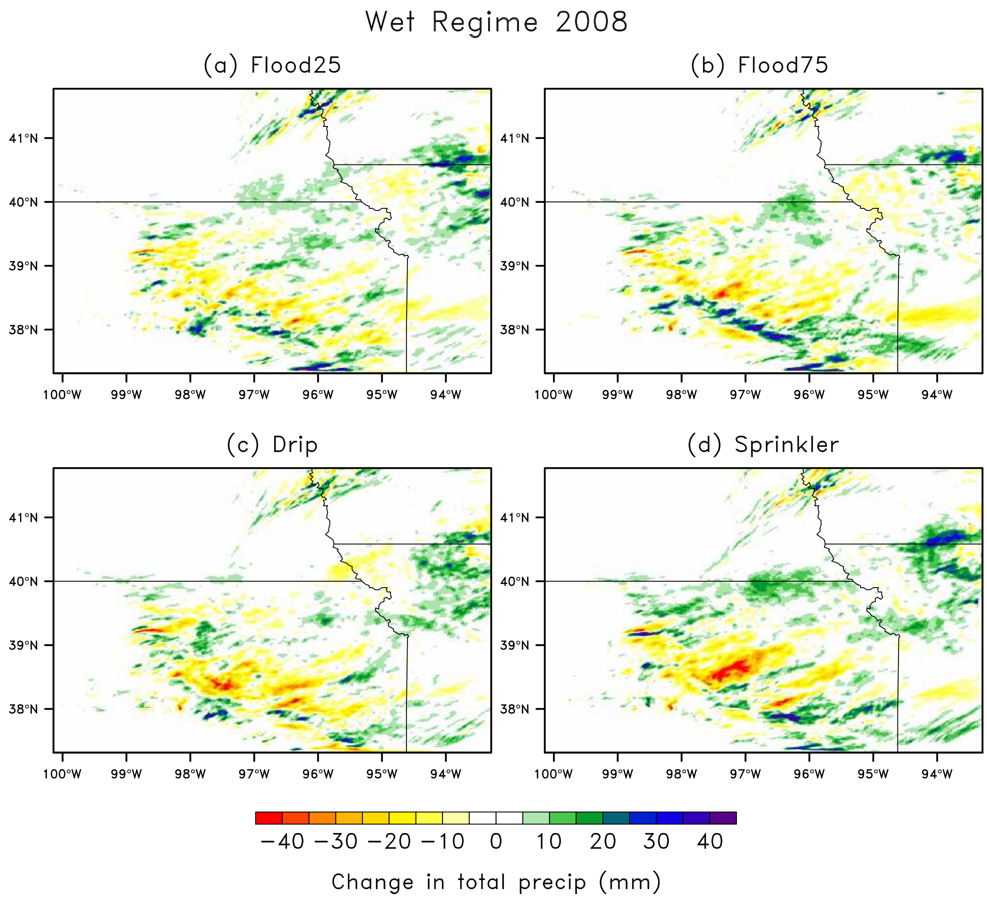

Figure 2.9. As in Figure 2.7, but for total accumulated precipitation over the 2-day LIS-WRF simulation on 25-26 May 2008 (wet regime).

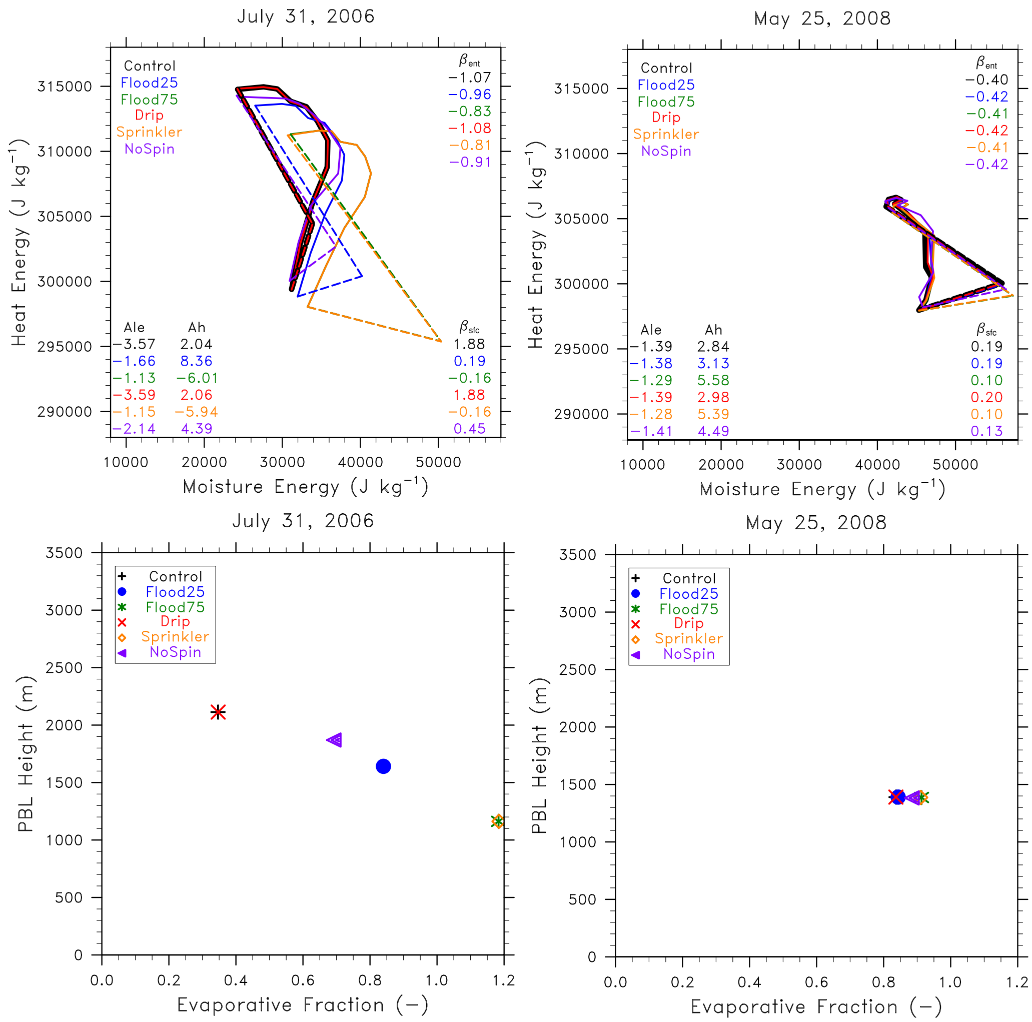

Figure 2.10. MDs for the LIS-WRF simulations during the (top-left) dry regime and (top right) wet regime at point A. The line representing the Control simulations is boldface. The solid lines are T2 and Q2 plotted in energy space from 0700 to 1700 LT. The tail of the surface vector has its tail at the final time point above. The entrainment ratio of heat Ah gives the proportion of sensible heat input to the PBL by entrainment Hent compared to that of the surface Hsfc and similarly for latent heat input Ale. (bottom left) Daytime mean evaporative fraction versus daily max PBLH at point A on 31 July (dry regime) and (bottom right) 25 May (wet regime). Each simulation is represented by a marker of a particular color and style. Note there is overlap in the markers in both the dry and wet regimes.

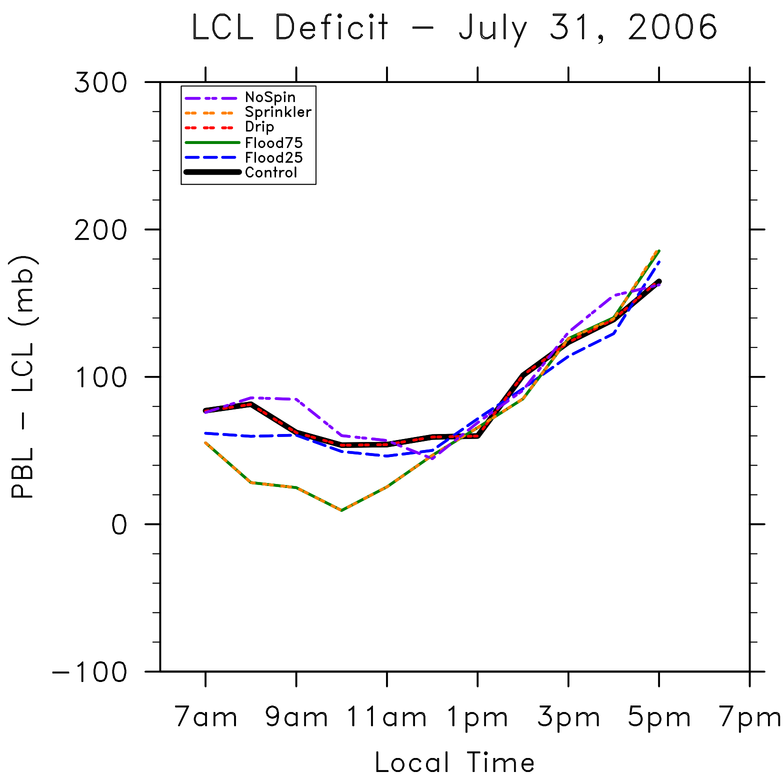

Figure 2.11. Hourly LCL deficit at point A on 31 July (dry regime).

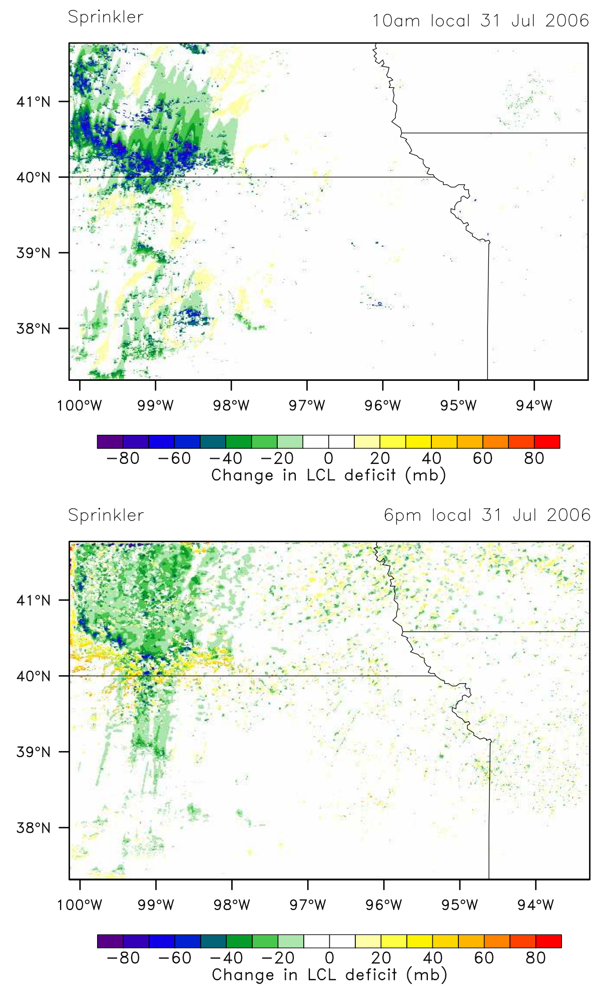

Figure 2.12. Change from Control in LCL deficit using the Sprinkler method at (top) 1000 and (bottom) 1800 LT 31 July (dry regime).

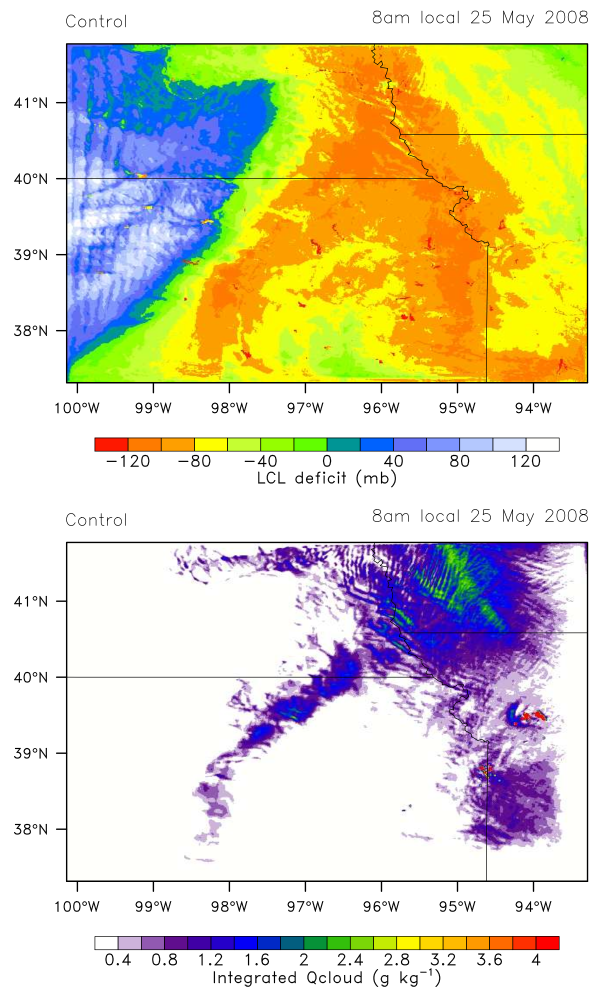

Figure 2.13. (top) The LCL deficit and (bottom) vertically integrated cloud water mixing ratio for the LIS-WRF Control simulation at 0800 LT 25 May (wet regime).

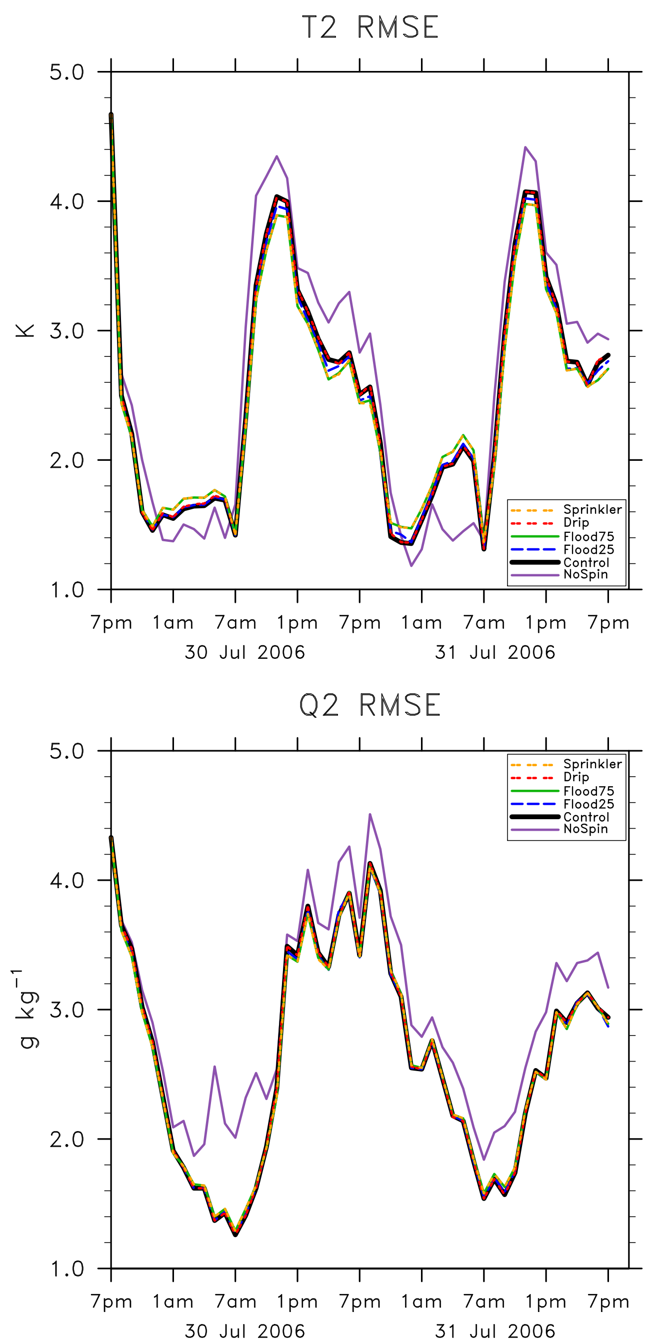

Figure 2.14. Hourly RMSE for (top) T2 and (bottom) Q2 for each of the LIS-WRF and the NoSpin simulations generated by the MET toolkit for the dry regime.

Chapter 3

ASSESSMENT OF IRRIGATION PHYSICS IN A LAND SURFACE MODELING FRAMEWORK AND EVALUATION WITH NON-TRADITIONAL AND HUMAN-PRACTICE DATASETS

3.1 Introduction

Irrigation is vital to feeding the world's population, but demands approximately 70% of global freshwater withdrawals (FAO, 2010), thereby altering the hydrologic cycle and raising questions about water resources sustainability. As a result, irrigation modeling studies have sought to understand the impacts of irrigation on ambient weather (Sorooshian et al., 2011, 2012), precipitation (Harding and Snyder 2012a,b), and regional to global climate (Lo and Famiglietti, 2013; Puma and Cook, 2010). Although the atmospheric response is often sensitive to the details of the irrigation scheme used in modeling studies, the observational data needed to fully vet an irrigation scheme (e.g., irrigation timing, practices, and co-located soil moisture) are generally not available or prohibitively challenging to acquire. As a result, most irrigation parameterizations are implemented in models without a robust evaluation of the irrigation physics or full understanding of the scheme behavior, making definitive conclusions about downstream impacts on regional weather, precipitation, and long term climate difficult.

The impact of water resources management practices such as irrigation on the water cycle is significant enough that the World Climate Research Program (WCRP) has identified anthropogenic changes to the continental water cycle as a Grand Science

Challenge to be addressed over the next 5 to 10 years (Trenberth and Asrar, 2014). In response, the Global Energy and Water Cycle Exchanges project's (GEWEX) Hydroclimatology Panel (GHP) and Global Land/Atmosphere System Study (GLASS) have begun a joint effort to advance the representation of human water resources management in land surface and coupled models (van Oevelen, 2016). To effectively meet these challenges, new, non-traditional datasets are needed to evaluate the current representation of irrigation in models and to assess the processes by which simulated irrigation impacts the water cycle.

The work presented here touches on each of these issues by comprehensively assessing a sprinkler irrigation algorithm in a land surface model (LSM) and evaluating the results with both conventional and non-traditional datasets. The paper is organized in the following way: Sect. 2 provides relevant background on recent irrigation modeling efforts with an emphasis on differences in irrigation schemes and previous evaluation efforts, and introduces gridded soil moisture from the Cosmic Ray Neutron Probe (CRNP) method as a potential tool for evaluation of land surface model irrigation. A description of the experimental design, including the land surface modeling framework and the irrigation algorithm, are presented in Sect. 3. Sect. 4 describes the results, first in the context of model sensitivity and secondly through an evaluation of the model simulations with observations. A discussion of the results and the applicability of this study to future irrigation modeling efforts are discussed in Sect. 5, and conclusions are stated in Sect. 6.

3.2 Background

3.2.1 Irrigation Physics

Irrigation increases soil moisture and therefore has the potential to influence local and regional clouds, precipitation, and ambient weather via land-planetary boundary layer (PBL) coupling processes (Santanello et al., 2011). By increasing latent and decreasing sensible heat fluxes, near surface temperature is reduced within irrigated areas (Bonfils and Lobell, 2007; Kanamaru and Kanamitsu, 2008). The irrigation-modified land energy balance alters the proportion of heat and moisture contributed to the PBL, thereby influencing PBL growth and entrainment (Kueppers and Snyder, 2011; Lawston et al., 2015). As a result, the PBL over irrigated areas is often shallower and moister, potentially resulting in alterations to convective cloud development (Adegoke et al., 2007; Qian et al., 2013). Irrigation applied over large areas not only affects local ambient weather, but models indicate that it can also modify precipitation patterns in areas remote from the source. Extensive irrigation projects, such as the Gezira Scheme in East Africa, have been shown to influence regional weather by changing circulation and precipitation patterns (Alter et al., 2015).

These significant potential impacts of irrigation on temperature, clouds, and precipitation necessitate an appropriate representation of irrigation in coupled land-atmosphere models. This need is has been addressed via irrigation parameterizations in LSMs that largely fall into three types of schemes: 1) defined increases to soil moisture in one or more soil layers (Kueppers and Snyder, 2011; de Vrese et al. 2016), 2) the addition of water as pseudo-precipitation to mimic sprinkler systems (Ozdogan et al., 2010; Yilmaz et al., 2014), and 3) modifications to vapor fluxes as a proxy for increased evapotranspiration resulting from highly efficient (e.g., drip) irrigation

(Douglas et al., 2006; Evans and Zaitchik, 2008). These schemes are generally dependent on parameter input datasets and user defined thresholds, affording a degree of customization, but also introducing uncertainty and potential error. Model sensitivity to the selection of datasets and thresholds is not trivial, as differences can alter the magnitude of irrigation-induced changes to the water and energy budgets. For example, a flood irrigation parameterization with a two different triggering thresholds resulted in up to 80 W m^{-2} difference in average seasonal latent heat flux increase in the U.S. Central Great Plains (Lawston et al., 2015). In another case, Vahmani and Hogue (2014) tested several irrigation demand factors and irrigation timing in their urban irrigation module, finding fluxes, runoff, and irrigation water are sensitive to both inputs. Additionally, the same parameterization used in a different model (Kueppers et al., 2008; Tuinenburg et al., 2014), or in the same model but at a different resolution (Sorooshian et al., 2011) has also produced different coupled atmospheric impacts.

3.2.2 Evaluation of Irrigation in LSMs

The sensitivity of atmospheric predictions to the details of the irrigation scheme makes it imperative to systematically evaluate irrigation parameterization, datasets, and thresholds in a controlled modeling study to determine the levels of uncertainty in the perturbation and subsequent results. However, datasets required for evaluation, such as irrigation amount, irrigation timing, and co-located continuous soil moisture observations, are not widely available, making it difficult to evaluate irrigation schemes (Kueppers et al., 2007). Modeling studies that have included some assessment of the irrigation scheme have used comparisons to annual water withdrawals for irrigation (Lobell et al., 2009; Pokhrel et al., 2012), outdoor water use

(Vahmani and Hogue, 2014), recommended amounts of irrigation (Sorooshian et al., 2011, 2012), or predicted irrigation requirements (Ozdogan et al., 2010). Bulk estimates, such as these, are often not used for robust evaluation, but rather indicate that the simulated results are reasonable.

In some cases, additional analysis of the observations has been successful in converting estimates to quantities usable for comparison. For example, Pei et al. (2016) used a potential evapotranspiration ratio to estimate June, July, and August irrigation usage from USGS yearly county-level estimates in order to validate irrigation amounts in the WRF-Noah Mosaic coupled model. The study found good agreement between the amounts simulated and that of the modified observations at 30 km horizontal resolution. In other cases, county and coarser resolution irrigation estimates have been used to constrain the irrigation algorithm output. Leng et al. (2013, 2014) calibrated the irrigation scheme in the Community Land Model (CLM) to reproduce county and water resources region irrigation water usage, respectively. Taken together, these studies exhibit recent progress made in irrigation modeling evaluation at regional to continental scales, but the datasets employed are insufficient for evaluation at high resolution and shorter (e.g. season to sub-monthly) time-scales.

As soil moisture is the primary control over fluxes and vegetation health, an evaluation of soil moisture sensitivity is equally as important as realistic irrigation estimates. Such evaluation is challenging as it demands soil moisture observations that are temporally and spatially continuous and at high enough resolution to resolve an irrigation signal. Satellite remote sensing has obvious potential to reach these goals, but retrievals of soil moisture are generally too coarse (i.e., ~25-40 km spatial resolution) and exhibit limited skill, at best, in detecting an irrigation signal (Kumar et al., 2015). At the other spatial extreme, point observations of soil moisture values are not representative of the larger area average (Entin et al., 2000). The aggregation of these observations into homogeneous, quality controlled datasets, such as the North American Soil Moisture Database (NASMD, Quiring et al. 2016) and the International Soil Moisture Network (ISMN, www.ipf.tuwien.ac.at/insitu), are promising for LSM evaluation more broadly, but in-situ measurements in irrigated fields, needed for irrigation scheme evaluation, are still sparse.

3.2.3 Cosmic Ray Neutron Probe (CRNP)

A potential solution to fill the gap between point and remote sensing observations of soil moisture is the Cosmic Ray Neutron Probe (CRNP), organized through the Cosmic Ray Soil Moisture Observing System (COSMOS, Zreda et al., 2012). CRNP is a new and novel way to obtain high-resolution, semi-continuous soil moisture observations, and as a result, has the potential to advance LSM and irrigation parameterization development. The CRNP is placed above the ground and measures neutrons produced by cosmic rays in the air and soil over a diameter of 300 m (+/- 150 m), depending on atmospheric pressure and humidity (Desilets and Zreda, 2013). The neutron density measured by the probe is inversely correlated with soil moisture and can be calibrated using local soil samples to an error of less than 0.03 $m^3 m^{-3}$ (Franz et al., 2012). The result is reliable, area-average soil water content integrated to a depth of 20-40 cm, depending on water content, bulk density, and lattice water, available at the same spatial scale as LSMs (Franz et al., 2012).

The characteristics of the CRNP, including the non-contact, passive data collection, make the CRNP portable and able to collect data while in motion. Desilets et al. (2010) first used a roving CRNP in Hawaii to obtain transects of soil moisture at highway speeds. More recently, Franz et al., (2015) mounted a large CRNP instrument to the bed of a pickup truck and completed roving surveys during the growing season of 2014 in a 12 x 12 km area of eastern Nebraska. The instrument collected ~300 neutron counts every minute and was driven at a maximum speed of 50 km per hour, allowing for high-resolution maps to be generation via geostatistical interpolation techniques. The spatial locations of each neutron measurement are given by the midpoint of successive rover locations and together are spatially interpolated via kriging to 250 m resolution. The surveys were completed every 3-4 days from May to September. In addition, 3 fixed probes were located inside the domain continuously recording soil moisture. Franz et al. (2015) used the fixed and roving data with a simple merging technique to produce 8-hour soil moisture products at 1, 3, and 12 km resolutions.

The work presented here uses the data and products gathered and generated in Franz et al. (2015) for evaluation of a sprinkler irrigation algorithm in a LSM environment, described in Sect 3. Specifically, the data are available for the 2014 growing season and include: timing and amount of irrigation water applied at two sites (one maize, one soybean), soil water content from a stationary COSMOS probe at these two irrigated sites, plus a rainfed site of mixed soybean and maize, and lastly, high-resolution gridded soil moisture at 3-4 day temporal resolution during the growing season (May to Sept) from the CRNP rover. The integration of human practice data (irrigation amount), physical observations (soil moisture point and spatial observations), and model simulations to evaluate the sprinkler algorithm and its impacts on soil moisture is a key and novel feature of this study. The main goals of this work are first to assess the physics of the simulated sprinkler irrigation, and secondly to evaluate the realism of the irrigation amounts and impacts to soil moisture.

3.3 Methods

3.3.1 Models and experiment design

NASA's Land Information System (LIS; Kumar et al., 2006) is used in this study to systemically assess the performance of the Sprinkler irrigation scheme. LIS is a land surface modeling and data assimilation system that allows users to choose from a suite of land surface models which can then be run offline while constrained and forced by best available surface and satellite observations. LIS can be fully coupled to the Weather Research and Forecasting model (WRF, Skamarock et al. 2005) in the NASA Unified WRF (NU-WRF, Peters-Lidard et al. 2015) framework. This configuration, LIS-WRF, has been used at the regional scale to assess the downstream impacts of irrigation on the PBL, but the performance of the irrigation scheme was not assessed (Lawston et al. 2015).

In this study, the Noah land surface model (Chen et al., 2007) version 3.3, was run offline within the LIS framework at 1 km spatial resolution over a 15 x 15 km area in eastern Nebraska, near the town of Waco. The size and location of the domain were designed to encompass the study area of Franz et al. (2015) to make use of the CRNP rover data, human practice information, and point and spatial observations yielded by their work, as discussed in Sect. 2.

The LIS simulations were run for 6 years (1 Jan 2009 to 31 Dec 2014) yielding daily output. The long-term simulation output was used to initialize restart-simulations for the growing seasons of 2012 and 2014 to produce hourly output for more detailed investigation during these periods, and the 3-5 year spinup periods, respectively, were shown to be sufficient for this region (Lawston et al. 2015). The analysis focuses on these two years (i.e., 2012 and 2014) to evaluate the irrigation algorithm during contrasting antecedent soil moisture conditions (e.g., relatively dry and wet, respectively), and to assess the performance of the scheme using the CRNP observations available in 2014.

To capitalize on the controlled nature of the study area and the irrigation scheme's dependence on greenness vegetation fraction (GVF) and irrigation intensity, discussed in detail in section 3.2, four types of simulations were completed and will hereafter be referred to as the 1) Control, 2) Standard, 3) Tuned, and 4) SPoRT simulations. The Control run is the only simulation that has the irrigation scheme turned off. The Standard simulation differs from Control only in that the sprinkler irrigation scheme is turned on and the Global Rainfed, Irrigated, and Paddy Croplands (GRIPC; Salmon et al., 2015) dataset is used to supply irrigation intensity at 1km resolution needed for the sprinkler algorithm. The GRIPC dataset prescribes irrigation intensity that is unrealistically high, as only 5% of the gridcells have intensity less than 100%. To correct for this overestimation, the Tuned simulation uses an irrigation intensity map created by reducing the GRIPC irrigation intensity according to a land use map generated from ground truth observations (Franz et al. 2015), thereby more accurately reflecting irrigation patterns in the study area (i.e. observationally tuned; Figure 1). The SPoRT run makes use of the GRIPC irrigation intensity dataset, like the Standard run, but uses a real-time GVF product from NASA-Marshall's Short Term Prediction, Research, and Transition Center (SPORT; (Case et al., 2014). This is in contrast to the other runs that use climatological GVF from the National Centers for Environmental Prediction (NCEP).

The SPoRT GVF is created using NDVI from MODIS satellite data and as such reflects the vegetation response to temperature and precipitation. In this way, the SPoRT GVF dataset captures interannual variability in vegetation that is missed by climatological GVF (Figure 2). Additionally, SPoRT GVF has higher spatial resolution (i.e., 3 km vs. ~16km for climatology) and has been shown to improve the simulated evolution of precipitation in a severe weather event as compared to GVF from climatology when using LIS coupled to a numerical weather prediction model (Case et al., 2014). The use of the SPoRT GVF dataset can be viewed as a middle-of-the-road approach between a simple representation of vegetation (e.g., climatology) and more sophisticated, but computationally-expensive methods, such a dynamic vegetation or crop growth models (e.g. Harding et al., 2015; Lu et al., 2015). As the SPoRT dataset is not available prior to 2010, the long-term SPoRT simulation uses climatological GVF for 2009-2010, and the SPoRT GVF dataset is incorporated in December 2010 and used throughout the rest of the simulation.

Additional datasets common to all simulations include Moderate Resolution Imaging Spectroradiometer – International Geosphere Biosphere Program (MODIS-IGBP) land cover, State Soil Geographic (STATS-GO) soil texture, University of Maryland (UMD) crop type, and National Land Data Assimilation System – Phase 2 (NLDAS2; Xia et al., 2012) meteorological forcing that includes bias corrected radiation and gauge-based precipitation.

3.3.2 Irrigation scheme

The preferred method of irrigation in Nebraska is the center pivot sprinkler system (NASS, 2014), and as such, we evaluate the sprinkler irrigation algorithm in LIS. The sprinkler scheme is described in Ozdogan et al. (2010) and was preliminarily tested and compared against two other irrigation schemes (drip and flood) available in LIS in Lawston et al. (2015). Sprinkler applies irrigation as precipitation when the root zone moisture availability falls below a user-defined threshold. In this study, we use a threshold of 50% of the field capacity, after Ozdogan et al. (2010).

In an effort to reproduce appropriate timing and placement of irrigation, a series of model checkpoints must be passed to allow for irrigation triggering. These checkpoints essentially boil down to four main questions:

1) Is the land cover irrigable?

2) Is there at least some irrigated land?

3) Is it the growing season?

4) Is the soil in the root zone dry enough to require irrigation?

The first two questions invoke direct tests against the static datasets (land cover and irrigation intensity, respectively), while the remaining two questions require additional calculations involving one or more time-varying datasets. The growing season, addressed in question three, is a function of the gridcell GVF as described in Ozdogan et al. (2010) and results in a season that spans roughly June through September in the study area. The last question, the determination of irrigation requirement, is dependent on two main features – the soil moisture and the definition of the root zone. Soil moisture is influenced by the meteorological forcing (e.g., how much rain falls and where) and soil texture (e.g., how long the moisture sticks around), while the root zone is the product of the maximum root depth (as defined by crop type) scaled by the GVF to mimic a seasonal cycle of root growth. Taken together, this means that the irrigation scheme is primarily controlled by six datasets: land cover, irrigation intensity, soil texture, crop type, meteorological forcing, and GVF.

For this limited study area, the land cover, crop type, and soil texture are homogenous throughout the domain (croplands, maize, and silt loam, respectively), meaning any heterogeneity in irrigation amounts and impacts can be attributed to only the meteorological forcing, GVF, and irrigation intensity. As the meteorological forcing is the same for all simulations, the experimental design leverages the unique characteristics of the controlled domain to assess the sensitivity of the irrigation algorithm specifically to changes in irrigation intensity and GVF; two important and common datasets in irrigation modeling. The irrigation algorithm is assessed first in the context of its physical response to forcing at the interannual, seasonal, and daily scales, and secondly, the results are evaluated against available observations in the growing season of 2014 (i.e., model performance).

3.4 Results

3.4.1 Model results at the interannual scale

Figure 3.3 shows the domain and monthly averaged irrigation amount applied for each of the three irrigation runs over the full six-year period. Interannual variability in the background precipitation (i.e., summer drought or pluvial periods) is reflected in the irrigation requirement, with dry seasons, such as 2012, exhibiting large irrigation demand, while wet seasons like 2011 and 2014 result in markedly less water applied. The average irrigation amount varies little between the experiments at this scale, around 1 mm day^{-1}, but a few features of the dataset differences are apparent.

The irrigation algorithm scales the amount of water applied by multiplying with the irrigation fraction value. The GRIPC irrigation dataset has greater irrigation intensity values everywhere in the domain, and as a result, the Standard run always applies more water than Tuned. The SPoRT run is less consistent in relation to the other methods; at times applying more water than both methods (e.g. July 2012), at others applying less (e.g. Sep 2012). This behavior is determined by the relative magnitude of the SPoRT GVF as compared to climatological GVF (Figure 3.2), as the GVF scales the root zone such that more water is applied by the irrigation scheme to more mature crops.

Figure 3.4 shows the percent change from control in soil moisture for each of the irrigation runs and each model soil layer. Irrigation increases soil moisture in all soil layers and all simulations. The spinup of the model is visible in the bottom soil layer behavior, shown ramping up through the first year of the simulation and then gradually equilibrating by July 2010. Increases in the third soil layer are quite consistent annually with a near doubling of the soil moisture when irrigation is turned on. The top and second layer fluctuations resemble the irrigation amount time series, indicating that the top two layers are more sensitive to the amount of irrigation water applied. These layers respond more quickly to irrigation, while percolation, and therefore time, is needed to impact the deeper soil layers. Differences between the irrigation runs are virtually undetectable in the top and second layers, but the cumulative impact of the differences in irrigation amounts and timing are reflected in differences in the third soil layer. The third and fourth layers are deeper and thicker (0.6 m and 1.0 m thickness, respectively) and as such are able to hold more water than the top and second layers (0.1 and 0.3 m thickness).

3.4.2 Model results at the seasonal scale

Figure 3.5 shows the average daily change from control in latent (Qle) and sensible (Qh) heat fluxes (left axis) as well as the daily precipitation amount from the NLDAS-2 meteorological forcing data (right axis) for May-October 2012 and 2014. Limited rainfall throughout the 2012 season resulted in the triggering of irrigation frequently throughout the growing season, including a stretch through July and August where irrigation was triggered somewhere in the domain every day (not shown). The 2014 growing season featured much more frequent precipitation, limiting consistent irrigation to late July and early August. The flux impacts follow the timing of irrigation triggering, steadily growing throughout the summer in 2012, up to 200 W m^{-2}, and emerging during dry down periods in 2014. Sharp decreases in flux impacts in the time series are the result of individual precipitation events, as the soil is not dry enough to trigger irrigation during and immediately following heavy rainfall events. In 2012, the SPoRT GVF is greater than climatology in June, resulting in more water applied and greater flux impacts in SPoRT than Tuned or Standard early in the season. However, in September, the SPoRT GVF detects the (negative) vegetation response to the July drought and irrigation amount and flux impacts are reduced. These seasonal scale impacts illustrate that the NLDAS-2 forcing (e.g. precipitation) data, via changes to soil moisture, drives the irrigation timing during the growing season and that the behavior of the irrigation scheme is consistent with expectations of human triggering of irrigation during dry and wet periods.

3.4.3 Model results at the local scale

At the interannual and seasonal scale, irrigation amounts and impacts are driven primarily by background rainfall regime, given by the forcing precipitation, with only small changes evident between the methods. At the diurnal scale, however, the choice of greenness and irrigation intensity datasets becomes more influential to irrigation impacts. Figure 3.6 shows the change from control in domain average latent heat flux for each of the irrigation runs for three diurnal cycles in July 2012 and the differences from control in latent heat flux at noon, spatially. All irrigation runs result in large increases to the latent heat flux, but while Tuned and Standard are relatively close in magnitude, the SPoRT run increases latent heat flux by more than 100 W m^{-2} more than Standard during peak heating. Spatially, the SPoRT simulation has a larger change from control everywhere in the domain as compared to Standard and Tuned, which exhibit similar magnitude of differences and spatial heterogeneity. The impacts on surface fluxes indicate that the choice of dataset, especially GVF, will likely impact coupled simulations, such as those with LIS-WRF.

In summary, the landcover, GVF, soil texture, meteorological forcing, irrigation fraction, and crop type all influence irrigation amounts in ways that are physically consistent with expectations for crop water use. For example, it is expected that the irrigation requirement is greatest for densely irrigated areas of mature crops with dry soil; the model reproduces this scenario by applying the greatest amount of water to gridcells that have high GVF (i.e., more mature crops and deeper roots), low soil moisture (from lack of precipitation), and high irrigation intensity.

3.4.4 Model performance

3.4.4.1 Evaluation of irrigation amounts and CRNP soil moisture evaluation

The simulation of irrigation amounts and timing as well as impacts on soil moisture are evaluated for the growing season of 2014 using field observations near

Waco, Nebraska, as described in Sect. 2.2. Figure 3.7 shows daily irrigation and rainfall amounts (right axis), as well as the volumetric soil water content (left axis) from the in-situ CRNP (solid black line) and all model simulations (green lines) at the rainfed and irrigated maize sites. The precipitation data confirm that 2014 was a relatively wet growing season, as was originally noted in the examination of Fig. 3.5b. The soil at the rainfed site gradually dries out between July 15 and August 5, the only consistent rain-free period of the summer (Fig. 3.7a). The dry down timing is simulated well in the Control and Tuned simulations, as irrigation is not included in Control and is prohibited at the rainfed site in Tuned, as defined by the edited irrigation intensity map (i.e., 0% for this gridcell). In contrast, the Standard and SPoRT simulations consider the rainfed gridcell to be 100% irrigated, as given by the GRIPC dataset, and as a result, both runs incorrectly trigger irrigation at this site, increasing SM during the dry down period.

At the irrigated maize site, irrigation is applied during the rain-free period in mid- July and early August and during a second, shorter stint late in August (red bars, Fig. 3.7b). The model simulations generally overestimate the amount of irrigation water at the irrigated site, applying an average of 8-15 mm day^{-1}(not shown), while the observations show that the irrigated field generally received 5 mm day^{-1}. In contrast to the rainfed site, the CRNP observations show SM increases or remains steady in mid-July through early August due to irrigation by the farmer at the maize site.

The triggering of irrigation during the dry down period is simulated well by the model as evidenced by the soil moisture differences between the Control and irrigated runs at the irrigated maize site (i.e. dry down versus steady SM levels, respectively). The SM given by the irrigated simulations matches the CRNP observations more closely than Control during the dry down period. This indicates that the combination of NLDAS-2 forcing and the triggering thresholds are sufficient to activate irrigation during rain-free periods, even in a wet year. Each irrigated LIS simulation applies enough irrigation water to maintain the SM levels, with small but inconsequential variations in the day to day to variability.

The soil water content observations are consistently greater than that of the model at both the rainfed and irrigated sites. However, it is common for soil moisture probes, other observations (e.g., satellite) and land surface models to exhibit different soil moisture climatologies that are largely a function of different representative depths of the soil (e.g. in model vs. CRNP). The spikes in soil moisture shown in the probe observations are represented well by the model, once again indicating the accuracy of the NLDAS-2 meteorological forcing data, even at this local scale. Overall, these results show that the irrigation scheme simulates well the irrigated versus rainfed soil moisture differences when the irrigation location is specified properly by the irrigation intensity dataset (in this case, the Tuned simulation).

3.4.4.2 Evaluation with CRNP gridded product

In order to assess whether soil moisture heterogeneity due to irrigation across the domain is captured accurately, simulations are evaluated against the CRNP gridded soil moisture product. The gridded product from Franz et al. (2015) uses the spatiotemporal statistics of the observed soil moisture fields, as obtained via the CRNP rover, and a spatial regression technique to create a 1-km, 8-hour gridded soil moisture product for the growing season (May – Sept, 388 values). In this study, we modify the spatial regression technique to treat irrigated and non-irrigated areas differently by using the CRNP (irrigated) rainfed data in the regression for (irrigated) non-irrigated gridcells. This results in a gridded soil moisture product that retains the spatiotemporal differences of the rainfed and irrigated areas.

The LIS-simulated soil moisture variability in time and space is evaluated using a comparison of the cumulative distribution functions (CDFs) generated from the LIS simulations and the modified COSMOS product, shown in Figures 3.8-3.9. Analyzed first is the CDF of all soil moisture values in the domain for two separate days, July 25 and July 30, during which irrigation was applied at the irrigated maize site (Fig. 3.8). As this CDF provides information about the variability of soil moisture spatially in the study area at one particular time, it is hereafter referred to as a 'spatial CDF' (Fig. 3.8). Also examined is a CDF of the domain-averaged soil moisture values from May 5 to Sept 22 at 8-hour intervals (the same as the COSMOS product; 388 values), hereafter referred to as the 'temporal CDF' (Fig. 3.9).

The spatial CDFs (Figs 3.8a-b) show uniformly dry soil in the control simulation while the irrigated runs exhibit a step-like behavior as a result of irrigation triggering and dry down timing across the domain. The different levels of steps within the irrigated simulations are a result of the input parameter datasets, as triggering and timing is dependent on these datasets The model distributions do not match the CRNP CDF, which instead shows a majority of soil moisture values that are wetter than the control simulation, but drier than the irrigated simulations and exhibit a smoother distribution. These CDFs suggest that the model, even with the irrigation algorithm turned on, is not able to accurately simulate the small-scale (i.e. field scale) heterogeneity in soil moisture values that is present in the CRNP data. The heterogeneity at this time and space scale results from the individual decisions made by farmers on and immediately preceding this date, and as such, is not captured by the strict soil moisture deficit based rules imposed by the irrigation algorithm, nor by the uniform land cover, soil type, and slowly varying irrigation fraction and GVF datasets at 1km resolution.

In contrast, the bulk temporal variability in soil moisture in both irrigated and non-irrigated areas during the growing season is simulated well by the model (Fig. 3.9). The temporal CDF shows that the model matches the COSMOS distribution more closely when the irrigation algorithm is turned on (Fig. 3.9a). Furthermore, when irrigated and non-irrigated areas are averaged separately, the irrigated (Control) simulations match the distribution of irrigated (non-irrigated) areas well (Fig. 3.9b). These results suggest that if this domain were one gridcell in a larger, coarser resolution domain (e.g. 15 km spatial resolution), the variation in the gridcell soil moisture (given here by the domain average) over the growing season would be representative of observations. That is, the heterogeneity and smaller scale processes resolved in the high-resolution domain, though unable to reproduce specific field-scale behavior, appropriately scale up to coarser resolution. At coarser time and space resolutions, the decisions made by individual farmers become less important, in favor of the larger scale features (e.g. timing of precipitation during the growing season), that influence and drive the collective behavior of human practices in this region.

3.5 Discussion

Although the exact response to irrigation physics is likely dependent on the LSM and irrigation scheme used, the results of this study are still applicable to irrigation modeling development as a whole. In particular, this study demonstrates the importance of supplying a land surface model with high-quality input datasets. Of primary importance are the datasets that control irrigation triggering (e.g., landcover, meteorological forcing, irrigated area), as the details of irrigation application are relevant only after irrigation is triggered in realistic locations and at the correct time during the season. Once reasonable timing and placement have been established, the datasets that regulate the amount of water applied (e.g., irrigation intensity, root depth, GVF) become important. These datasets may require a certain degree of customization, depending on the available information about irrigation practices and land use in the study area, to ensure an appropriate amount of water is applied.

The root systems of crops generally mirror the vegetative state above ground (i.e., GVF), and as such, the model represents root growth by scaling the maximum root depth by the GVF (Ozdogan et al. 2010) and applying a proportional amount of irrigation water. Although the crop type is uniform maize for the limited domain, as given by the UMD crop dataset, Franz et al. (2015) shows a mix of maize and soybeans in the study area. An additional run was completed in which a tuned crop type map was supplied to the model to distinguish between maize and soybean gridcells based on the land use map of Franz et al. (2015) and the maximum root depth was altered to be 1 m for maize and 1.2 meters for soybean. The results of this analysis showed very little differences between this simulation and the others, indicating that the model is quite insensitive to the maximum root depth change and that the scaling by GVF tends to be more important than small changes (up to 20% in this case) in maximum root depth. However, models that contain a more complex treatment of crops may have a greater dependency on crop root depth.

The method for determining the start and end of the growing season, based on the 40% annual range in climatological GVF, proved to be reliable for this study area and climate. However, in arid or semi-arid regions, the 40% threshold applied to a small annual range in GVF can result in a year round irrigation season that may not be representative of regional irrigation practices. Thus, where the annual range in GVF is small (e.g., southern California), more tailoring may be needed to ensure that irrigation occurs only during the local irrigation season.

This study shows model sensitivity to the irrigation intensity dataset, in terms of where and how much irrigation water is applied. Historically, the Global Map of Irrigated Areas (GMIA; Döll and Siebert, 1999) has been the most widely used irrigation dataset in irrigation modeling studies (Bonfils and Lobell, 2007; Boucher et al., 2004; Guimberteau et al. 2012; among many others) as it was the first reliable global irrigation map, making use of cartographic and FAO statistics. However, progress in satellite remote sensing and ease of access to required datasets will likely result in a growing number of options for irrigation intensity datasets in the coming years. As such, the results of this study, detailing the potential effects of choice of irrigation intensity dataset on irrigation amounts will likely become more relevant with the expansion in choices of irrigation-related datasets.

3.6 Conclusions

This study provided an assessment of the sprinkler irrigation physics and model sensitivity to irrigation intensity and GVF datasets in a LSM framework, and evaluated the results with novel point and gridded soil moisture observations. For all experiments, model results show that irrigation increases soil moisture and latent heat flux, and decreases sensible heat flux. Differences between experiments are small at the interannual scale, but become more apparent in analysis at seasonal and particularly diurnal time scales. The irrigation scheme uses GVF as a proxy for plant maturity and scales the amount of water applied accordingly to represent differences in irrigation scheduling based on growth stage. This behavior and the impacts of irrigation on soil moisture and fluxes are physically consistent with expectations of irrigation effects on the land surface.

The evaluation with CRNP observations revealed both limitations and strengths of the irrigation algorithm. The field-scale heterogeneity resulting from the individual actions of farmers is not captured by the model and the amount of irrigation applied by the model exceeds that applied at the two irrigated fields. However, the timing of irrigation during the growing season (i.e., late July to early August), which coincided with a stretch of limited rainfall, is simulated well by the scheme. Additionally, the smaller scale processes resolved in the small domain appropriately scale up to coarser time and space resolution, indicating the scheme could be used reliably at coarser resolution (e.g. 15 km) in this region. The model skill is due in large part to the accuracy of NLDAS-2 meteorological forcing, land cover, and irrigation intensity datasets, which are all critical to reproducing the seasonal timing and location of irrigation triggering. Overall, these results underscore the importance of supplying a LSM with high-quality datasets.

This study has also shown that CRNP distributed soil moisture data can be valuable in LSM and irrigation parameterization evaluation. The ability to compare the LSM output for the irrigated and control runs against soil moisture at irrigated and non-irrigated sites, as well as against a gridded soil moisture dataset, afforded a unique opportunity to evaluate the performance of the scheme in a way that would not have been possible without these data. The CRNP observations provide valuable information about the impact of irrigation on soil moisture, how it changes over time, and in the future could possibly be used to help identify where and when irrigation occurs. Irrigation timing information is particularly valuable at the scales of this study and larger, where the ability to obtain such information from each farmer is unrealistic. The USDA census of agriculture contains some of the most detailed information on the state of agriculture in the U.S., including estimates of irrigated acreage, irrigation method, and crop cultivated. However, the census occurs only once every five years and lacks irrigation timing information. CRNP soil moisture and in the future, high resolution soil moisture and evapotranspiration from satellites, could serve as a proxy to determine seasonal timing of irrigation as well as help identify irrigation acreage between census years.

The flexibility of the LIS framework, and in particular the ability for the user to choose the irrigation scheme, parameters, and model of choice, makes LIS a premiere framework for irrigation studies. However, the general conclusions of this study, as they pertain to irrigation scheme impacts and sensitivity to dataset changes, are applicable to irrigation modeling more broadly. The continued evaluation and improvement of irrigation parameterizations, as discussed here, is an important step towards better understanding human influences on the water cycle and the impacts of such activities in a changing climate.

3.7 Data availability

Fixed and mobile cosmic-ray neutron probe data is available in Franz et al. (2015) or by request from Trenton Franz.

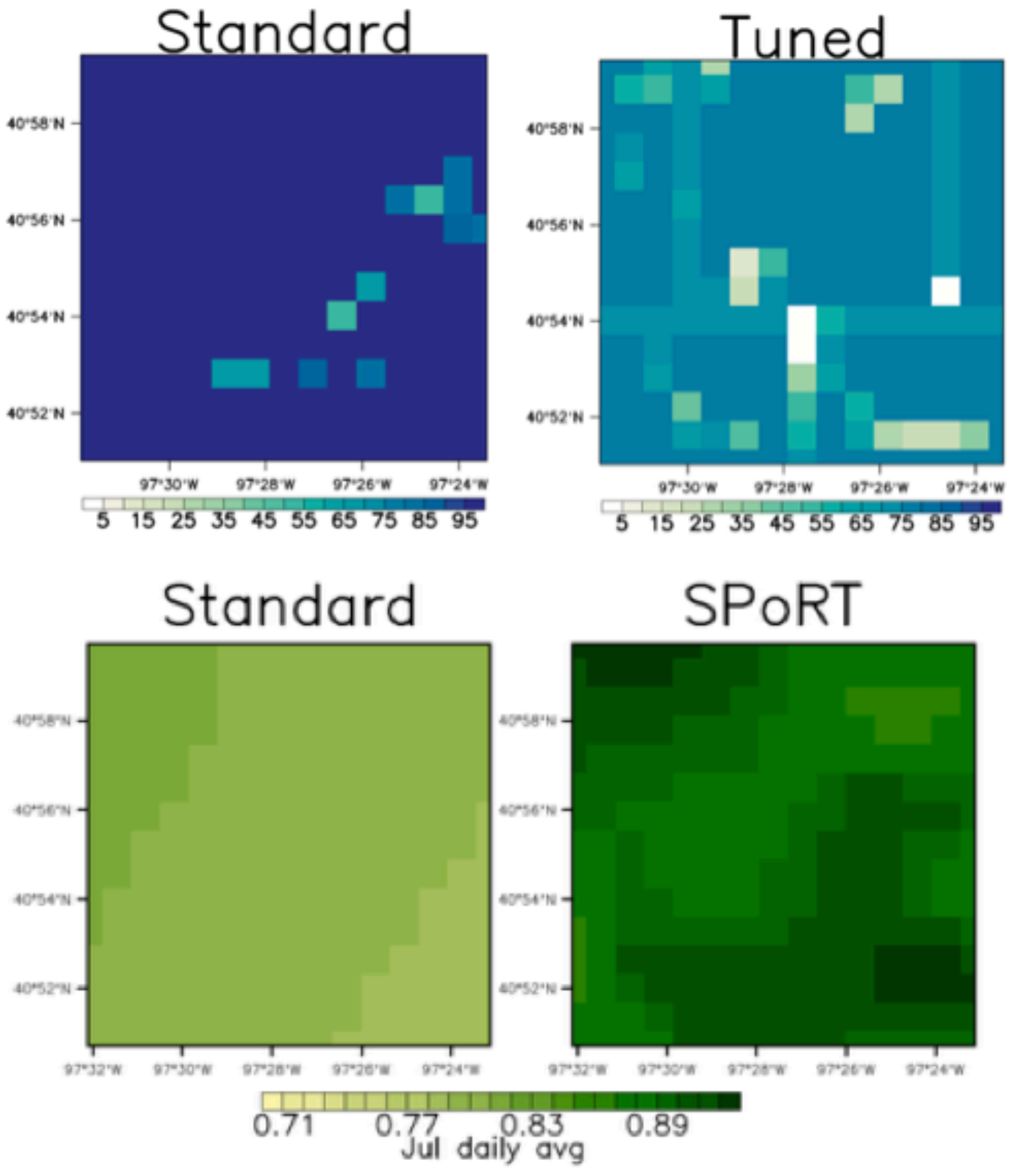

Figure 3.1 (Top) Comparison of the GRIPC irrigation intensity given by Salmon et al. (2015, left) used in the Standard and SPoRT simulations and the observationally tuned irrigation intensity (right) used in the Tuned simulation. (Bottom) Average July 2012 greenness vegetation fraction given by NCEP climatology (left) used in the Standard and Tuned simulations and (right) SPoRT real-time dataset used in the SPoRT run.

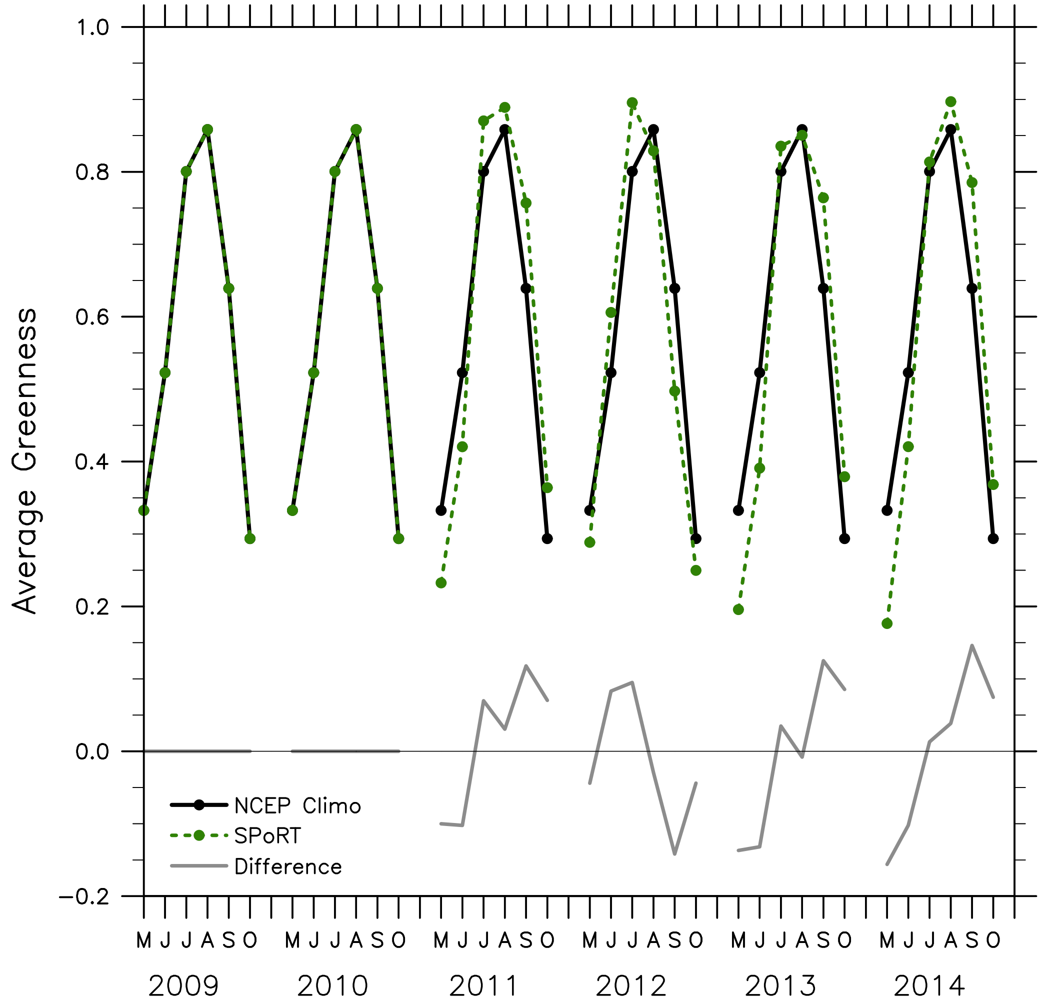

Figure 3.2 Domain and monthly averaged GVF from the NCEP climatological GVF dataset, used in the Standard run, the SPoRT GVF dataset used in the SPoRT run, and the difference between the two (SPoRT – Climatology).

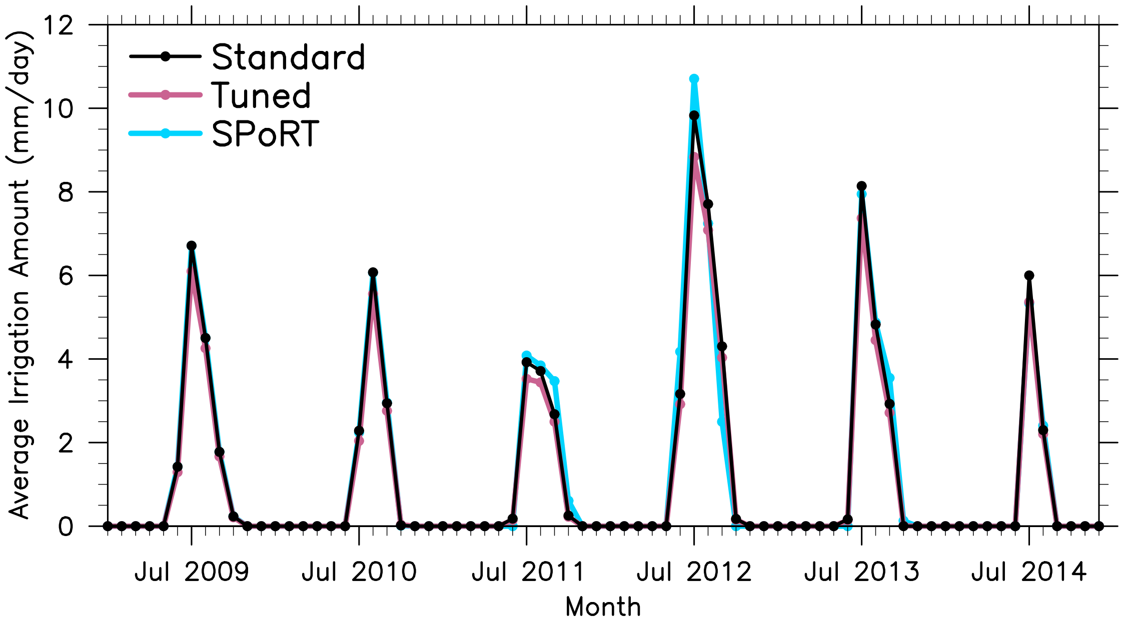

Figure 3.3 Domain and monthly averaged irrigation amount for each irrigation simulation.

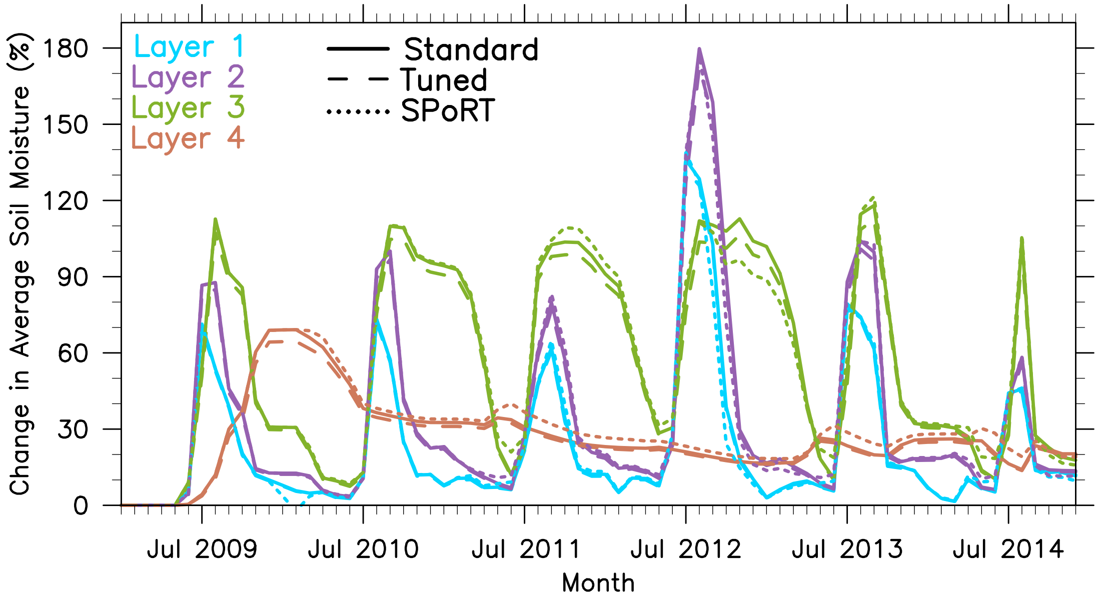

Figure 3.4 Change from control (IRR - CTRL) in soil moisture for each experiment (line style) and each layer (line color). Layer designations are the Noah LSM default layers Layer 1 (top layer) is 0 to 10 cm depth, layer 2 is 10 to 40 cm (delta Z = 30cm), layer 3 is 40 cm to 1 m (delta Z = 60 cm) and layer 4 is 1 m to 2 m (100 cm depth).

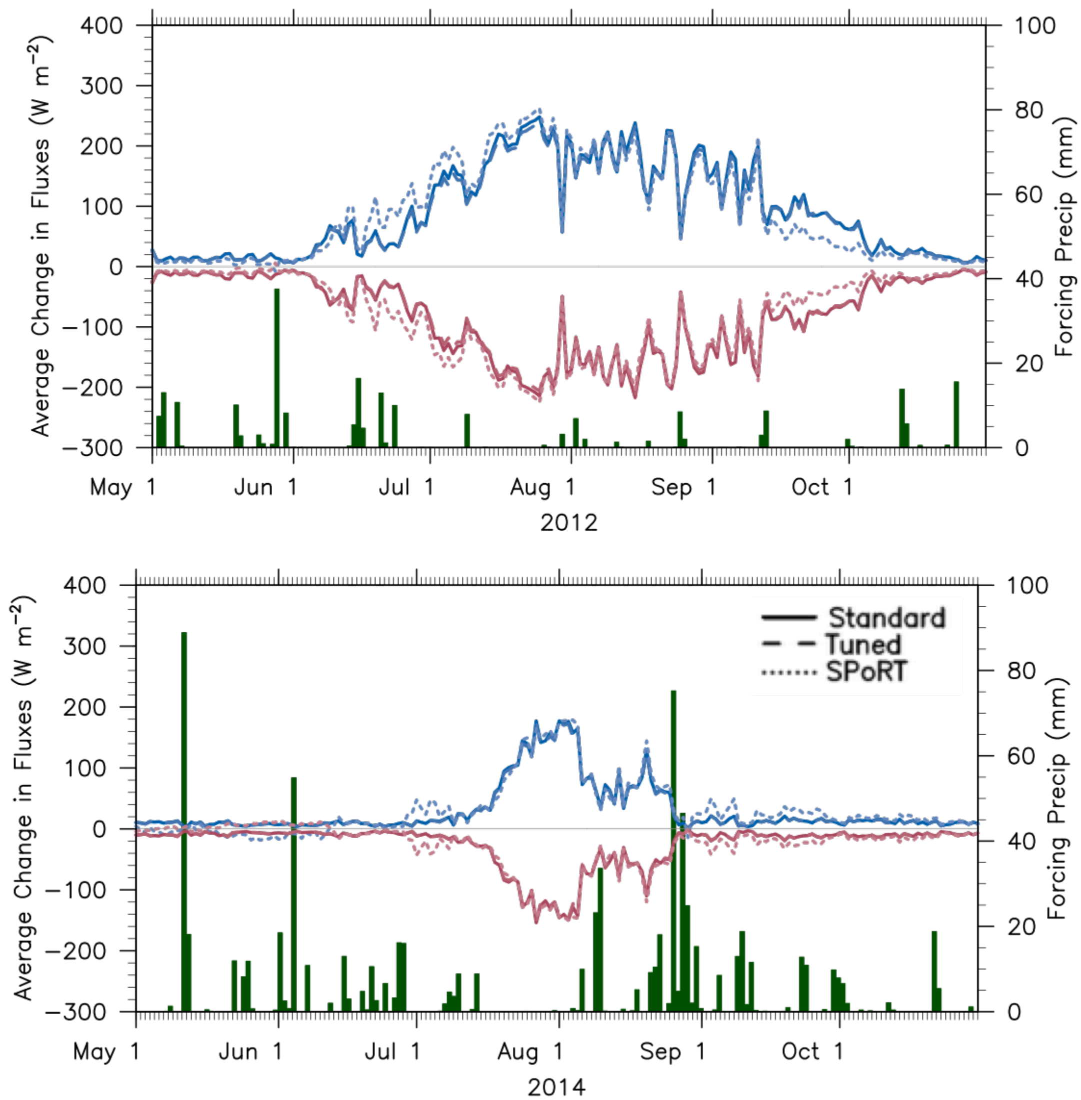

Figure 3.5 May to September 2012 (top) and 2014 (bottom) domain average daily change from control (IRR-CTRL) in latent (blue) and sensible (red) heat fluxes for each irrigation simulation (left axis) and domain average daily accumulated precipitation from the NLDAS2 forcing data (right axis).

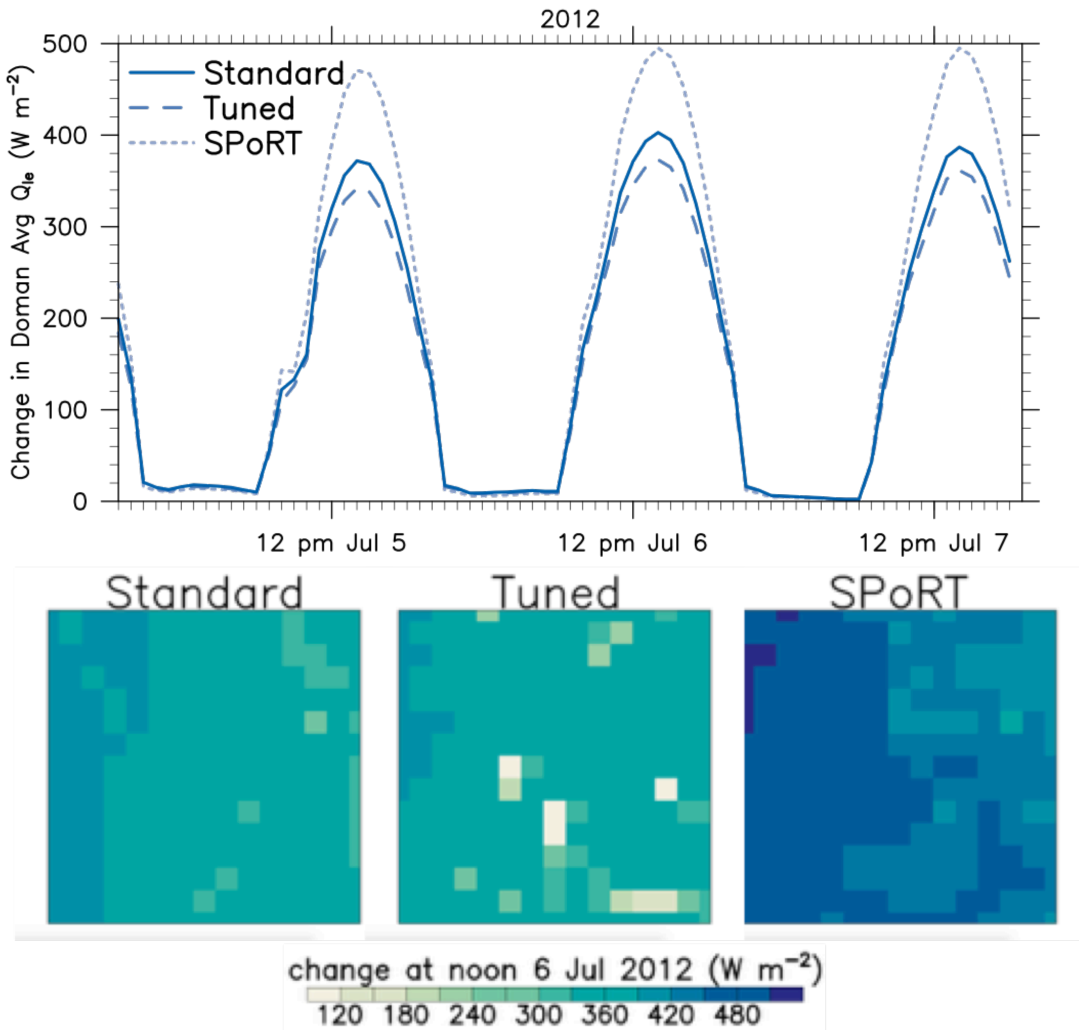

Figure 3.6 Domain average change in latent heat flux for three diurnal cycles in July 2012 (top). Change in latent heat flux (IRR-CTRL) at noon on July 6, 2012 for each irrigation simulation (bottom).

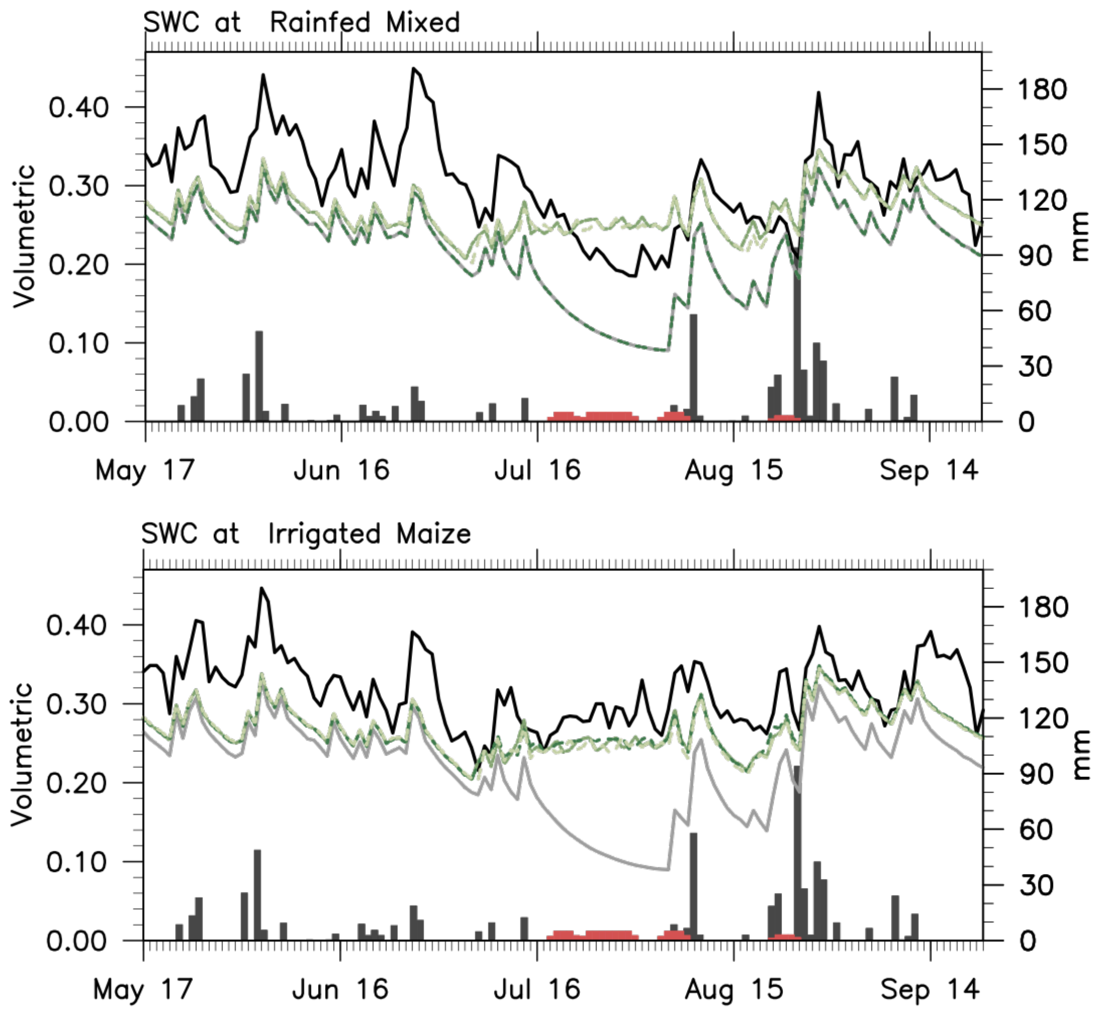

Figure 3.7 Volumetric soil water content at the rainfed (top) and irrigated maize (bottom) sites (left axis). The black solid line shows observations from the CRNP probe, the gray and green lines show the LIS control and irrigation simulations, respectively. Dark gray bars show accumulated daily precipitation from the Automated Daily Weather Network in York, Nebraska and pink bars show the accumulated irrigation amount at the irrigated maize and soybean sites (right axis).

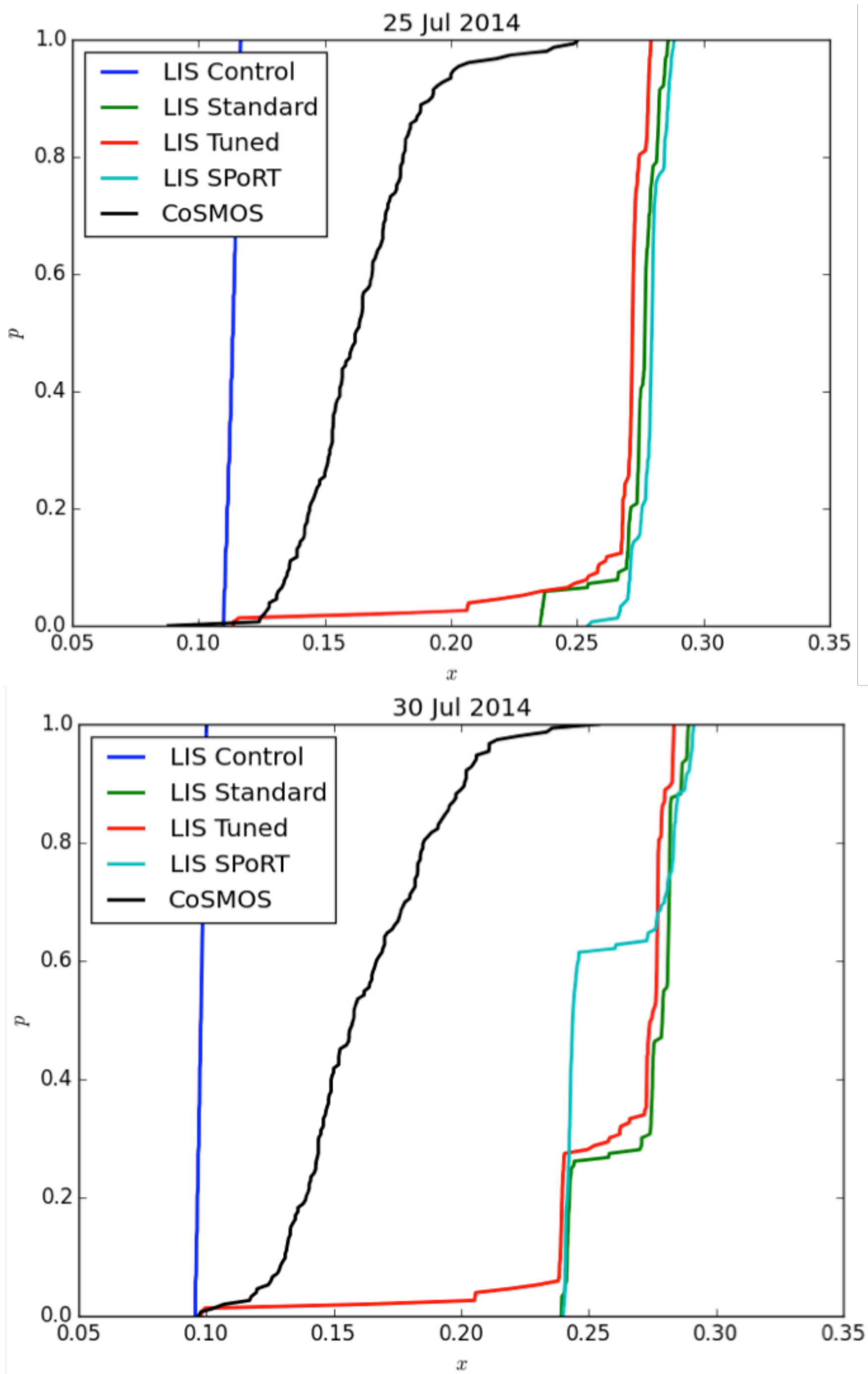

Figure 3.8 Spatial CDF for 25 July 2014 (top) and 30 Jul 2014 (bottom), two dates when irrigation was applied at the irrigated maize and soybean sites in practice and in the model simulations.

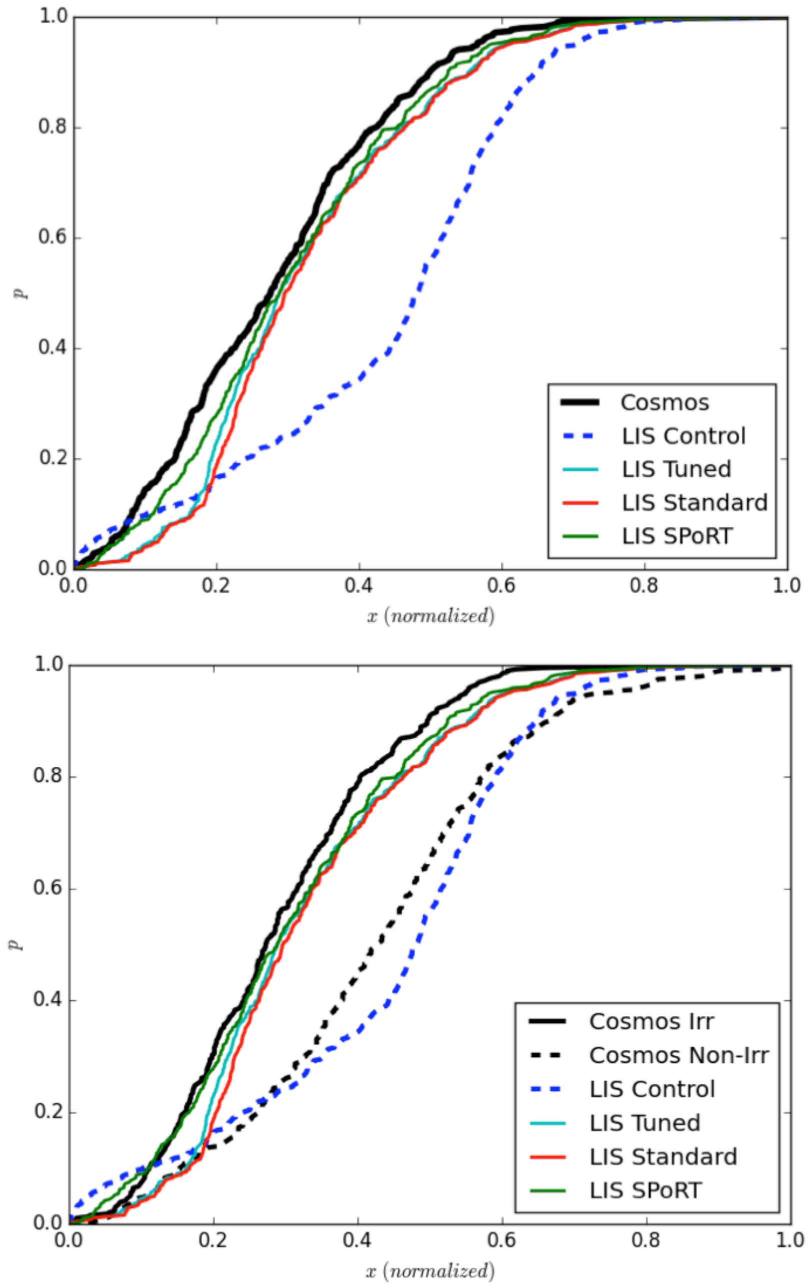

Figure 3.9 Temporal CDF of normalized domain averaged (top) and irrigated/non-irrigated spatial average (bottom) SWC values from May 5 to Sept 16 from the COSMOS observational product (black) and the model simulations (colors).

Chapter 4

ASSESSMENT OF IRRIGATION AND WIND TURBINE WAKE EFFECTS ON LAND-ATMOSPHERE INTERACTIONS IN A DESERT REGIME

4.1 Introduction

Irrigation has been shown to modify local hydrology and regional climate through a repartitioning of water among the surface, soil, and atmosphere with potential to drastically change the terrestrial energy budget in agricultural areas during the growing season(Qian et al. 2013). Vegetation cover and soil moisture primarily control water and energy fluxes from the surface into the planetary boundary layer (PBL), so accurate representation of the land surface characteristics is key to determining and predicting atmospheric conditions.

In the United States, the most commonly irrigated regions are often also areas that boast great wind power resource potential (NREL, 2016). The small spatial footprint of turbine design and installation allows farmers to grow crops close to the base of the turbines and the supplemental income gained from leasing the land to a utility company can provide an economic safety net in years of low crop yield (UCS, 2016). Wind turbines, however, also have the potential to impact local land-atmosphere (L-A) interactions within and downwind of the farm. The extraction of kinetic energy by the turbine to produce electricity creates a wake in which wind speed is reduced and turbulent kinetic energy (TKE) is increased (Baidya Roy et al. 2004). As few observations exist within operational wind farms, previous studies have used large eddy simulations (LES; Calaf et al. 2011; Lu and Porté-Agel 2011), mesoscale models (Fitch et al. 2013; Cervarich et al. 2013) and global models (Wang and Prinn 2009)to explore the persistence of wind turbine wakes and their impact on near surface vertical mixing, surface fluxes, and temperature. While several mesoscale modeling studies found enhanced vertical mixing near the surface (Baidya Roy and Traiteur 2010), LES studies have shown reduced vertical mixing near the ground (Calaf et al. 2010; Xie and Archer 2015), highlighting a need for further study of turbine impacts on microclimate.

Despite the fact that turbines are often located in agriculturally productive, potentially irrigated farms, the combined influence of turbines and irrigation has not been investigated. As the realization of climate change continues to spur renewable energy initiatives, it is likely that turbines will further encroach on agricultural areas. The sign and magnitude of turbine impacts on microclimate is particularly important in agriculturally productive farms, as fluxes of heat, moisture, and carbon dioxide are critical for crop development and yield (Rajewski et al. 2013). As such, it is vital to quantify the impact of turbines on the transfer of energy and moisture, especially in irrigated regions where artificially increased soil moisture already presents complex L-A interactions.

The main objective of this study is to better understand the impacts of irrigation and turbines, individually and in concert, on surface heat and moisture fluxes and near surface meteorology. This goal is achieved via a series of high resolution model simulations using newly developed physics modules that explicitly represent irrigation and wind turbine wake effects. Section 2 describes relevant previous studies related to irrigation and wind turbine wake effects with an emphasis on turbine impacts in agricultural regions and the potential mechanisms by which turbines and irrigation may interact. Section 3 details the model set up and experimental design, and Section 4 presents an analysis of the simulation results, first in the context of irrigation and turbines individually, and then the combined impacts. A discussion of the limitations of the study and the role of the results in the context of the literature base is included in Section 5. Finally, conclusions are presented in Section 6.

4.2 Background

4.2.1 Irrigation

Irrigation makes it possible to grow the food necessary to feed the world's population, but also results in alterations to the energy and water cycles. Wet soil resulting from irrigation increases the potential for evaporation (latent heat), thus repartitioning the surface energy balance. Flux changes due to irrigation have been detected at a range of spatial scales and increases in latent heat can reach up to 100 W m-2 locally (Ozdogan et al. 2010), 9 W m-2 regionally (Douglas et al. 2006), or 0.03 to 0.1 W m-2 globally (Boucher et al. 2004). These changes are met with a complimentary decrease in sensible heat flux and a reduction in daytime surface temperature. Cooling effects due to irrigation have been well documented and can have far-reaching implications when discussed in the context of global climate change. Past expansion of irrigation coincides with greenhouse gas increases and therefore could potentially be masking the full warming signal due to greenhouse gas increases (Kueppers et al. 2007; Lobell et al. 2009; Cook et al. 2010).

For large areas of irrigated acreage, modifications to the surface energy balance can be significant enough to impact local and regional circulations and precipitation patterns. In the summer months, decreases in surface temperature and increases in near surface humidity result in a reduction in PBL height of up to 1500 m and a lowering of the lifting condensation level (cloud base) (Kueppers et al. 2007; Qian et al. 2013). These alterations to the PBL can affect atmospheric stability and influence precipitation patterns and intensity (Alter et al. 2015a; Douglas et al. 2009; DeAngelis et al. 2010). Irrigation has been shown to result in a net water deficit as the loss due to increased evapotranspiration outweighs that of the return due to the positive feedback on precipitation, and most recycled precipitation falls away from the source (Harding and Snyder 2012; Wei et al. 2013).

4.2.2 Wind Turbines

Global models typical represent the kinetic energy extraction of turbines through increased aerodynamic surface roughness. Results of these simulations have shown up to a 1°C warming (Wang and Prinn 2009), changes in global circulation patterns (Keith et al. 2004; Kirk-Davidoff and Keith 2008), and even modifications to the development and path of North Atlantic cycles (Barrie and Kirk-Davidoff 2010). However, parameterizations that represent turbines as an elevated momentum sink and source TKE, as opposed to surface roughness approximation, generally produce results more consistent with wind tunnel experiments (Fitch et al. 2013).

Regional studies using the elevated source/sink parameterization have most often found increased vertical mixing near the surface due to the expansion of the turbine wakes (Fitch et al. 2012). A nighttime surface warming due to the mixing of warming air down to the ground has been show in mesoscale models (Baidya Roy et al. 2004; Cervarich et al. 2013) and is supported by remote sensing observations (Zhou et al. 2012; Slawsky et al . 2015). In contrast, fine-scale simulations show reduced vertical mixing near the ground and weaker surface fluxes in stable conditions (Calaf et al. 2010, 2011; Lu and Porté-Agel 2011; Xie and Archer 2015). Literature also varies on the turbine impacts on daytime temperatures. Results range from cooling (Baidya Roy and Traiteur 2010), to warming (Walsh-Thomas et al. 2012), to no significant temperature impact (Rajewski et al. 2013; Cervarich et al. 2013; Slawsky et al. 2015). The range of outcomes may be due in part to the variability of background atmospheric stability conditions, with more instability leading to a greater degree of cooling (Baidya Roy 2011).

As a result of the potential for turbines to impact surface energy and moisture fluxes and the frequent co-location of wind turbines and agriculturally productive sites, a few recent studies have investigated the interaction between wind turbines and agriculture. The Crop Wind Energy Experiment (CWEX; Rajewski et al. 2013) field campaign took place in Iowa in the summers of 2011 and 2012 in an effort to determine whether turbines can create measurable changes to the microclimate over crops and to investigate the potential implications of those changes, if they exist, on crop growth and yield potential. Up to six flux towers and two Windcube lidar instruments were deployed in cornfields near two lines of 1.8 MW wind turbines.

Results from two daytime case studies, one during a southwesterly flow event and the other during a frontal passage, indicate that turbines modify fluxes of heat and carbon dioxide, both important quantities for crop development. In each case, daytime average upward latent and sensible heat fluxes and downward CO_2 flux at 4.5 m were increased at a downwind tower as compared to an upwind flux tower. The CWEX data also reveal that fluxes of water can be enhanced by a factor of five in the lee of the turbines when wind flow is perpendicular to the row of turbines during the day, but impacts are negligible for other wind directions (Rajewski et al. 2014). These observational results partially support those of the modeling studies (Baidya Roy et al. 2004; Baidya Roy and Traiteur 2010) finding enhanced vertical mixing near the ground during stable conditions.

CWEX indicated that turbines can effect agriculture, but the reverse may be true as well; that is, crop management also may also impact wind energy. Using the WRF model and the Fitch turbine parameterization, Vanderwende and Lundquist (2016) explored the impact of crop height on wind energy production. The reduced surface drag of soybeans (e.g. short crop) as compared to maize (i.e., taller and greater surface roughness) reduced rotor-layer wind shear and increased hub-height wind speed by a statistically significant amount. The crop type switch resulted in 14% increase in wind farm energy output and demonstrates the importance of taking into account agricultural land management practices in the discussion of wind energy topics.

4.2.3 Turbines and Irrigation

Despite the fact that efforts to determine the effects of wind turbines on agriculture have been gaining interest, and that in some regions agricultural production is virtually inseparable from irrigation (e.g., used on 80% of farms cultivating vegetables, orchards, or berries; NASS, 2012), the combined impacts of irrigation and turbines on microclimate have not been addressed. In cases where turbines and irrigation result in the same type of atmospheric impacts, the combined effect could amplify the influence of what would be given individually. For example, turbines and irrigation individually can reduce daytime temperature, making it possible that the combined impact is an even greater cooling in daytime temperature. Even more consequentially, irrigation and turbines individually have been linked to drought. Pei et al. (2016) showed that irrigation may have worsened the 2012 U.S. High Plains drought and according to Abbasi et al. (2016), an unprecedented drought in Mongolia developed faster in areas with operational wind turbines.

However, the impacts of irrigation on the atmosphere and the sensitivity of turbine wake effects to atmospheric properties makes it likely that non-linear feedbacks due to the interaction of turbine wakes and irrigation exist. For example, irrigation can increase atmospheric stability (Alter et al. 2015b), which may increase the longevity of turbine wake effects, change the sign of surface flux and temperature changes, and alter the amount of power produced by turbines. Irrigation has also been shown to induce or alter mesoscale circulations (de Vrese et al. 2016), thereby impacting wind speed and direction, and potentially power production. Similarly, a turbine-induced increase in moisture flux away from the surface (e.g. near surface drying; Rajewski et al. 2014) may increase the irrigation requirement. The interactions and potential feedbacks between irrigation and turbines make it necessary to address these issues in a coupled modeling environment that includes model physics that explicitly represent both irrigation and wind turbines, as is done in this study for the first time.

4.3 Methods

4.3.1 Model Configuration and Study Area

This study uses NASA's Land Information System (LIS; Kumar et al. 2006) version 7.1 coupled to NASA's Unified Weather Research and Forecasting (NU-WRF; Peters-Lidard et al., 2015) model, version 8. NU-WRF contains all features of

NCAR's standard WRF model, but includes additional physics options, the ability to run coupled simulations with LIS, and make it possible to spinup the land surface through offline LIS simulations on the same grid used by WRF. The Fitch wind farm parameterization (WFP; Fitch et al. 2012) and WRF model together have shown skill in reproducing turbine-induced power deficits at the scale of wind farms and has been identified as an appropriate framework to investigate downstream impacts of wind farms (Fitch et al. 2013; Jimenez et al. 2015). In addition, LIS features three irrigation parameterizations that can be used offline and in coupled simulations with WRF. The sprinkler irrigation scheme, first tested and compared to other irrigation in Lawston et al. (2015) and evaluated in Lawston et al. (2016) is used in this study. These features of the LIS and NU-WRF modeling systems, as they relate to simulating irrigation and turbines, make this system the ideal framework for investigating the combined impacts of irrigation and turbines.

The offline LIS and coupled LIS-WRF simulations use a nested domain configuration of 9, 3, and 1 km spatial resolution (Figure 4.1) centered on the border of Oregon and Washington in the Pacific Northwest United States. Each running domain contains 249 x 315 grid points and uses the MODIS International Geosphere Biosphere Program (IGBP) landcover dataset for the land use classification information and NCEP climatological greenness. The atmospheric boundary and initial conditions are provided by the North American Mesoscale forecast system (NAM) at 6-hourly intervals.

The Fitch scheme represents turbines by introducing an elevated momentum sink and modifying the turbulent kinetic energy (TKE) to include additional TKE produced by wind turbines (Fitch et al. 2012). The Mellor-Yamada after Nakanishi-

Niino (MYNN; Nakanishi and Niino 2006) 2.5 closure PBL scheme was used, as it is a requirement for the Fitch turbine parameterization. The latitude and longitude of each turbine in the study area was obtained from the USGS Windfarm product (available via: eerscmap.usgs.gov/windfarm), totaling 2735 turbines. The turbines are placed only in the innermost domain using the actual latitude and longitude (Figure 4.2), resulting in the placement of multiple turbines per gridcell in some cases. The characteristics of the turbines are defined using the WRF default wind turbine specifications and include a hub height of 75 m, 85 m rotor diameter, 0.130 standing thrust coefficient, and 2.0 MW nominal power. The LIS-WRF simulations use and 42 vertical levels.

The sprinkler irrigation parameterization, described in detail in Lawston et al. (2016) and Ozdogan et al. (2010), applies irrigation water as precipitation in the morning when the soil moisture availability drops below a user defined threshold. In this study, we use a triggering threshold of 50% of field capacity. Several other thresholds were tested with 50% of field capacity giving a reasonable seasonal cycle of irrigation application. The Global Rainfed and Irrigation Paddy Cropland (GRIPC; Salmon et al. 2015) irrigation intensity dataset is used to determine the location of irrigation triggering and to scale the amount of water applied by the scheme.

This study area was chosen as it features both sweeping areas of irrigation and large wind farms (Figure 4.2). There are areas of semi-isolated irrigation in the north-central portion of the domain (along 119°W), as well as irrigated areas downwind of turbines (along the Washington-Oregon border). There are 76 gridcells that are both irrigated and contain at least one turbine. Furthermore, the direct impacts of irrigation have been shown to be greatest in dry antecedent soil moisture conditions, suggesting irrigation impacts will be strong in this semi-arid climate. This region also contains several observational points, which will be used in a future study to validate the model simulations.

4.3.2 Experimental Design

The Noah land surface model, version 3.3 (Chen et al. 2007) was run offline (uncoupled) within the LIS framework for three years to allow for the spinup of land surface states and fluxes. The offline runs were forced with meteorological data from the National Land Data Assimilation System – Phase 2 (NLDAS-2, Xia et al. 2012) and Global Data Assimilation System (GDAS) forcing for international areas in the outer domains. Two offline simulations were completed; a control simulation (no irrigation) and an irrigated spinup. These simulations were analyzed to confirm proper functioning of the irrigation scheme and are used to provide the initial conditions for the coupled LIS-WRF runs.

Four categories of LIS-WRF coupled runs are initialized from the offline control and irrigated simulations. The control spinup was used to initialize a coupled control run (no irrigation, no turbines; hereafter referred to CTRL) and a turbine run (no irrigation, turbines; WIND). The irrigated spinup was used to initialize a simulation without turbines (irrigation, no turbines; IRR) and one with turbines (irrigation, turbines; WIND_IRR). This matrix of simulations allows for analysis of the individual impacts of irrigation and turbines in this region (IRR-CTRL and WIND-CTRL, respectively) as well as the combined impacts (WIND_IRR – CTRL) as simulated by the modeling system.

Three, two-day periods were chosen from the month of July 2015 as the case studies for the coupled LIS-WRF runs. The selected case studies, 1-3 July, 16-18 July, and 23-25 July, (hereafter referred to as case 1, 2, 3, respectively) are rain-free days, span the month of July, and represent a range of soil moisture perturbations, as indicated by analysis of the irrigated and control spinup simulations (Figure 4.3). Case 1 follows soon after a rain event, and as a result had the smallest soil moisture perturbation at initialization, around 0.04 to 0.1 m^3 m^{-3} (i.e., ~30%) increase in top layer soil moisture. In contrast, a persistent rain-free period in mid-July resulted in consistent irrigation application throughout the month, increasing top layer soil moisture by about 0.14 and 0.17 m^3 m^{-3} (i.e. ~55% and 70%) in cases 2 and 3, respectively.

The LIS-WRF simulations are run for a total of two days and 6 hours. As the impacts of both irrigation and turbines have been shown to depend on atmospheric conditions (i.e. radiation, stability), this study focuses on the impacts of each of these perturbations throughout the diurnal cycle. The first six hours are considered a period of atmospheric spinup and are ignored, and the remaining 48 hours of each simulation are analyzed. This results in two diurnal cycles per case, for a total of 6 diurnal cycles. The impact of irrigation on surface latent and sensible heat fluxes (hereafter referred to as Qle and Qh, respectively), near surface temperature (T2), and humidity (Q2) is analyzed first, followed by the turbine impacts on these quantities, and lastly the combined impacts.

4.4 Results

4.4.1 Irrigation Impacts

Figure 4.4 shows the change from control (IRR – CTRL) in Qle and Qh over irrigated gridcells, plotted in the lighter blue and red colors, respectively, for all six daily cycles from the three case. The darker shades of red and blue represents the case average. The wet soil resulting from irrigation repartitions the surface Qle and Qh. Latent heat flux increases by 70 to 115 W m^{-2} at midday, while Qh is reduced by approximately the same amount. These plots confirm that in this moisture-limited regime, the addition of irrigation water has a large and immediate impact on evaporation. Case 3 (case 1), which exhibited the greatest (smallest) increase in soil moisture at initialization, also features the greatest (smallest) increase in Qle and decrease in Qh.

Figure 4.5 shows the change from control in near surface (2 m) humidity and temperature over the irrigated gridcells for each diurnal cycle and the case average. Irrigation supplies more moisture, resulting in increased humidity at all times of day and in all cases. Overnight, the humidity increase is steady, with a small uptick soon after sunrise, possibly due to turbulent eddies mixing the stable humid area. Another peak in specific humidity occurs soon after sunset in 4 of the 6 diurnal cycles. The temperature is cooler over irrigated areas by up to 0.8 K during the day as a result of increased evaporation and changes to soil properties. Wet soil has a higher heat capacity and thermal conductivity than dry soil, making it slower to heat up during the day, contributing to the reduced daytime temperature. At night, the temperature is warmer by an average of 0.2 to 1.2 K over irrigated areas as the heat stored in the wet soil during the day is slowly released overnight. Figure 4.8 shows the contrasts in day and nighttime temperature differences spatially for case 3. Locally temperature can increase by up to 3-4 K at night and decrease by a similar amount during the day. Irrigation cooled air is mixed and advected a short distance (~5-10 km depending on atmospheric conditions; not shown).

4.4.2 Turbine Impacts

Figure 4.7 shows the average latent and sensible heat fluxes in the CTRL simulation as well as the difference from CTRL in fluxes when turbines are included (WIND – CTRL) for each diurnal cycle and the case average. These plots represent the spatial average of gridcells containing at least one turbine. The CTRL fluxes show that in this semi-arid region, limited moisture keeps latent heat fluxes small, while the sensible heat fluxes are large, reaching an average of 500 W m^{-2} at midday (Fig 4.7a). During the day, a negative difference in Qh between WIND and CTRL indicates weaker fluxes in the turbine simulation, as Qh is positive in the daytime. (Fig 4.7b). At night, when Qh is negative, fluxes are smaller again in the turbine simulation, resulting in a positive Qh difference. Thus, these results indicate that the inclusion of turbines in the simulation weakens surface sensible heat fluxes within the farm. The turbine impacts to latent heat flux within the farm are negligible.

The magnitude of the Qh changes are small (4 to 5 W m^{-2}) but should be considered in the context of the proportion of the total Qh throughout the diurnal cycle. During the day, when Qh is great (~ 500 W m-2), the reduction due to turbines in the latent heat flux is negligible. However, at night when Qh is small (~ 40 W m^{-2}), the percent change due to turbines can reach up to 12%. The proportional difference in fluxes is reflected in the near surface temperature changes, shown in 4.8. During the day, the negligible change in Qh results in no substantial temperature change. However, at night the weakened Qh due to turbines results in a cooling at 2 m. These results are the first to suggest cooling at night due to turbines in a mesoscale modeling environment. No substantial changes to Q2 are shown in in the wind farm area as a result of the turbines, likely due to the fact that there is limited moisture available to perturb.

4.4.3 Combined Impacts

The combined impacts to T2 and Q2 resulting from the WIND_IRR simulation are assessed and compared against an approximation of the impacts given by the linear sum of the individual turbine and irrigation impacts. Figure 4.9a shows the difference from control in T2 over all irrigated and turbine gridcells as given by the WIND_IRR simulation. The relative impacts of irrigation on T2 are greater than those due to turbines and as a result the diurnal changes in T2 more closely resemble those seen over irrigated areas (Fig. 4.5b). Although turbines, when analyzed independently of irrigation, resulted in a small nighttime cooling, that impact is swamped by the larger contribution of nighttime warming due to irrigation (e.g. ~0.4 K average). Figure 4.9b shows the difference between the WIND_IRR impacts to T2 (WIND_IRR – CTRL) and the linear sum of the WIND and IRR impacts (WIND-CTRL and IRR –CTRL, respectively). The comparison of these two quantities gives and indication of the nonlinear impacts revealed in the WIND_IRR simulation that are not captured by the linear sum approximation. The difference, in this case, is close to zero and varies little throughout the day, indicating that the nonlinear impacts on temperature are small.

The WIND_IRR difference from control in Q2, shown in Figure 4.10a, shows a consistent increase, around 0.5 g kg^{-1}, and also resembles the IRR impacts more closely than the turbine impacts, due to the addition of moisture in the irrigated run. Although turbines showed very little impact on Q2 independently (Fig 4.8b), the combined impact of irrigation and turbines results in a greater increase in Q2 than with irrigation alone and greater than that estimated by the linear sum of the two perturbations (Fig 4.10b). These results imply that the weaker surface sensible heat fluxes induced by the turbines may reduce drying near the surface, resulting in greater values of Q2 in the combined run.

To date, no mesoscale modeling studies of turbine impacts have included irrigation, and as such, we assess the effects of the inclusion of irrigation on the turbine runs by comparing the WIND_IRR and WIND simulations. Figure 4.11 shows the difference (WIND_IRR – WIND) in Qh (x-axis) compared with the difference in power output (y-axis). The color of each dot denotes the hour in local time of each data point. These results show that during the day, irrigation reduces sensible heat flux is to an even greater degree than would have otherwise occurred in the turbine simulation only. The largest reductions occur at the midday, when irrigation diverts radiation that would have been used for Qh into Qle. This figure also indicates that there is small reduction in daytime power production by the turbines when irrigation is included.

4.5 Discussion

This is the first mesoscale modeling study to show a turbine-induced reduction of surface sensible heat fluxes and nighttime cooling. However, single and infinite wind farms in large eddy simulations (LES) have shown reduced vertical mixing at the surface and weaker surface fluxes (Lu and Porté-Agel 2011; Xie and Archer 2015; Calaf et al. 2010, 2011). Using the same WFP used here in an idealized setting in WRF, Fitch et al. (2013) found warming in nighttime T2 and that turbines strengthened nighttime (negative) Qh. However, they noted that their results could have been impacted by the prescribed skin temperature, and therefore, represented an upper bound on the nighttime warming. They suggest that feedbacks impacting surface skin temperature could reduce the warming and expressed a need for future studies with fully coupled models to investigate this and other feedbacks, as done here. In addition, the characteristics of the turbines (i.e. thrust and power coefficient) needed for the WFP are not publicly available for manufactured turbines and as such, this study used the default WRF settings, which may impact the model response (Fitch 2016).

The small sample size used in this study (i.e., three cases and six diurnal cycles) precludes broad conclusions about combined impacts of turbines and irrigation at other times of the year or in different climate regimes. However, the impacts of each case are generally of consistent sign, despite spanning the month of July and a range of soil moisture perturbations. As such, these results are likely applicable for most calm conditions in mid-summer in this study area.

4.6 Conclusions

This study used a high-resolution mesoscale modeling environment with parameterizations for irrigation and turbines to assess the individual and combined impacts of each perturbation in a semi-arid region. Results show that irrigation repartitions surface sensible and latent heat fluxes, reduces daytime temperatures and increases temperatures at night. Turbines weaken surface sensible heat fluxes minimally during the day but enough at nighttime to slightly reduce near surface temperature. The simulations that include both turbines and irrigation show that wind power production is slightly reduced when irrigation is included and irrigation contributes to a greater reduction in daytime surface sensible heat fluxes than would be realized with only turbines. The linear sum of the turbine and irrigation impacts can be used to approximate the combined impact of irrigation and turbines on temperature but doesn't perform as well for humidity, suggesting that non-linear processes play a stronger role in near surface humidity impacts in this typically moisture-limited regime.

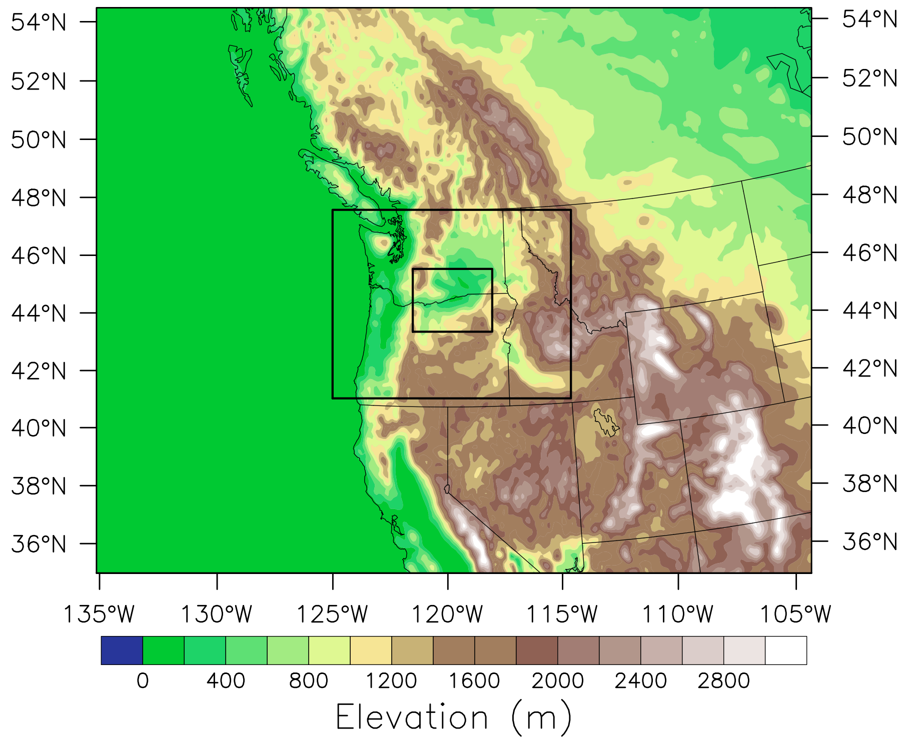

Figure 4.1 The nested domain configuration for the LIS-WRF simulation. Each domain contains 249 x 315 grid points. The spatial resolution of each nest is 9 km, 3 km, and 1 km, for the outermost, middle, and innermost domains, respectively.

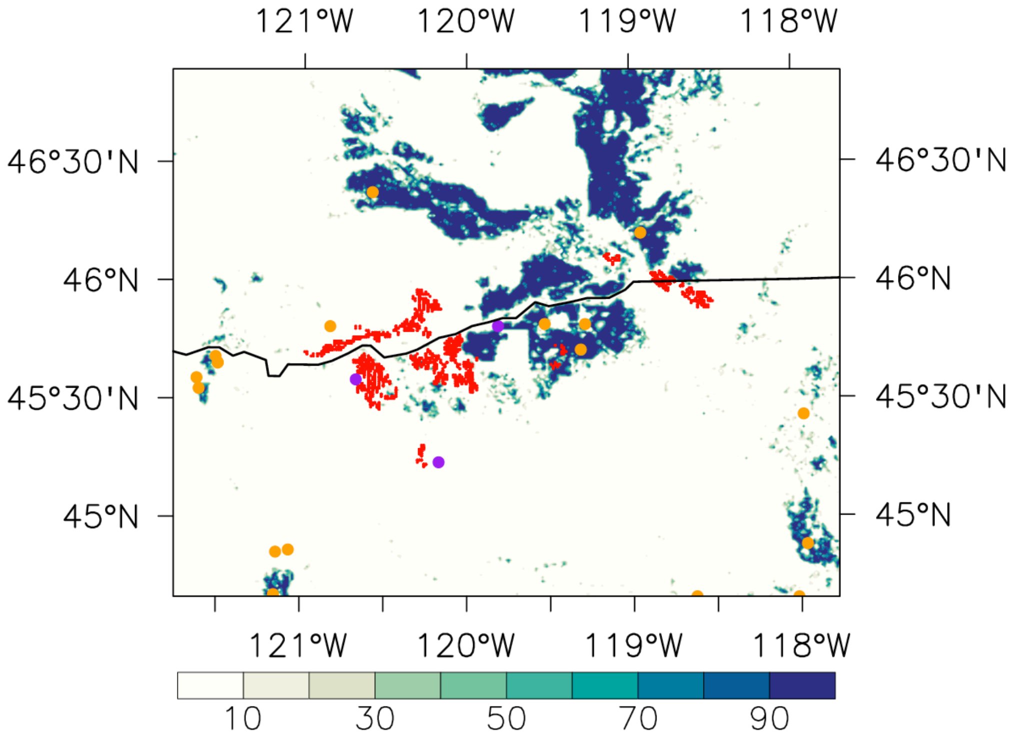

Figure 4.2 Locations of individual turbines (red) overlaid on the irrigation intensity map (shades of blue) in the innermost (1 km resolution) domain. The locations of surface based temperature (orange) and wind profiling (purple) instruments are also noted and will be used in future studies to validate the model results.

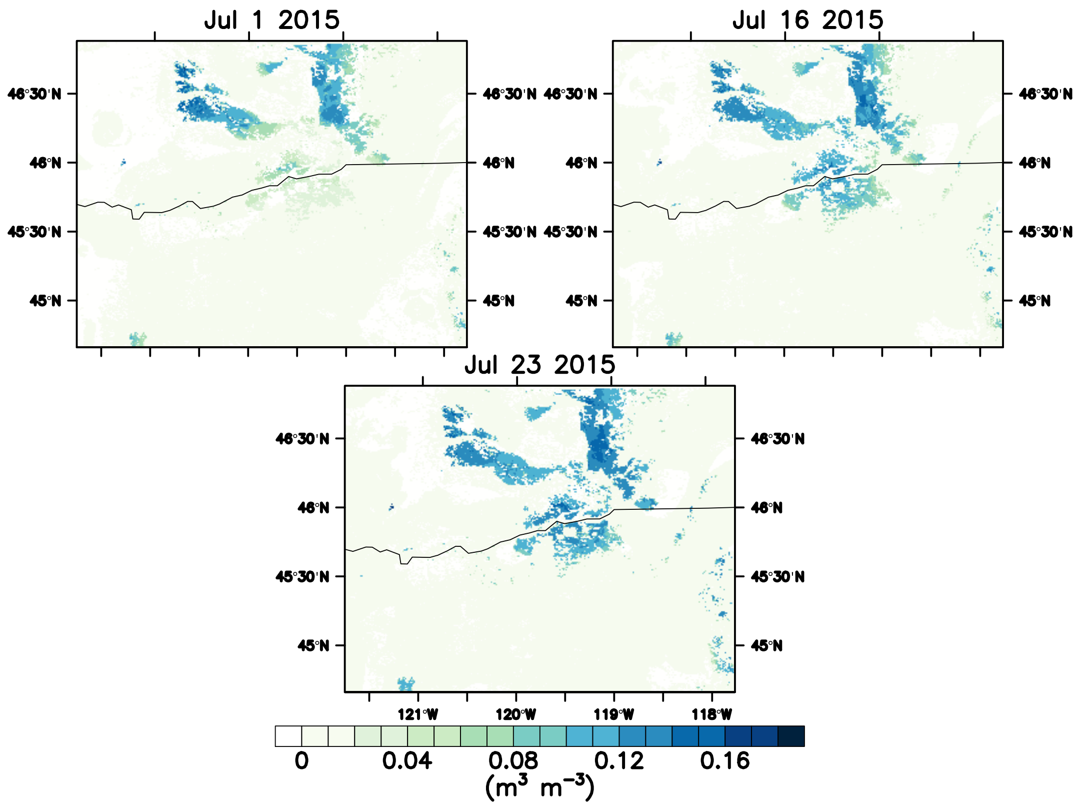

Figure 4.3 Change from control (IRR – CTRL) in top layer soil moisture at the time of initialization for each of the coupled LIS-WRF cases.

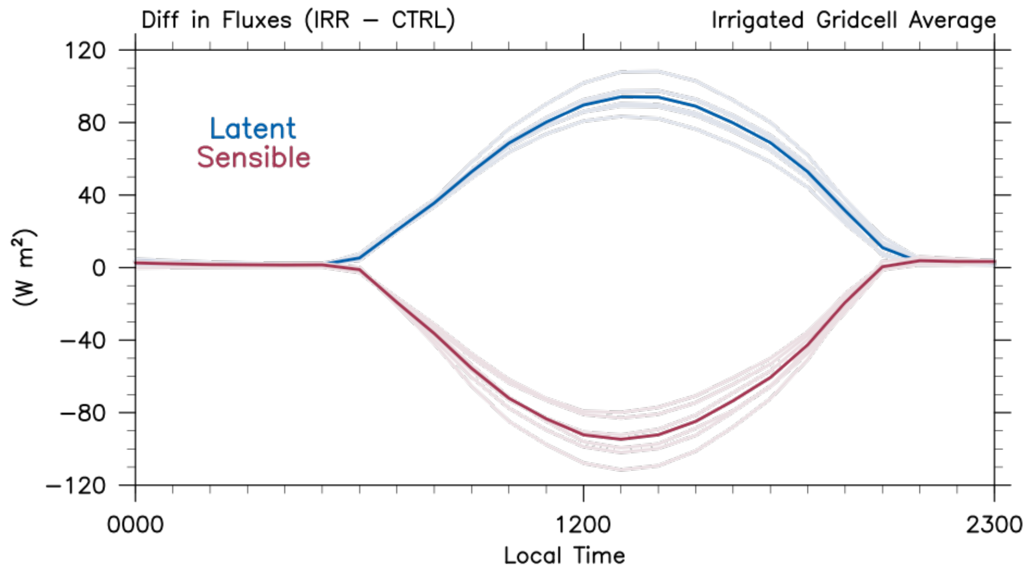

Figure 4.4 Change from control (IRR – CTRL) in surface latent (blue) and sensible (red) fluxes averaged over all gridcells with irrigation intensity greater than zero. Light colors show the six diurnal cycles for the three cases. The darker shades of blue and red are the case averages of latent and sensible heat fluxes, respectively.

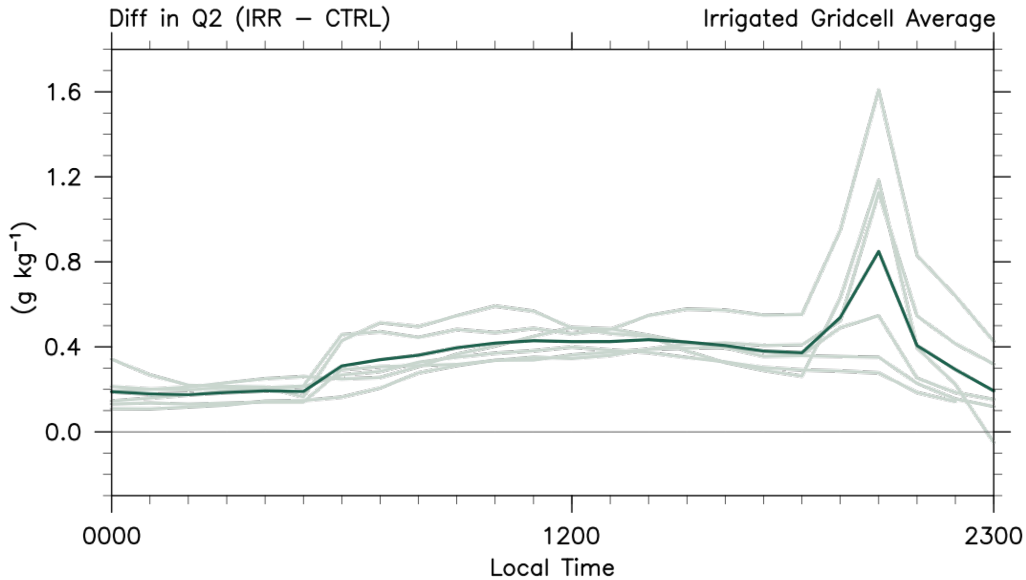

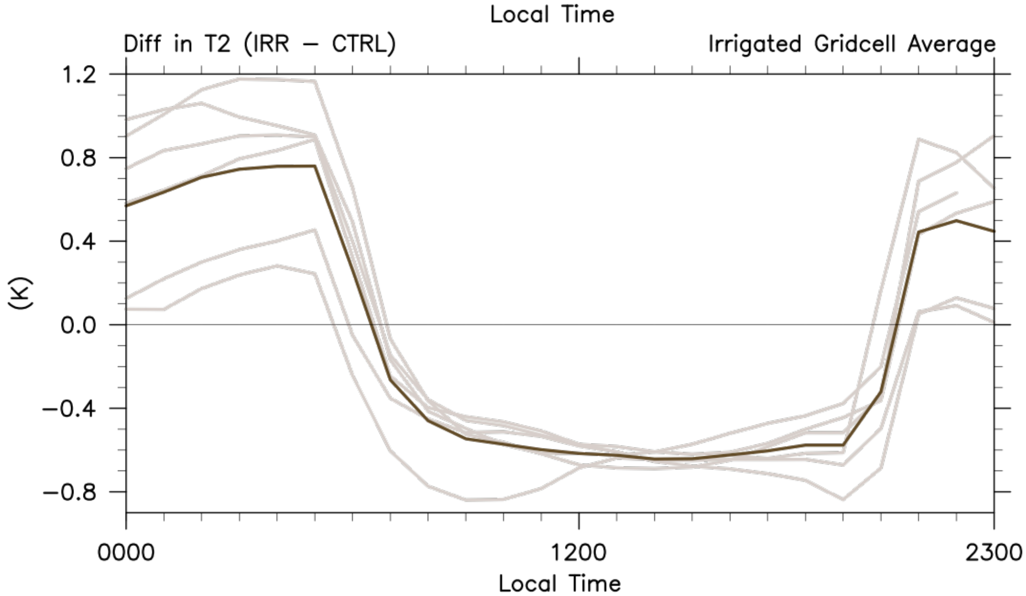

Figure 4.5 As in Figure 4.4, but for (a) near surface humidity (b) and near surface temperature.

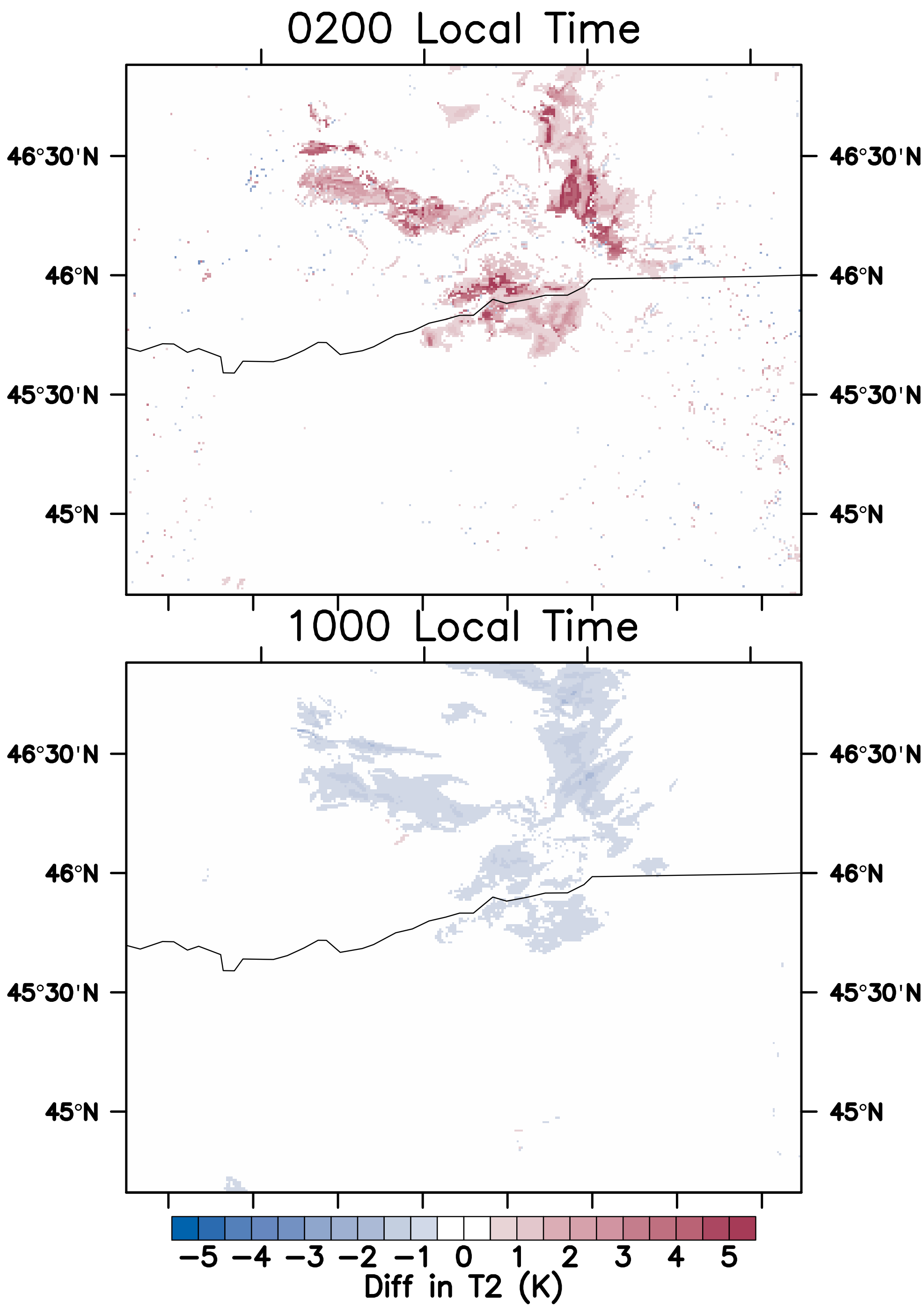

Figure 4.6 Change from control (IRR – CTRL) in near surface temperature at 2 am (top) and 10am (bottom) on the first day of case study 3.

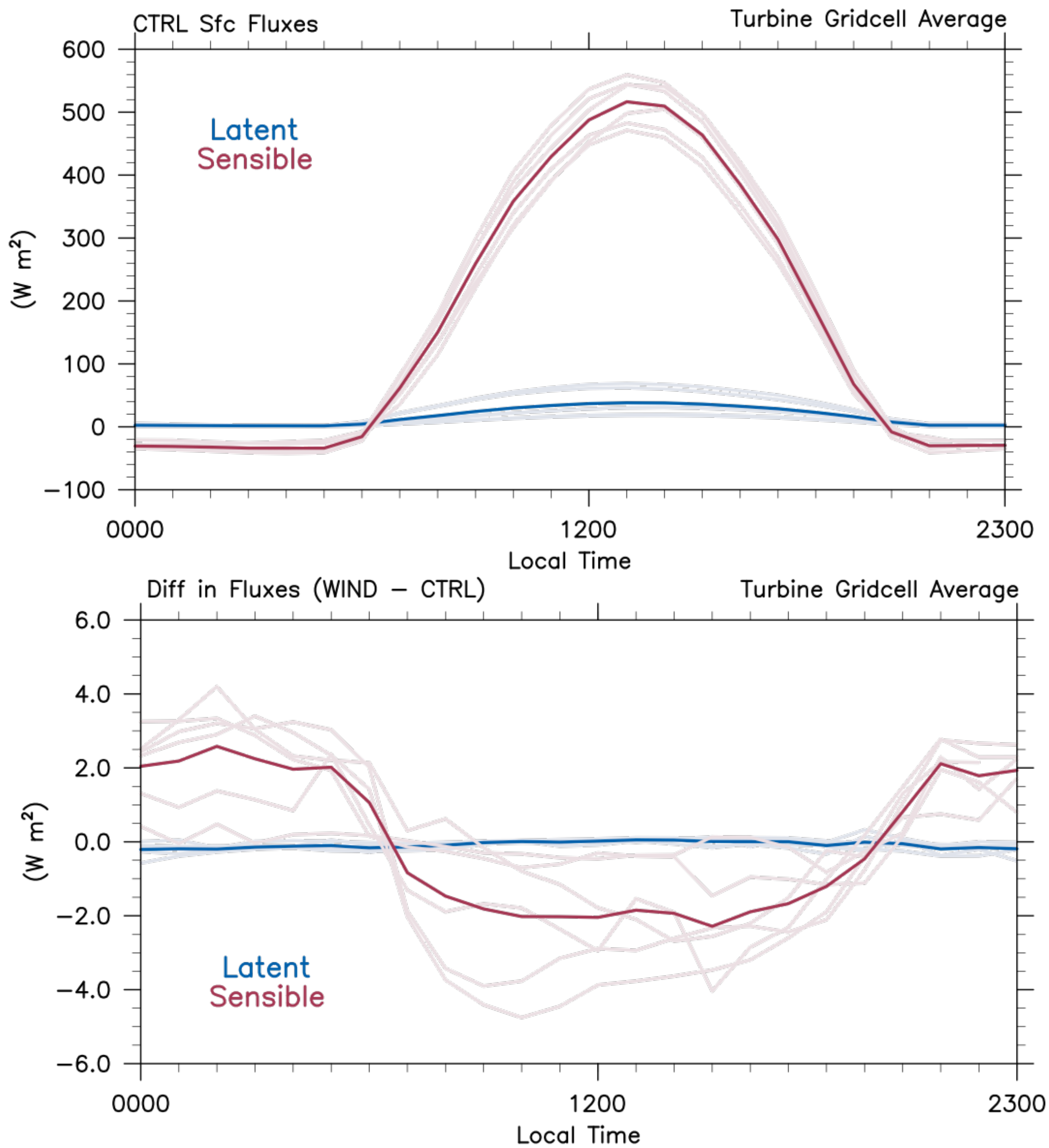

Figure 4.7 Hourly surface latent (blue) and sensible heat (red) fluxes in CTRL averaged over all gridcells containing at least one turbine (top). As in (top) but for change from control (WIND – CTRL).

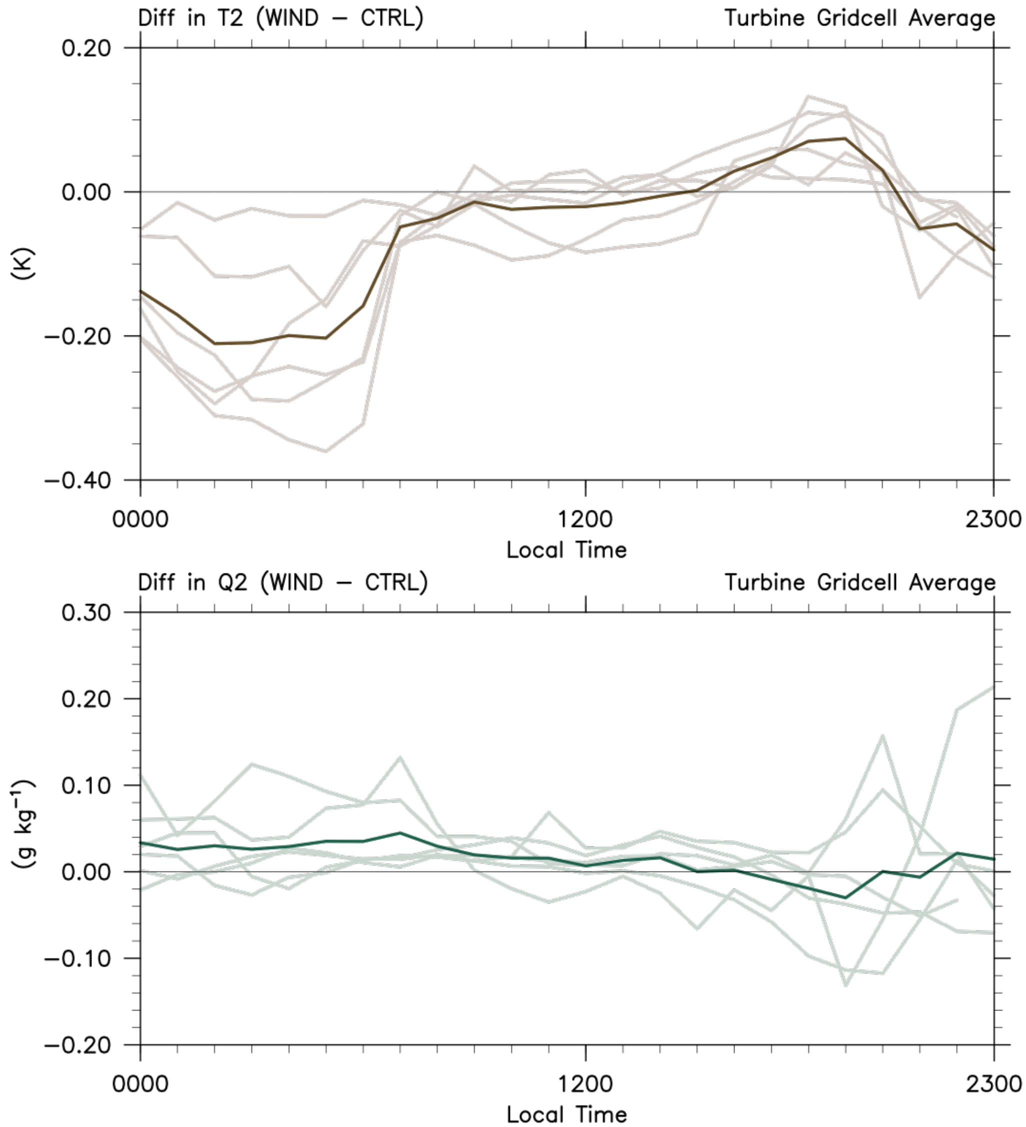

Figure 4.8 As in Figure 4.7 but for near surface temperature (top) and humidity (bottom).

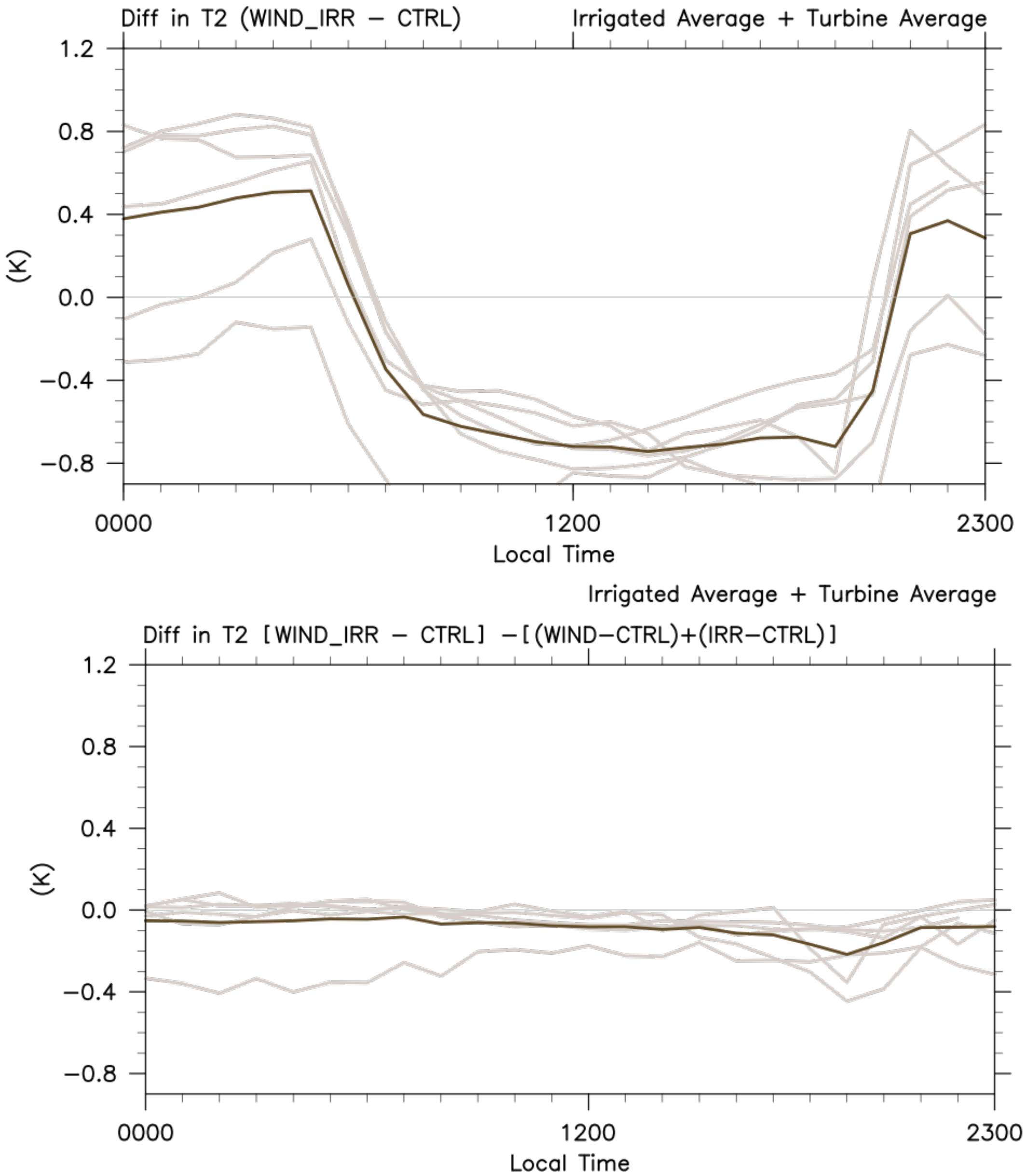

Figure 4.9 Change from control in T2 resulting from the simulation that includes both turbines and irrigation (WIND_IRR – CTRL) averaged over gridcells that are irrigated added to the average over turbine gridcells (top) Difference between WIND_IRR impacts (WIND_IRR – CTRL) and the sum of the linear impacts of irrigation and turbines individually (bottom; IRR – CTRL and WIND – CTRL, respectively).

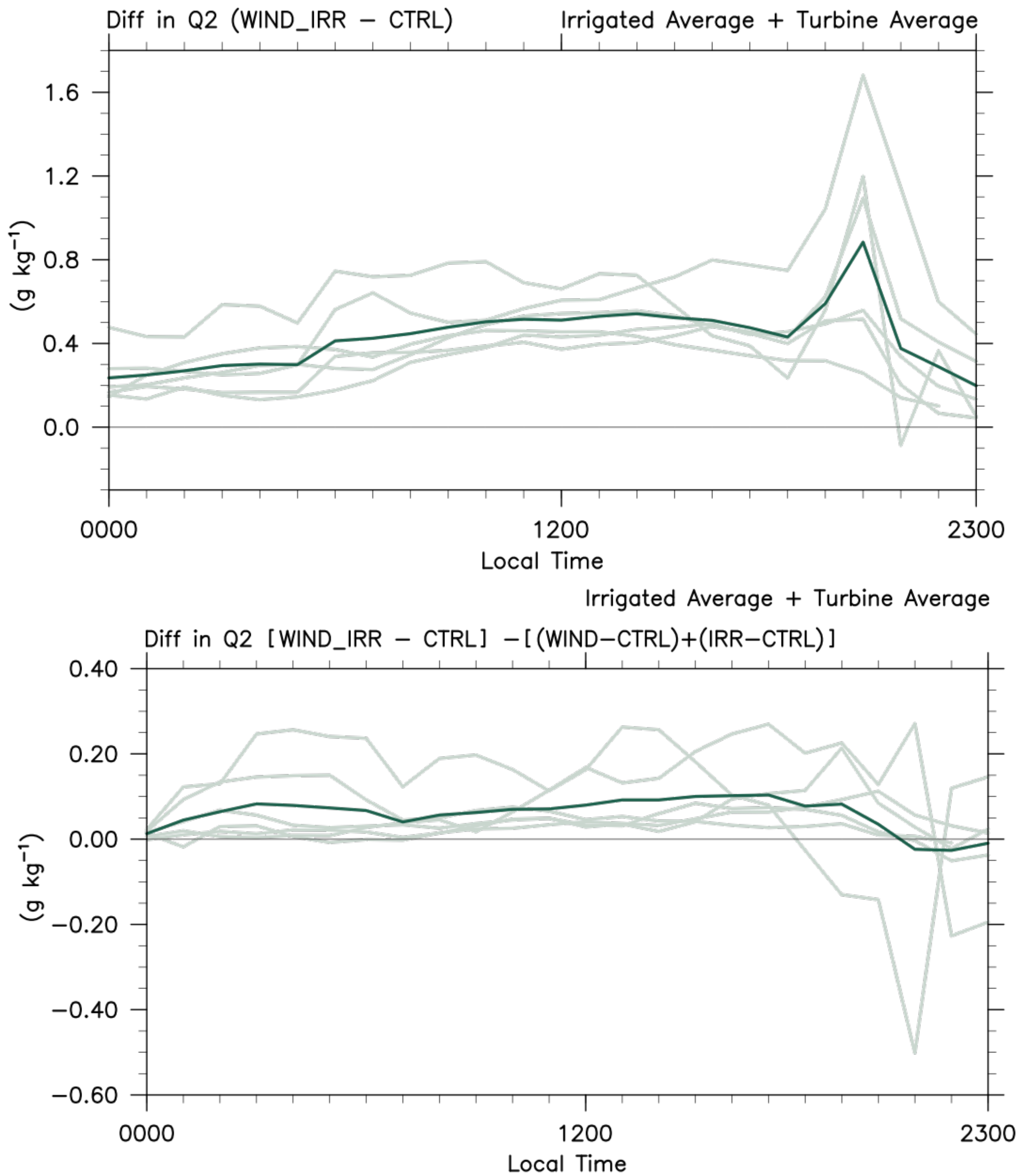

Figure 4.10 As in Figure 4.9, but for near surface humidity.

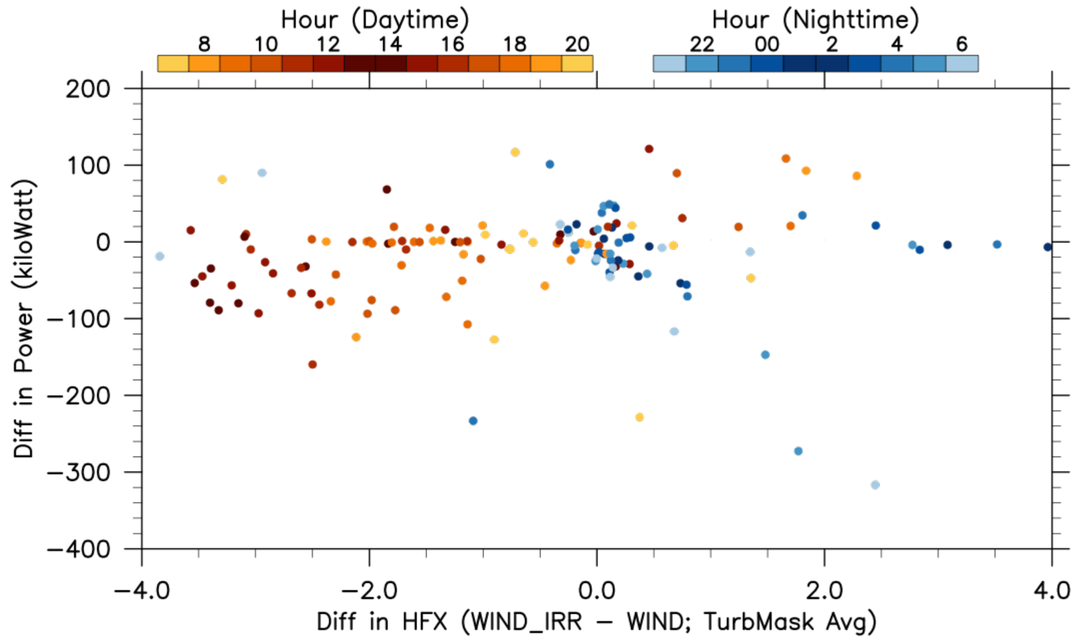

Figure 4.11 Scatterplot of the hourly difference in sensible heat flux in the simulation that contains both irrigation and turbines as compared to only using turbines and the corresponding difference in power produced. All differences are (WIND_IRR – WIND) and color of the dots indicates the hour of the day of each data point.

Chapter 5

CONCLUSIONS

These three studies showcase the dramatic effects that human-induced changes to the land surface can have on surface fluxes of latent and sensible heat and downstream impacts on near surface temperature, humidity, and ultimately the evolution of the planetary boundary layer. The first study showed that regional irrigation impacts are sensitive to time, space, and method and that irrigation cools and moistens the surface over and downwind of irrigated areas, ultimately resulting in both positive and negative feedbacks on the PBL. However, with a high-resolution simulation, evaluation of the irrigation methods with point observations proved to be difficult because of a number of factors, including the underrepresentation of irrigated areas in the USGS landuse classification data. Biophysical characteristics that determine transpiration amounts differ between crops, but the vegetation parameters in LIS–Noah do not account for different crop types. Thus, these land-use category differences not only complicated the point observations for the LSM evaluation by turning off irrigation and thus any differences between the methods at the Mead sites, but they also likely contributed to the underestimation of latent heat (through less ET) simulated by the model.

The second study addressed evaluation issues that arose in the first study by assessing the sprinkler irrigation physics and model sensitivity to irrigation intensity and GVF datasets in a LSM framework, and evaluating the results with novel point and gridded soil moisture observations. For all experiments, model results show that irrigation increases soil moisture and latent heat flux, and decreases sensible heat flux. Differences between experiments are small at the interannual scale, but become more apparent in analysis at seasonal and particularly diurnal time scales. The irrigation scheme uses GVF as a proxy for plant maturity and scales the amount of water applied accordingly to represent differences in irrigation scheduling based on growth stage. This behavior and the impacts of irrigation on soil moisture and fluxes are physically consistent with expectations of irrigation effects on the land surface. The continued evaluation and improvement of irrigation parameterizations, as discussed here, is an important step towards better understanding human influences on the water cycle and the impacts of such activities in a changing climate.

The third study used a high resolution mesoscale modeling environment with parameterizations for irrigation and turbines to assess the individual and combined impacts of each perturbation in a semi-arid region. Results show that irrigation repartitions surface sensible and latent heat fluxes, reduces daytime temperatures and increases temperatures at night. Turbines weaken surface sensible heat fluxes minimally during the day but enough at nighttime to slightly reduce near surface temperature. The simulations that include both turbines and irrigation show that wind power production is slightly reduced when irrigation is included and irrigation contributes to a greater reduction in daytime surface sensible heat fluxes than would be realized with only turbines. The linear sum of the turbine and irrigation impacts can be used to approximate the combined impact of irrigation and turbines on temperature but doesn’t perform as well for humidity, suggesting that non-linear processes play a stronger role in near surface humidity impacts in this typically moisture-limited regime.

Taken together, these studies suggest that human impacts to land use can be considerable and should be included in the context of climate change projections. As the demand for food and fuel increases with a growing world population, the need to efficiently produce high crop yields will likely lead to further expansion of irrigated fields. The inclusion of irrigation physics then has the potential to improve forecasts, which will offer farmers a better tool to adapt to increasing crop demands.

REFERENCES

Abbasi, S. A., and T. Abbasi, 2016: Impact of wind-energy generation on climate : A rising spectre. *Renew. Sustain. Energy Rev.*, **59**, 1591–1598, doi:10.1016/j.rser.2015.12.262. http://dx.doi.org/10.1016/j.rser.2015.12.262.

Adegoke, J. O., R. A. S. Pielke, J. Eastman, R. Mahmood, and K. G. Hubbard, 2003: Impact of Irrigation on Midsummer Surface Fluxes and Temperature under Dry Synoptic Conditions : A Regional Atmospheric Model Study of the U . S . High Plains. **131**, 556–564.

——, R. Pielke, and A. M. Carleton, 2007: Observational and modeling studies of the impacts of agriculture-related land use change on planetary boundary layer processes in the central U.S. *Agric. For. Meteorol.*, **142**, 203–215.

Alter, R. E., Y. Fan, B. R. Lintner, and C. P. Weaver, 2015a: Observational evidence that Great Plains irrigation has enhanced summer precipitation intensity and totals in the Midwestern US. *J. Hydrometeorol.*, 1717–1736, doi:10.1175/JHM-D-14-0115.1. http://dx.doi.org/10.1175/JHM-D-14-0115.1.

——, E.-S. Im, and E. A. B. Eltahir, 2015b: Rainfall consistently enhanced around the Gezira Scheme in East Africa due to irrigation. *Nat. Geosci*, **8**, 763–767. http://dx.doi.org/10.1038/ngeo2514.

Baidya Roy, S., 2011: Simulating impacts of wind farms on local hydrometeorology. *J. Wind Eng. Ind. Aerodyn.*, **99**, 491–498, doi:10.1016/j.jweia.2010.12.013. http://dx.doi.org/10.1016/j.jweia.2010.12.013.

——, and J. J. Traiteur, 2010: Impacts of wind farms on surface air temperatures. *Proc. Natl. Acad. Sci. U. S. A.*, **107**, 17899–17904, doi:10.1073/pnas.1000493107.

Baidya Roy, S., S. W. Pacala, and R. L. Walko, 2004: Can large wind farms affect local meteorology? *J. Geophys. Res. D Atmos.*, **109**, 1–6, doi:10.1029/2004JD004763.

Barrie, D. B., and D. B. Kirk-Davidoff, 2010: Weather response to a large wind turbine array. *Atmos. Chem. Phys.*, **10**, 769–775.

Betts, A. K., 1992: FIFE atmospheric boundary layer budget methods. *J. Geophys. Res.,* **97**, 18523-18531.

Bonfils, C., and D. Lobell, 2007: Empirical evidence for a recent slowdown in irrigation-induced cooling. *Proc. Natl. Acad. Sci. U. S. A.*, **104**, 13582–13587.

Boucher, O., G. Myhre, and A. Myhre, 2004: Direct human influence of irrigation on atmospheric water vapour and climate. *Climate Dynamics,* **22**(6-7), 597-603.

Calaf, M., C. Meneveau, and J. Meyers, 2010: Large eddy simulation study of fully developed wind-turbine array boundary layers. *Phys. Fluids*, **22**, 1–16, doi:10.1063/1.862466.

——, M. B. Parlange, and C. Meneveau, 2011: Large eddy simulation study of scalar transport in fully developed wind

Cervarich, M. C., S. B. Roy, and L. Zhou, 2013: Spatiotemporal Structure of Wind Farm-atmospheric Boundary Layer Interactions. *Energy Procedia*, **40**, 530–536, doi:10.1016/j.egypro.2013.08.061.

Chase, T. N., R. A. Piekle Sr, T. G. F. Kittel, J. S. Baron, and T. J. Stohlgren, 1999: Potential impacts on Colorado Rocky Mountain weather due to land use changes on the adjacent Great Plains. *J. Geophys. Res.*, **104**, 16673–16690.

Chen, F., and Coauthors, 2007: Description and Evaluation of the Characteristics of the NCAR High-Resolution Land Data Assimilation System. *J. Appl. Meteorol. Climatol.*, **46**, 694–713.

Cook, B. I., M. J. Puma, and N. Y. Krakauer, 2010: Irrigation induced surface cooling in the context of modern and increased greenhouse gas forcing. *Clim. Dyn.*, **37**, 1587–1600, doi:10.1007/s00382-010-0932-x.

DeAngelis, A., F. Dominguez, Y. Fan, A. Robock, M. D. Kustu, and D. Robinson, 2010: Evidence of enhanced precipitation due to irrigation over the Great Plains of the United States. *J. Geophys. Res.*, **115**, D15115.

Desilets, D. and Zreda, M. 2013: Footprint diameter for a cosmic-ray soil moisture probe: Theory and Monte Carlo simulations.Water Resour. Res., 49(6), 3566–3575, doi:10.1002/wrcr.20187.

Döll, P., Siebert, S., 1999: A Digital Global Map of Irrgated Areas. Report A9901, Center for Environmental Systems Research, University of Kassel, Kurt Wolters Strasse 3, 34109 Kassel, Germany.

Douglas, E. M., D. Niyogi, S. Frolking, J. B. Yeluripati, R. a. Pielke, N. Niyogi, C. J. Vörösmarty, and U. C. Mohanty, 2006: Changes in moisture and energy fluxes due to agricultural land use and irrigation in the Indian Monsoon Belt. *Geophys. Res. Lett.*, **33**, L14403.

——,, a. Beltrán-Przekurat, D. Niyogi, R. a. Pielke, and C. J. Vörösmarty, 2009: The impact of agricultural intensification and irrigation on land-atmosphere interactions and Indian monsoon precipitation - A mesoscale modeling perspective. *Glob. Planet. Change*, **67**, 117–128, doi:10.1016/j.gloplacha.2008.12.007.

Entin, J. K., Robock, A., Vinnikov, K. Y., Hollinger, S. E., Liu, S. and Namkhai, A, 2000: Temporal and spatial scales of observed soil moisture variations in the extratropics, J. Geophys. Res., 105(D9), 865–877.

Evans, J. P., and B. F. Zaitchik, 2008: Modeling the large-scale water balance impact of different irrigation systems. *Water Resour. Res.*, **44**, W08448.

Fitch, A. C., 2016: Notes on using the mesoscale wind farm parameterization of Fitch et al . (2012) in WRF. 1757–1758, doi:10.1002/we.

——., J. B. Olson, J. K. Lundquist, J. Dudhia, A. K. Gupta, J. Michalakes, and I. Barstad, 2012: Local and Mesoscale Impacts of Wind Farms as Parameterized in a Mesoscale NWP Model. *Mon. Weather Rev.*, **140**, 3017–3038, doi:10.1175/MWR-D-11-00352.1.

——, ——, and ——, 2013: Parameterization of wind farms in climate models. *J. Clim.*, **26**, 6439–6458, doi:10.1175/JCLI-D-12-00376.1.

Franz, T. E., Zreda, M., Ferre, T. P. A., Rosolem, R., Zweck, C., Stillman, S., Zeng, X. and Shuttleworth, W. J., 2012: Measurement depth of the cosmic ray soil moisture probe affected by hydrogen from various sources, Water Resour. Res., 48(8), 1–9, doi:10.1029/2012WR011871.

Franz, T. E., Wang, T., Avery, W., Finkenbiner, C. and Brocca, L., 2015: Combined analysis of soil moisture measurements from roving and fixed cosmic ray neutron probes for multiscale real-time monitoring, Geophys. Res. Lett., (May), 1–8, doi:10.1002/2015GL063963.

Guimberteau, M., Laval, K., Perrier, A. Polcher, J., 2012: Global effet of irrigation and its impact on the onset of the Indian summer monsoon. Clim Dyn. 39: 1329. doi:10.1007/s00382-011-1252-5.

Harding, K. J., and P. K. Snyder, 2012a: Modeling the Atmospheric Response to Irrigation in the Great Plains. Part II: The Precipitation of Irrigated Water and Changes in Precipitation Recycling. *J. Hydrometeorol.*, **13**, 1687–1703.

——, and ——, 2012b: Modeling the Atmospheric Response to Irrigation in the Great Plains. Part I: General Impacts on Precipitation and the Energy Budget. *J. Hydrometeorol.*, **13**, 1667–1686.

Huber, D., D. Mechem, and N. Brunsell, 2014: The Effects of Great Plains Irrigation on the Surface Energy Balance, Regional Circulation, and Precipitation. *Climate*, **2**, 103–128.

Hutson, S. S., N. L. Barber, J. F. Kenny, K.S. Linsey, D.S. Lumia, and M.A. Maupin, 2004: Estimated use of water in the United States in 2000. U.S. Geological Survey Circular 1268, USGS. 46 pp.

Im, E., M. P. Marcella, and E. A. B. Eltahir, 2014: Impact of Potential Large-Scale Irrigation on the West African Monsoon and Its Dependence on Location of Irrigated Area. *J. Clim.*, **27**, 994–1009.

Irmak, A., I. Ratcliffe, P. Ranade, K. Hubbard, R. K. Singh, B. Kamble, and J. Kjaersgaard, 2011: Estimation of Land Surface Evapotranspiration with a Satellite Remote Sensing Procedure. *Gt. Plains Res.*, **21**, 73–88.

Janjic, Z. I., 1994: The Step-Mountain Eta Coordinate Model: Further Developments of the Convection, Viscous Sublayer, and Turbulence Closure Schemes. *Mon. Weather Rev.*, **122**, 927–945.

Jiang, L., E. Ma, and X. Deng, 2014: Impacts of Irrigation on the Heat Fluxes and Near-Surface Temperature in an Inland Irrigation Area of Northern China. *Energies*, **7**, 1300–1317.

Jimenez, P. A., J. Navarro, A. M. Palomares, and J. Dudhia, 2015: Mesoscale modeling of offhsorewind turbine wakes at the wind farm resolving scale: a composite-based analysis with the Weather Research and Forecasting model over Horns Rev. *Wind Energy*, **18**, 559–566, doi:10.1002/we. http://onlinelibrary.wiley.com/doi/10.1002/we.1608/full.

Kanamaru, H. and Kanamitsu, M., 2008: Model Diagnosis of Nighttime Minimum Temperature Warming during Summer due to Irrigation in the California Central Valley, J. Hydrometeorol., 9(5), 1061–1072, doi:10.1175/2008JHM967.1.

Keith, D. W., J. F. Decarolis, D. C. Denkenberger, D. H. Lenschow, S. L. Malyshev, S. Pacala, and P. J. Rasch, 2004: The influence of large-scale wind power on global climate. *Proc. Natl. Acad. Sci. U. S. A.*, **101**, 16115–16120, doi:10.1073/pnas.0406930101.

Kirk-Davidoff, D. B., and D. W. Keith, 2008: On the Climate Impact of Surface Roughness Anomalies. *J. Atmos. Sci.*, **65**, 2215–2234, doi:10.1175/2007JAS2509.1.

Koster, R. D., P. A. Dirmeyer, A. N. Hahmann, R. Ijpelaar, L. Tyahla, P. Cox, and M. J. Suarez, 2002: Comparing the Degree of Land – Atmosphere Interaction in Four Atmospheric General Circulation Models. **3**, 363–375.

Kueppers, L. M., and M. A. Snyder, and L. C. Sloan, 2007: Irrigation cooling effect: Regional climate forcing by land-use change. *Geophys. Res. Lett.*, **34**, L03703.

——, ——, 2011: Influence of irrigated agriculture on diurnal surface energy and water fluxes, surface climate, and atmospheric circulation in California. *Clim. Dyn.*, **38**, 1017–1029.

——, and Coauthors, 2008: Seasonal temperature responses to land-use change in the western United States. *Glob. Planet. Change*, **60**, 250–264.

Kumar, S. V, and Coauthors, 2006: Land information system : An interoperable framework for high resolution land surface modeling. *Environ. Model. Softw.*, **21**, 1402–1415.

——, Peters-Lidard, C. D., Santanello, J., Harrison, K., Liu, Y., and Shaw, M., 2012: Land surface Verification Toolkit (LVT) – a generalized framework for land surface model evaluation. *Geosci. Model Dev.*, **5**, 869-886, doi:10.5194/gmd-5-869-2012, 2012.

——, Peters-Lidard, C. D., Santanello, J. A., Reichle, R. H., Draper, C. S., Koster, R. D., Nearing, G. and Jasinski, M. F., 2015: Evaluating the utility of satellite soil moisture retrievals over irrigated areas and the ability of land data assimilation methods to correct for unmodeled processes, Hydrol. Earth Syst. Sci., 19(11), 4463–4478, doi:10.5194/hess-19-4463-2015.

Lawrence, D. M., and J. M. Slingo, 2005: Weak Land – Atmosphere Coupling Strength in HadAM3 : The Role of Soil Moisture Variability. *J. Hydrometeorol.*, **6**, 670–680.

Lawston, P. M., J. A. Santanello, B. F. Zaitchik, and M. Rodell, 2015: Impact of Irrigation Methods on Land Surface Model Spinup and Initialization of WRF Forecasts. *J. Hydrometeorol.*, **16**, 1135–1154, doi:10.1175/JHM-D-14-0203.1.

Leng, G., M. Huang, Q. Tang, H. Gao, and L. R. Leung, 2014: Modeling the Effects of Groundwater-Fed Irrigation on Terrestrial Hydrology over the Conterminous United States. *J. Hydrometeorol.*, **15**, 957–972.

Lo, M.-H., and J. S. Famiglietti,2013: Irrigation in California's Central Valley strengthens the southwestern U.S. water cycle, *Geophys. Res. Lett.,* **40**, 301–306, doi:10.1002/grl.50108.

Lobell, D., G. Bala, A. Mirin, T. Phillips, R. Maxwell, and D. Rotman, 2009: Regional Differences in the Influence of Irrigation on Climate. *J. Clim.*, **22**, 2248–2255.

Lu, H., and F. Porté-Agel, 2011: Large-eddy simulation of a very large wind farm in a stable atmospheric boundary layer. *Phys. Fluids*, **23**, doi:10.1063/1.3589857.

Lu, Y., Jin, J. and Kueppers, L. M., 2015: Crop growth and irrigation interact to influence surface fluxes in a regional climate-cropland model (WRF3.3-CLM4crop), Clim. Dyn., 45(11–12), 3347–3363, doi:10.1007/s00382-015-2543-z.

Mahmood, R., T. Keeling, S. a. Foster, and K. G. Hubbard, 2013: Did irrigation impact 20th century air temperature in the High Plains aquifer region? *Appl. Geogr.*, **38**, 11–21.

Mesinger, F., and Coauthors, 2006: North American Regional Reanalysis. *Bull. Amer. Meteor. Soc.,* **87,** 343-360.

Model Evaluation Tools (MET) User's Guide, cited June 2014. Available online ww.dtcenter.org/met/users/docs/users_guide/MET_Users_Guide_v4.1.pdf

Moore, N., and S. Rojstaczer, 2002: Irrigation’s influence on precipitation: Texas High Plains, U.S.A. *Geophys. Res. Lett.*, **29**, 2–1–2–4.

Nakanishi, M. and H. Niino, 2006: An Improved Mellor--Yamada Level-3 Model: Its Numerical Stability and Application to a Regional Prediction of Advection Fog", *Boundary-Layer Meteorology*, **119**, 397-407.

National Agricultural Statistics Survey (NASS), 2009: *2007 Census of Agriculture Farm and Ranch Irrigation Survey (2008)*.

NASS: 2012 census of agriculture: Farm and ranch irrigation survey, (3) Special studies, Part 1, Rep. AC-12-ss-1, National Agricultural Statistics Service, USDA, 266pp., 2014

NREL, cited 2016: National Renewal Energy Lab Wind Maps [available via: www.nrel.gov/gis/wind.html].

van Oevelen, P., 2016: Water for Food Baskets of the World. GEWEX News. 26 (2), 2.

Ozdogan, M., and G. Gutman, 2008: A new methodology to map irrigated areas using multi-temporal MODIS and ancillary data: An application example in the continental US. *Remote Sens. Environ.,* **112,** 3520-3537.

——, M. Rodell, H. K. Beaudoing, and D. L. Toll, 2010: Simulating the Effects of Irrigation over the United States in a Land Surface Model Based on Satellite-Derived Agricultural Data. *J. Hydrometeorol.*, **11**, 171–184.

Pei, L., N. Moore, S. Zhong, A. D. Kendall, D. W. Hyndman, and Z. Gao, 2016: Effects of irrigation on the summer climate over the United States. *J. Clim.*, **29**, 3541–3558, doi:10.1175/JCLI-D-15-0337.1.

Peters-Lidard, C. D., and Coauthors, 2015: Integrated modeling of aerosol, cloud, precipitation and land processes at satelliteresolved scales. Environ. Modell. Software, 67, 149–159, doi:10.1016/j.envsoft.2015.01.007.

Pokhrel, Y., N. Hanasaki, S. Koirala, J. Cho, P. J.-F. Yeh, H. Kim, S. Kanae, and T. Oki, 2012: Incorporating Anthropogenic Water Regulation Modules into a Land Surface Model. *J. Hydrometeorol.*, **13**, 255–269.

Qian, Y., M. Huang, B. Yang, and L. K. Berg, 2013: A Modeling Study of Irrigation Effects on Surface Fluxes and Land–Air–Cloud Interactions in the Southern Great Plains. *J. Hydrometeorol.*, **14**, 700–721.

Quiring, Steven, M., Ford, Trent, W., Wang, Jessica, K., Khong, A., Harris, E., Lindgren, T., Goldberg, D. W. and Li, Z., 2016: The North American Soil Moisture Database: Development and Applications, 20(8), 585–601, doi:10.1175/BAMS-D-12-00050.1.

Rajewski, D. a., and Coauthors, 2013: Crop wind energy experiment (CWEX): Observations of surface-layer, boundary layer, and mesoscale interactions with a wind farm. *Bull. Am. Meteorol. Soc.*, **94**, 655–672, doi:10.1175/BAMS-D-11-00240.1.

Rajewski, D. A., E. S. Takle, J. K. Lundquist, J. H. Prueger, R. L. Pfeiffer, J. L. Hatfield, K. K. Spoth, and R. K. Doorenbos, 2014: Agricultural and Forest Meteorology Changes in fluxes of heat , H 2 O , and CO 2 caused by a large wind farm. *Agric. For. Meteorol.*, **194**, 175–187, doi:10.1016/j.agrformet.2014.03.023. http://dx.doi.org/10.1016/j.agrformet.2014.03.023.

Salmon, J. M., M. A. Friedl, S. Frolking, D. Wisser, and E. M. Douglas, 2015: Global rain-fed, irrigated, and paddy croplands: A new high resolution map derived from remote sensing, crop inventories and climate data. *Int. J. Appl. Earth Obs. Geoinf.*, **38**, 321–334, doi:10.1016/j.jag.2015.01.014. http://www.sciencedirect.com/science/article/pii/S0303243415000240.

Santanello, J. A., C. D. Peters-Lidard, S. V. Kumar, C. Alonge, and W.-K. Tao, 2009: A Modeling and Observational Framework for Diagnosing Local Land–Atmosphere Coupling on Diurnal Time Scales. *J. Hydrometeorol.*, **10**, 577–599.

——, ——, and ——, 2011a: Diagnosing the Sensitivity of Local Land–Atmosphere Coupling via the Soil Moisture–Boundary Layer Interaction. *J. Hydrometeorol.*, **12**, 766–786.

——. and Coauthors, 2011b: Results from Local Land-Atmosphere Coupling (LoCo) Project. *GEWEX Newsl.*, **21**, 7–9.

——, C. D. Peters-Lidard, A. Kennedy, and S. V. Kumar, 2013a: Diagnosing the Nature of Land–Atmosphere Coupling: A Case Study of Dry/Wet Extremes in the U.S. Southern Great Plains. *J. Hydrometeorol.*, **14**, 3–24.

——, S. V. Kumar, C. D. Peters-Lidard, K. Harrison, and S. Zhou, 2013b: Impact of Land Model Calibration on Coupled Land–Atmosphere Prediction. *J. Hydrometeorol.*, **14**, 1373–1400.

Segal, M., Z. Pan, R. W. Turner, and E. S. Takle, 1998: On the Potential Impact of Irrigated Areas in North America on Summer Rainfall Caused by Large-Scale Systems. *J. Appl. Meteorol.*, **37**, 325–331.

Skamarock, W. C., J. B. Klemp, J. Dudhia, D. O. Gill, D. M. Barker, W. Wang, and J. G. Powers, 2005: *A Description of the Advanced Research WRF Version 2*. NCAR Tech Note NCAR/TN-468+STR, 88 pp.

Slawsky, L. M., L. Zhou, S. B. Roy, G. Xia, and M. Vuille, 2015: Observed Thermal Impacts of Wind Farms Over Northern Illinois. 14981–15005, doi:10.3390/s150714981.

Sorooshian, S., J. Li, K. Hsu, and X. Gao, 2011: How significant is the impact of irrigation on the local hydroclimate in California's Central Valley? Comparison of model results with ground and remote-sensing data. *J. Geophys. Res.*, **116**, D06102.

——, ——, ——, and ——, 2012: Influence of irrigation schemes used in regional climate models on evapotranspiration estimation: Results and comparative studies from California's Central Valley agricultural regions. *J. Geophys. Res.*, **117**, D06107.

Tang, Q., S. Peterson, R. H. Cuenca, Y. Hagimoto, and D. P. Lettenmaier, 2009: Satellite-based near-real-time estimation of irrigated crop water consumption, *J. Geophys. Res*., **114**, D05114.

Tuinenburg, O. A., R. W. A. Hutjes, T. Stacke, A. Wiltshire, and P. Lucas-Picher, 2014: Effects of Irrigation in India on the Atmospheric Water Budget. *J. Hydrometeorol.*, **15**, 1028–1050.

Trenberth, K. E. and Asrar, G. R., 2014: Challenges and Opportunities in Water Cycle Research: WCRP Contributions, Surv. Geophys., 35(3), 515–532, doi:10.1007/s10712-012-9214-y.

UCS, cited 2016: Farming the wind: Wind power and agriculture [available online at www.ucsusa.org/clean_energy/technology_and_impacts/impacts/farming-the-wind-wind-power.html]

Vahmani, P., and T. S. Hogue, 2014: Incorporating an Urban Irrigation Module into the Noah Land Surface Model Coupled with an Urban Canopy Model. *J. Hydrometeorol.*, **15**, 1440–1456.

Vanderwende, B., and J. K. Lundquist, 2016: Could Crop Height Affect the Wind Resource at Agriculturally Productive Wind Farm Sites ? *Boundary-Layer Meteorol.*, **158**, 409–428, doi:10.1007/s10546-015-0102-0. "http://dx.doi.org/10.1007/s10546-015-0102-0.

de Vrese, P., S. Hagemann, and M. Claussen, 2016: Asian irrigation, African rain: Remote impacts of irrigation. *Geophys. Res. Lett.*, doi:10.1002/2016GL068146.

Walsh-Thomas, J. M., G. Cervone, P. Agouris, and G. Manca, 2012: Further evidence of impacts of large-scale wind farms on land surface temperature. *Renew. Sustain. Energy Rev.*, **16**, 6432–6437, doi:10.1016/j.rser.2012.07.004. http://dx.doi.org/10.1016/j.rser.2012.07.004.

Wang, C., and R. G. Prinn, 2009: Potential climatic impacts and reliability of very large-scale wind farms. *Atmos. Chem. Phys. Discuss.*, **9**, 19081–19102, doi:10.5194/acpd-9-19081-2009.

Wei, J., P. a. Dirmeyer, D. Wisser, M. G. Bosilovich, and D. M. Mocko, 2013: Where Does the Irrigation Water Go? An Estimate of the Contribution of Irrigation to Precipitation Using MERRA. *J. Hydrometeorol.*, **14**, 275–289.

Xia, Y. L., Mitchell, K., Ek, M., Sheffield, J., Cosgrove, B., Wood, E., Luo, L. F., Alonge, C., Wei, H. L., Meng, J., Livneh, B., Lettenmaier, D., Koren, V., Duan, Q. Y., Mo, K., Fan, Y. and Mocko, D., 2012: Continental-scale water and energy flux analysis and validation for the North American Land Data Assimilation System project phase 2 (NLDAS-2): 1. Intercomparison and application of model products, J. Geophys. Res., 117, doi:Artn D03109\rDoi 10.1029/2011jd016048.

Xie, S., and C. Archer, 2015: Self-similarity and turbulence characteristics of wind turbine wakes via large-eddy simulation. *Wind Energy*, **18**, 1815–1838, doi:10.1002/we. http://onlinelibrary.wiley.com/doi/10.1002/we.1608/full.

Yilmaz, M. T., M. C. Anderson, B. Zaitchik, C. R. Hain, W. T. Crow, M. Ozdogan, J. A. Chun, and J. Evans, 2014: Comparison of prognostic and diagnostic surface flux modeling approaches over the Nile River basin. *Water Resour. Res.*, **50**, 386–408.

Zaitchik, B. F., J. Evans, and R. B. Smith, 2005: MODIS-Derived Boundary Conditions for a Mesoscale Climate Model : Application to Irrigated Agriculture in the Euphrates Basin. *Mon. Weather Rev.*, **133**, 1727–1743.

Zhou, L., Y. Tian, S. Baidya Roy, C. Thorncroft, L. F. Bosart, and Y. Hu, 2012: Impacts of wind farms on land surface temperature. *Nat. Clim. Chang.*, **2**, 539–543, doi:10.1038/nclimate1505.

Zreda, M., Shuttleworth, W. J., Zeng, X., Zweck, C., Desilets, D., Franz, T. and Rosolem, R., 2012: COSMOS: The cosmic-ray soil moisture observing system, Hydrol. Earth Syst. Sci., 16(11), 4079–4099, doi:10.5194/hess-16-4079-2012.

Appendix

PERMISSIONS

Chapter 1 ©American Meteorological Society. Used with permission. Lawston, P. M., J. A. Santanello, B. F. Zaitchik, and M. Rodell, 2015: Impact of Irrigation Methods on Land Surface Model Spinup and Initialization of WRF Forecasts. J. Hydrometeorol., 16, 1135–1154, doi:10.1175/JHM-D-14-0203.1.